HI OBSERVATIONS OF DUST CLOUDS

Thesis by

Kwong Wah Chu

In Partial Fulfillment of the Requirements

for the Degree of

Doctor of Philosophy

California Institute of Technology

Pasadena, California

1975

(Submitted August 29, 1974)

ACKNOWLEDGMENTS

It is difficult to adequately thank everyone who has provided assistance in carrying out this project. To thank everyone individually is not possible for which the writer can only apologize. Nevertheless, a number of people deserve special mention.

Much thanks must go to my fellow graduate students J. Bieging, J. C. Pigg, J. Romney and W. Wright. Without their help in pushing buttons into the wee hours of the morning, the observing program could not have been accomplished.

R. Crutcher and N. Scoville provided considerable assistance. The former helped reduce the autocorrelator data, and the latter provided some important CO observations.

Special thanks goes to my thesis advisor, D. H. Rogstad, for suggesting this project in the beginning and providing the necessary encouragement to continue when things looked bleak.

Finally I wish to express my appreciation to G. Stanley, OVRO Director, and the entire OVRO staff. Without their support and cooperation, this work would not have been possible.

ABSTRACT

Aperture synthesis observations of three dust clouds, L134, L1495 and L1517, were made at 21 cm. A 7 arc min diameter beam was synthesized, and the velocity resolution was 0.2 km/sec. In addition to interferometer observations, single dish measurements were carried out to provide large scale information. Two dust clouds, L134 and L1495, were detected in absorption against background 21 cm emission. In both cases the 21 cm absorption line is at a velocity coincident with molecular lines detected in the dust clouds. The hydrogen responsible for the absorption line has a spin temperature less than 20° K, and the columnar atomic hydrogen density through the dust clouds is between 10^{19} cm^{-2} and 10^{20} cm^{-2}. Based upon optical extinction and normal cosmic abundances, the expected hydrogen content is 10^{22} cm^{-2}. It is presumed that most of the hydrogen is in molecular form.

L134 consists of two velocity components separated by 2 km/sec. Fragmentation of a larger cloud into two smaller components may explain the data, but more evidence is needed to draw any firm conclusion. Within an individual velocity component, no significant substructure was detected in L134 or L1495. The optical appearance of L1517 strongly suggests a fragmented structure, but this dust cloud was not detectable at 21 cm. L1517 may be sufficiently dense that the

amount of residual atomic hydrogen is too small to detect, but this conjecture remains to be substantiated.

TABLE OF CONTENTS

I. INTRODUCTION

One of the fundamental problems in astronomy is to understand the process by which stars are born. Based upon the large amount of scientific knowledge accumulated to date, the idea that star formation is a continuing process is now commonly accepted as fact. Theoretical work attempting to describe how matter condenses from interstellar-like densities (10^{-24} gm/cm^3) to stellar-like densities (1 gm/cm^3) has recently been reviewed by Larson (1973). In principle current knowledge about the fundamental physical laws governing gravitational and electromagnetic interactions should be sufficient to describe star formation up to the point where nuclear reactions become important. However, the problem is so complicated and initial conditions are so poorly known that star formation is not a well understood process.

Observational astronomy is of great importance because it provides a framework of facts (initial conditions and boundary conditions) within which physical laws may be applied to understand the birth of stars. The presence of dark areas in the sky strikingly deficient in stars compared to surrounding regions had long been noticed, but only after many years did it become accepted that dense clouds of dust obscuring stars in the background were responsible for the phenomena (Lynds 1968). It has long been speculated

that dark dust clouds represent the initial stages of star formation (Bok and Reilly 1947). If true, knowledge about physical conditions in these dust clouds is important for understanding how stars might eventually form.

In recent years many molecular lines (e.g. OH, CO, and H_2CO) have been detected in the dust clouds (Cudaback and Heiles 1969; Penzias et al. 1972; Dieter 1973). Hydrogen is by far the most abundant element, and from a naive viewpoint, one would expect the 21 cm emission to be an easy means by which dust clouds may be observed. The common models for dust grains and normal cosmic abundances would lead one to expect that the total columnar hydrogen density N is

$$N \simeq 10^{21} A_v \text{ cm}^{-2}$$

where A_v is the visual extinction of the dust cloud in magnitudes. Dust clouds often produce several magnitudes of absorption, and if all the hydrogen predicted by the above equation is present and in atomic form, dust clouds should be easily detected at 21 cm. In reality the situation is quite complex. In surveys covering the general interstellar field, excess 21 cm emission seems associated with increased obscuration by dust (Lilley 1955; Heiles 1967; Sturch 1969). However, when attempts are made to correlate dust and 21 cm emission on a detailed basis, the results are varied:

occasionally excess 21 cm emission is associated with dust (Raimond 1966; Heiles 1969); more often 21 cm emission decreases when obscuration increases (Davies 1956, 1958; McGee et al. 1963; Garzoli and Varsavsky 1966, 1970; Quiroge and Varsavsky 1970; Sancisi and Wesselius 1970; Sancisi 1971; Knapp 1974); but quite often no correlation is detected between dust clouds and 21 cm emission (Bok et al. 1955; Kerr and Garzoli 1968; Heiles 1969). Several factors can help explain the various results: (1) the 21 cm emission comes from cold hydrogen and the emission line is saturated; (2) the hydrogen is mostly in molecular form; (3) foreground hydrogen and variations in the background brightness may mask observable effects produced by the hydrogen in the dust cloud; (4) physical conditions in dust clouds differ significantly from cloud to cloud. Obviously more detailed observations are needed to help clarify the situation.

Interstellar dust and gas are nonuniformly distributed within the galaxy. Concentrations of dust and gas vary on a scale size from many hundreds of parsecs (spiral arms) down to a small fraction of a parsec (small globules seen projected against emission nebulae). To minimize problems introduced by nonuniform background brightness, it is advantageous to observe as compact a dust cloud as possible but still retain reasonable angular resolution. Previous

21 cm studies of dust clouds were made with a single antenna, and therefore the angular resolution was limited (typically 0.5°). Interferometric observations of compact dust clouds using an aperture synthesis technique are advantageous for two reasons: (1) high angular resolution may be achieved; (2) uniform background emission is automatically resolved out. Because radio interferometry appeared to be a promising method to gain more information about compact dust clouds, a decision was made to carry out an observational program.

Dust clouds called "large globules" by Bok were chosen for study. The particular globules picked were highly opaque and had a size suitable for interferometer observations (diameter $\simeq$ 20'). The objective was to measure the 21 cm brightness distribution of the globules with as good an angular resolution, velocity resolution and sensitivity as were commensurate with equipment and time limitations. In any case the interferometer was expected to produce data significantly superior to any single dish measurements made up to date. Due to the increased angular resolution available by interferometry techniques, the structure and kinematics of large globules can be studied. With greater knowledge about physical conditions in the large globules, a better evaluation may be made about their role in star formation.

II. OBSERVATIONS

SELECTION OF THE DUST CLOUDS

Certain considerations should be taken in selecting suitable objects for observations. Because an aperture synthesis program was to be undertaken, it was obvious at the start only a few objects could be studied due to the limited observing time available. For each dust cloud, the important factors which need to be evaluated are: (1) size of the dust cloud compared to the antenna beam size; (2) how well the visibility can be sampled in the (u,v) plane; (3) the amount of information already available about the dust cloud. A great uncertainty was the degree of spatial structure occurring in the 21 cm background. Its effect would be to confuse the brightness temperature due to the dust cloud. The amount of foreground HI would also influence the ease with which dust clouds could be detected. The only way to resolve these uncertainties was to do some observations. Initially four dark dust clouds were chosen for a feasibility study.

Dust cloud L134 (Lynds 1962) was selected as the primary cloud to be observed for a variety of reasons. First, L134 lies at a 35° galactic latitude, and it was hoped that

the background HI emission would be relatively simple in its spatial and velocity dependence as compared to regions at lower galactic latitudes. Second, a considerable amount of information was already available about L134 (Heiles 1968; Palmer et al. 1969; Zuckerman et al. 1969; Penzias et al. 1972). Molecular lines of OH, H_2CO and CO had been detected in the direction of L134, but HI observations (Sancisi 1971), while showing a HI emission minimum in the direction of L134, indicated that this minimum was at a velocity 2 km/sec less than that of the molecular lines. It was felt further HI observations with greater velocity and angular resolution would be worthwhile. Third, the size of L134 as inferred from photographs is smaller than the beam of the 90 ft. antenna (32') which makes it well suited for interferometer observations.

The remaining three clouds were chosen in order that some object would always be visible. B361 is a cloud suggested by Bok et al. (1970) as a candidate for further study. Since it filled a convenient time slot in the observing program, it was initially included in the observations. B361 lies within 1° of the galactic equator and initial observations during March 1972 indicated a considerable amount of spatial structure was present in the 21 cm emission over at least a 50 km/sec velocity range. No

detection of molecular lines in B361 existed; therefore, it was not possible to determine at which velocity the HI data should be examined to see if the dust cloud was visible. At this point B361 was dropped from any further consideration.

L1517 and L1495 are two dust clouds which lie within the Taurus dust complex. L1517 was chosen mainly because its optical appearance suggested it to be ideal for this project. It has an overall diameter of about 20', and most interestingly it appears to consist of about four subcondensations approximately 5' in size (see fig. 5-1). There is one known T Tauri star within 30' of the cloud center and a B9 peculiar emission line star within 5' of the center (Herbig 1960). The available evidence suggests that L1517 is now or was very recently in an area of star formation. The hope that 21 cm observations would show structure like that suggested by photographs provided the incentive for observing this cloud.

L1495 is a large dust cloud which Lynds (1962) estimates to be 2.6 square degrees. The observations are centered on a section of L1495 which coincides with a position where OH has been detected (Cudaback and Heiles 1969). This position is about 1° north of the position listed

by Lynds (1962) for L1495. There are four known T Tauri stars in the immediate vicinity of this dust cloud (Herbig 1962). Despite being larger than the antenna beam, L1495 was selected to see what substructure might exist.

Table 2-1 gives a summary of the dust clouds that were studied. The antennas were pointed at the adopted position during the interferometer observations. The diameter is a crude estimate obtained by viewing the Palomar Sky Survey print. In this paper the center of the dust cloud will be taken as the adopted position despite where the true centroid of the dust distribution might lie.

TABLE 2-1

OBSERVED DUST CLOUDS

NAME	ADOPTED POSITION RA(1950)	DEC(1950)	GALACTIC COORD l	b	DIAM.
L134	15^h 51.1^m	-04° 31.6'	4.2°	35.7°	20'
L1495	04^h 15.5^m	28° 18.0'	168.7°	-15.5°	1°
L1517	04^h 51.5^m	30° 32.0'	172.4°	-8.0°	20'

INSTRUMENT

The interferometer observations were conducted with the OVRO twin-element interferometer, and single dish observations were obtained with the 130 ft. diameter antenna using a 100 channel autocorrelator. The interferometer consists of two 90 ft. antennas, and its operation as a 21 cm line aperture synthesis instrument has been described by Rogstad and Shostak (1971). A block diagram showing the basic interferometer logic is shown in fig. 2-1. A detailed description of the interferometer will not be given except for factors important in planning the observing program.

Because these particular observations do not benefit from a wide bandpass, the IF bandpass (nominal center frequency 10 MHz) was purposely limited to 5 MHz by inserting filters into the IF line coming from each antenna. This had the beneficial effect of rejecting continuous wave interference which at times got injected into the IF lines for reasons not entirely clear. In this paper "wideband channel" refers to this 5 MHz bandpass correlated without further filtering. The wideband channel was used for observing continuum sources in the sky. Such observations are necessary to perform instrumental calibration as will be discussed in a later section.

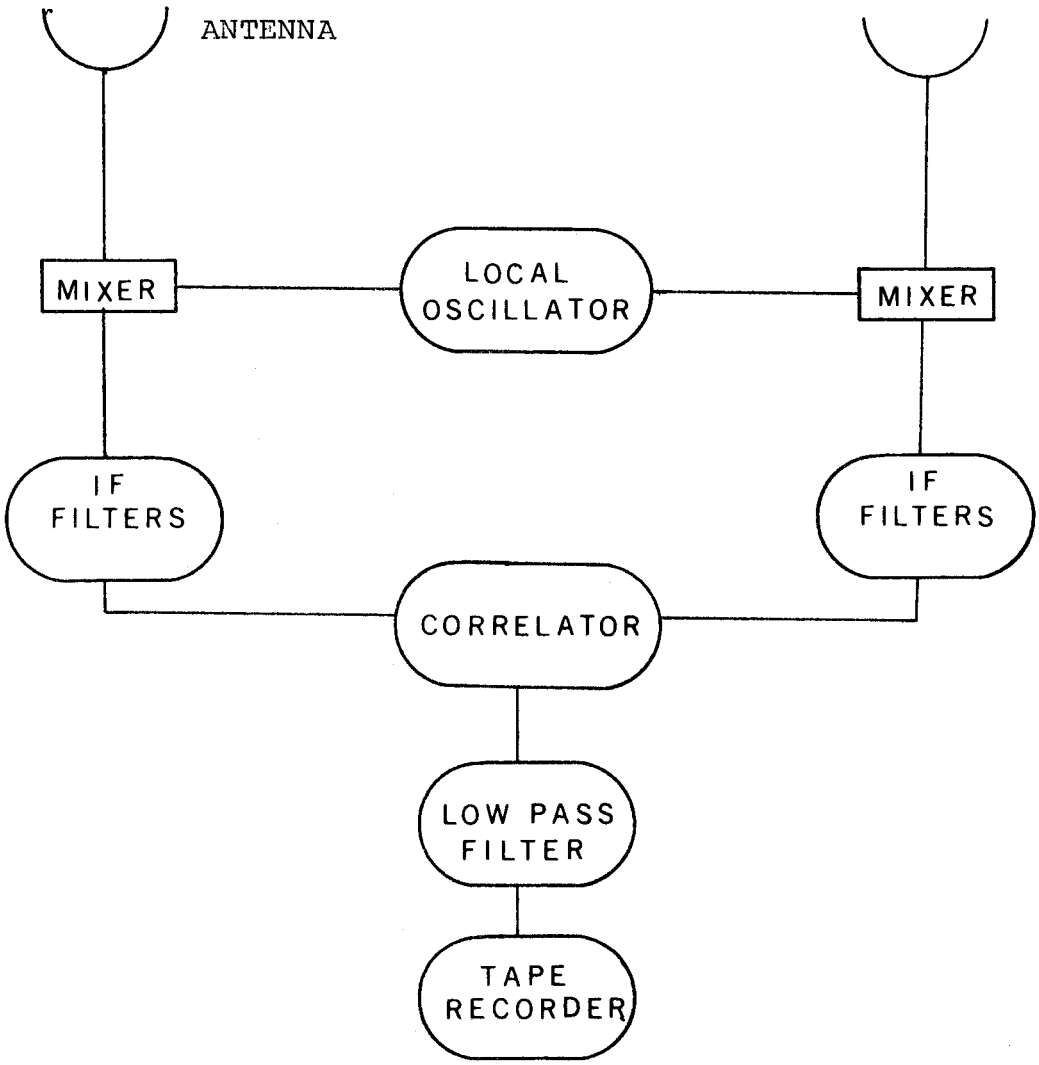

FIGURE 2-1. Block diagram of interferometer logic

Part of the IF signal is split and divided into 47 narrow bandpasses by the use of filters. Each of these narrow bandpasses is then correlated and produces what is called a "narrowband channel." At any given time, a maximum of 47 narrowband channels and one broadband channel could be recorded. The characteristics of the filters are as follows. The twenty-four 1 kHz filters (actually 24 pairs of matched filters, one for each antenna) have a nominal center frequency ranging from 9.965 MHz to 10.011 MHz and are spaced 2 kHz apart. The half-power width is 1 kHz and the true center frequency is within 0.1 kHz of the nominal frequency center. The forty-eight 4 kHz filters range from 9.812 MHz to 10.188 MHz and are spaced 8 kHz apart. The half-power width and nominal center frequency tolerance are 4 kHz and 0.1 kHz respectively. During the March 1972 observations, only the 4 kHz filters were used and the remaining observations used all twenty-four 1 kHz filters and twenty-three 4 kHz filters.

Just before dividing the IF signal into the various channels, there is an IF amplifier with automatic gain control capability. Assuming that the receiver temperature is constant and the antenna temperature is always a small fraction of the receiver temperature, it is desirable to use AGC in order to minimize gain variations. The typical

receiver temperature is 80° K, and assuming an aperture efficiency of 0.5, a 10 f.u. source will produce a 1° K antenna temperature. The observed dust clouds contain no continuum sources greater than 0.2 f.u. The HI emission brightness temperature may be comparable to 80° K; however, it is confined to a bandwidth narrow compared to 5 MHz. Based upon these facts, use of the AGC should not introduce any systematic errors greater than 1%, and accordingly AGC was used throughout the interferometer observations.

Based upon the experience of others (Greisen 1972; Bieging 1973), it was decided that narrowband channel calibration could best be performed by injecting correlated noise into the front end receiver of each antenna. In this manner one has an absorption-free source which could be turned on or off at will. On the whole this was a satisfactory method for calibrating the narrowband channels despite some difficulties due to the detector characteristics of the narrowband channels. A more detailed discussion is given under the section about calibrations.

OBSERVING PROGRAM

In this section a description is given of how the observations were carried out. Table 2-2 gives a chronological summary of the observations. The major purpose of the March 1972 observations was to determine whether or not the proposed observations would be feasible. The conflicting requirements to cover a wide velocity range but still achieve good velocity resolution were best balanced by using the 4 kHz filters. Based upon the size of the dust clouds, it was known that the shortest spacing would be important, but the longest spacings needed would depend upon the amount of small scale structure,and this was not known.

The March 1972 observations showed there was appreciable visibility amplitude (10 f.u. for L134) at only the shortest spacings. At the 300 ft. EW spacing where the projected baseline varied from 240 to 430 wavelengths, the visibility amplitude was less than or close to the noise level of 0.5 f.u. Based upon the need of obtaining better signal to noise, maximum effort was made in September and November 1972 to obtain all the shortest spacings available where signals had already been detected. At the same time, some evaluation was needed as to whether the small visibility amplitude at the 300 ft. EW spacing indicated a true

TABLE 2-2 SUMMARY OF OBSERVATIONS

DATE	SPACING FT	OBJECT	VELOCITY COVERAGE KM/SEC (LSR)	VELOCITY RESOLUTION KM/SEC
March 2, 1972 to March 15, 1972	300 EW 200 EW 105 NS 200 NS	L134	-40 to +40	1
		L1495	-40 to +40	1
		L1517	-40 to +40	1
Sept. 8, 1972 to Sept. 21, 1972	200 EW 100 EW 105 N 100 E 105 N 100 W	L134	-3 to +7 -18 to +18	0.2 1
		L1495	+2 to +12 -13 to +23	0.2 1
		L1517	-13 to -3 -28 to +8	0.2 1
Nov. 1, 1972 to Nov. 15, 1972	200 NS 105 NS 105 N 200 E 105 N 200 W	SAME AS FOR SEPTEMBER 1972		
Dec. 26, 1973 to Jan. 1, 1974	SINGLE DISH	L134	-4 to +9 -60 to +65	0.13 1.3
		L1495	-6 to +14 -60 to +65	0.13 1.3
		L1517	-14 to +11 -60 to +65	0.13 1.3

lack of small scale structure or whether it was due to an instrumental limitation.

At this point a few comments upon the sensitivity of the interferometer to small scale structure is needed. A priori a reasonable model is for cold HI in the dust cloud to absorb radiation from background HI emission. It is apparent that for any fixed interferometer baseline, there is an optimal size dust cloud which will produce maximum visibility amplitude; if the cloud is too large, it will be resolved out, but if it is too small, the cloud produces no appreciable flux. A model was made using circular Gaussian sources with a peak temperature T. For any baseline u, there is an optimal source diameter d which will give maximum visibility amplitude. The results are shown in fig. 2-2. Based upon this model, the small visibility amplitude at the 300 ft. EW spacing is not entirely due to instrumental limitations, i.e. brightness temperature fluctuations with a reasonable spatial scale and amplitude could produce a visibility amplitude greater than the noise level. For example, a 5' diameter, 25° K source observed at a 350 wavelength spacing will have a visibility amplitude of 1.5 f.u., about 3 times the noise level. On the other hand, brightness temperature fluctuations with somewhat smaller scale or amplitude than the example just mentioned would

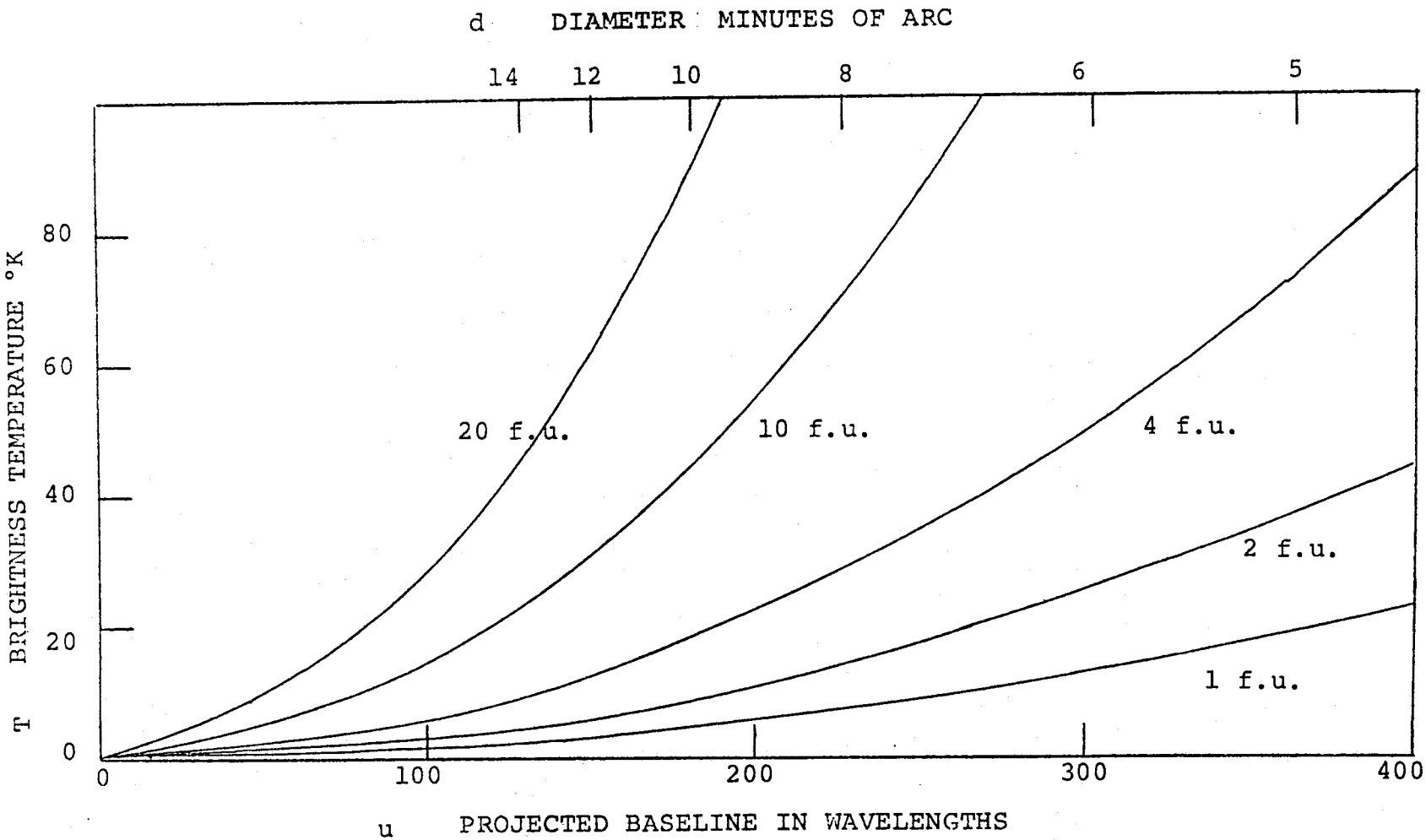

FIGURE 2-2. Contour map of the maximum visibility amplitude produced by circular Gaussian sources with a given peak brightness temperature (ordinate) and observed at a given projected baseline spacing (abscissa). For any baseline spacing, there is a corresponding radius at which the circular Gaussian source will produce maximum fringe amplitude; the diameter (half intensity point) is given at top of the figure.

not have been detected. The small visiblity amplitude at the 300 ft. spacing suggests there is no small scale structure, but obviously brightness temperature fluctuations with a sufficiently small scale or amplitude would be undetected.

For L134 and L1495 the data indicated that the fringe amplitude was greatest within a narrow velocity range coincident with molecular line velocities (see fig. 5-10, 4-7). This fact provided the necessary confidence to continue the observations after March 1972. At that time no molecular line known to the observer had been detected in L1517; therefore, it was assumed that the velocity of maximum fringe amplitude (-7 km/sec) was the dust cloud velocity. It was decided that the September and November 1972 observations would use 1 kHz filters to cover a velocity range of about 10 km/sec centered upon the suspected velocity of the cloud. The OVRO interferometer is capable of recording 47 narrow-band channels but only twenty-four 1 kHz filters were available; therefore, 4 kHz filters were used in the remaining 23 channels to provide greater redundancy and greater velocity coverage (about 40 km/sec).

A few points need to be mentioned about the filter arrangement. The 1 kHz filters are 1 kHz wide but center frequencies are spaced 2 kHz apart. Consequently if fine

velocity coverage is needed, one must make two sets of observations where the LO frequency differs by an odd number of kHz. Shifting by only one kHz can be a disadvantage for the following reason. Suppose there is one faulty channel which is not detected during the calibration procedure; if a shift of only 1 kHz is made, the complex visibilities measured by this one channel will be at two adjacent velocities and may be hard to distinguish from some real feature which is 2 kHz wide. During the course of observations there is no easy on-line procedure by which the performance of the narrowband channels may be checked. In order to circumvent the possibility of one faulty channel producing a gap in the velocity coverage, one can shift the local oscillator frequency by an even number of kHz. In this manner, the visibility at any velocity is measured by at least two physically distinct channels. The foregoing considerations would be important if one was attempting to measure narrow spectral lines as was the case for these observations. Accordingly during the interferometric observations, the LO frequency was shifted by 1 kHz, 3 kHz and 4 kHz higher than the lowest LO frequency. Such a technique produces greater problems during data reduction, but it enhances the reliability of the observations.

Typical (u,v) coverage for L134 and L1495 is shown in fig. 2-3 and 2-4. The coverage for L1517 is similar to L1495 since the two sources are at about the same declination. The corresponding synthesized beams (also called the dirty beam) are shown in fig. 2-5 and 2-6. If one wishes to map an area 30' by 30', then according to the sampling theorem, the (u,v) plane must be sampled by a rectangular grid of points spaced 115 wavelengths apart. In reality measurements by the interferometer cannot conform to such a sampling scheme. As will be discussed later, the greatest problem with the (u,v) sampling is the lack of measurements near the origin at spacings less than 130 wavelengths.

The usual observation routine was to track each dust cloud from -4^h to $+4^h$ hour angle except at some short spacings where one antenna blocked the view of the other antenna,resulting in a more limited hour angle coverage. The usual procedure was to calibrate and then observe the dust cloud making 4 separate 12 minute records. For each record the LO frequency was shifted in order to obtain the four shifts previously mentioned and to compensate for motion with respect to the local standard of rest. This cycle was repeated during the 8 hours that the dust cloud was tracked. A calibration consisted of observing an unresolved source in the sky with a well determined position

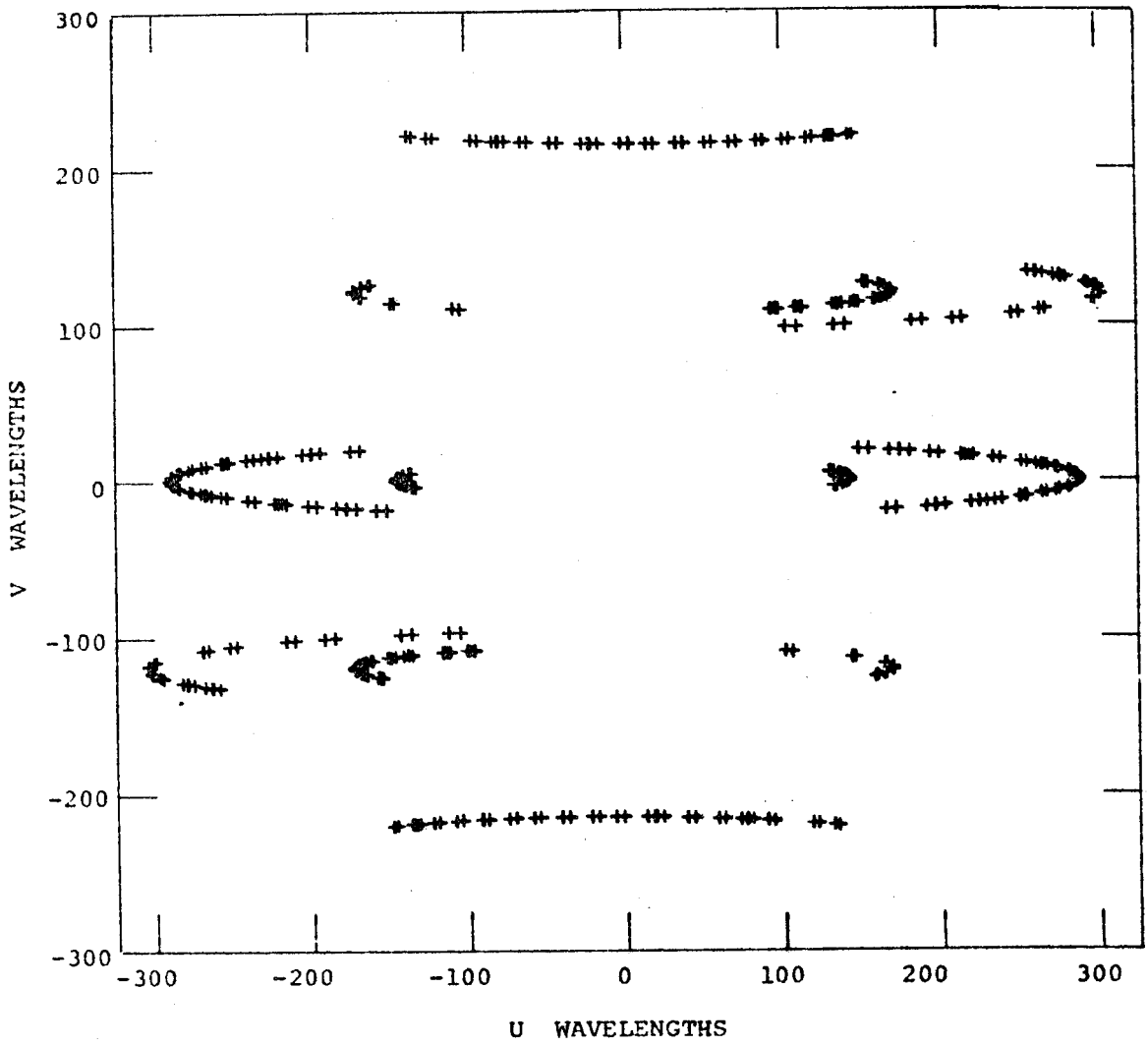

FIGURE 2-3. Typical sampling in (u,v) plane for L1134.

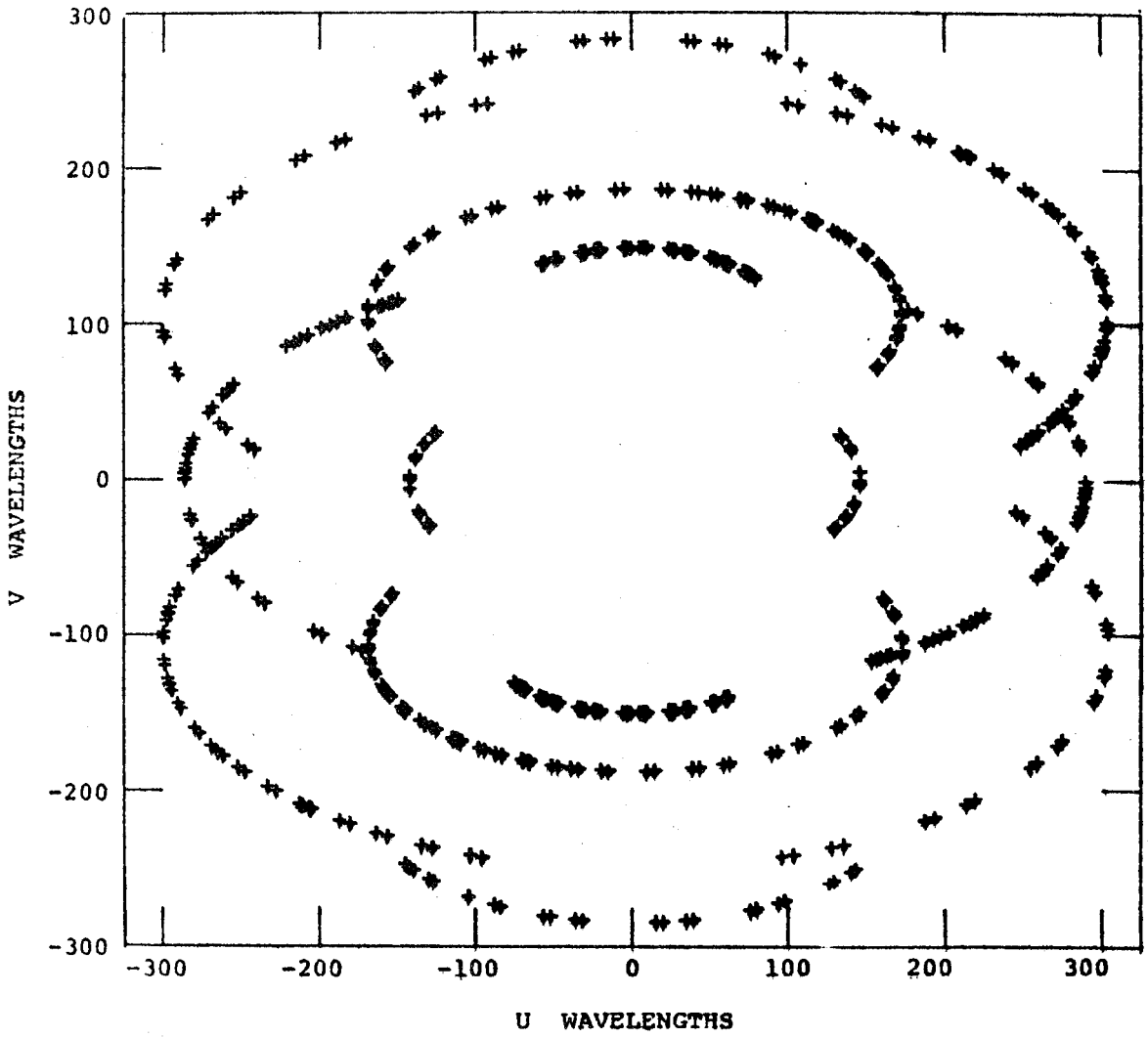

FIGURE 2-4. Typical sampling in (u,v) plane for L1495.

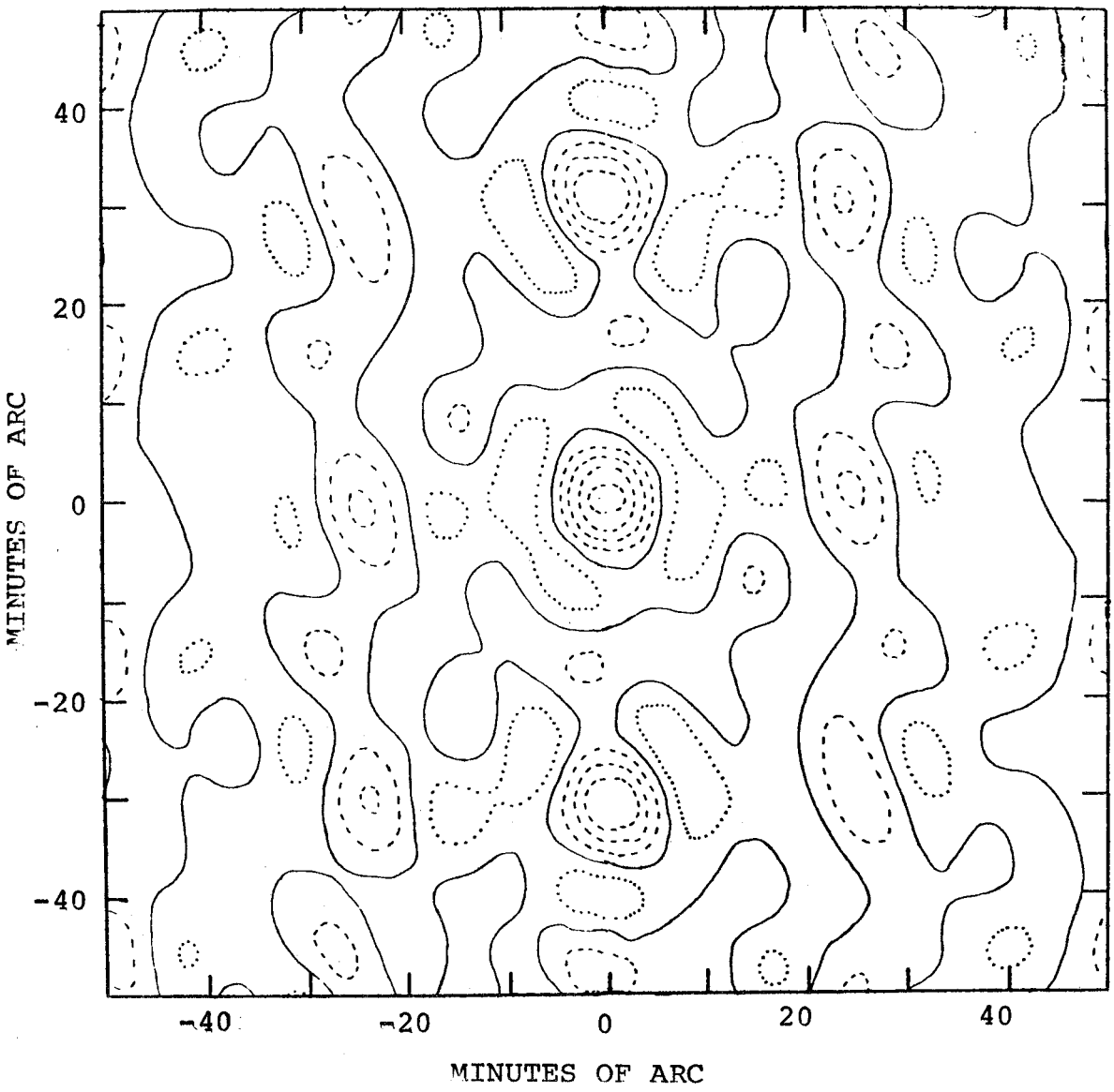

FIGURE 2-5. Synthesized beam for L134. Peak amplitude at center is normalized to 1.0. Contour interval is 0.2. Dashed contour lines are positive, dotted contour lines are negative, and solid line is the zero contour line.

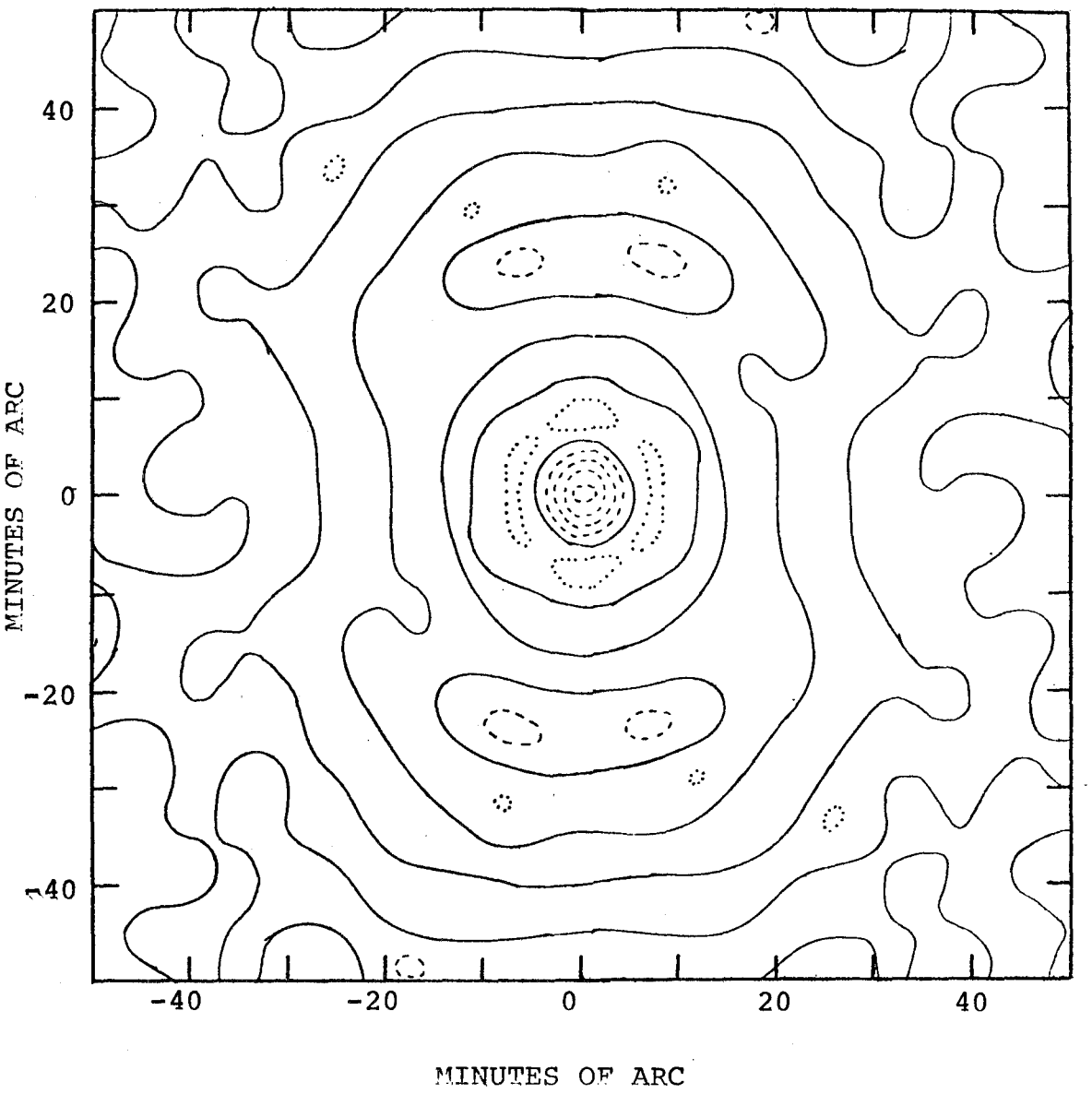

FIGURE 2-6. Synthesized beam for L1495. Peak amplitude at center is normalized to 1.0. Contour interval is 0.2. Dashed contour lines are positive, dotted contour lines are negative, and solid line is the zero contour line.

and flux, and observing a noise diode to determine the phase and amplitude of each narrowband channel relative to the broadband. This was necessary because continuum sources in the sky are not free from 21 cm absorption and consequently cannot be easily used to calibrate the narrowband channels.

In December 1973 single dish observations with a 130 ft. diameter antenna and a 100 channel autocorrelator were made for the three dust clouds. These observations were necessary to obtain zero spacing information and very short spacing information not available from the interferometric data. The hydrogen line emission profile was obtained on a grid of points about 2° 20' on a side centered upon the dust cloud. The spacing of points within the inner 1 square degree was 10' and in the outer regions about 20'. Preceding and following observations of each dust cloud, the telescope was pointed at a mountain to calibrate the bandpass shape. The baseline level was determined by making observations with a 625 kHz bandpass and assuming there was no significant hydrogen emission where the spectrum was flat at high and low velocities with respect to the local standard of rest. A 62.5 kHz bandwidth was used to measure the hydrogen emission profile at the suspected dust cloud velocity.

DATA REDUCTION AND CALIBRATION

A rough outline of the data reduction routine is shown as a block diagram in fig. 2-7. The following section provides a sketchy description of the reduction programs but brief digressions are made at some points where more detailed explanations are appropriate. Wherever a paragraph begins describing a particular block, the number of that block (see fig. 2-7) is placed at the beginning of the paragraph.

(1) The tape inspection program serves merely to check that the data are properly recorded on tape. For example, tape parity errors are detected. No actual data reduction is done at this stage.

(2) The phase-frequency correction and baseline are determined from special sets of observations made explicitly for such purposes. The phase-frequency correction is necessary in order that phase shifts produced by changing the local oscillator frequency can be calculated.

(3) After the phase-frequency correction and baseline are determined, the data on the dust clouds and calibrators are analyzed to produce raw flux and phase measurements.

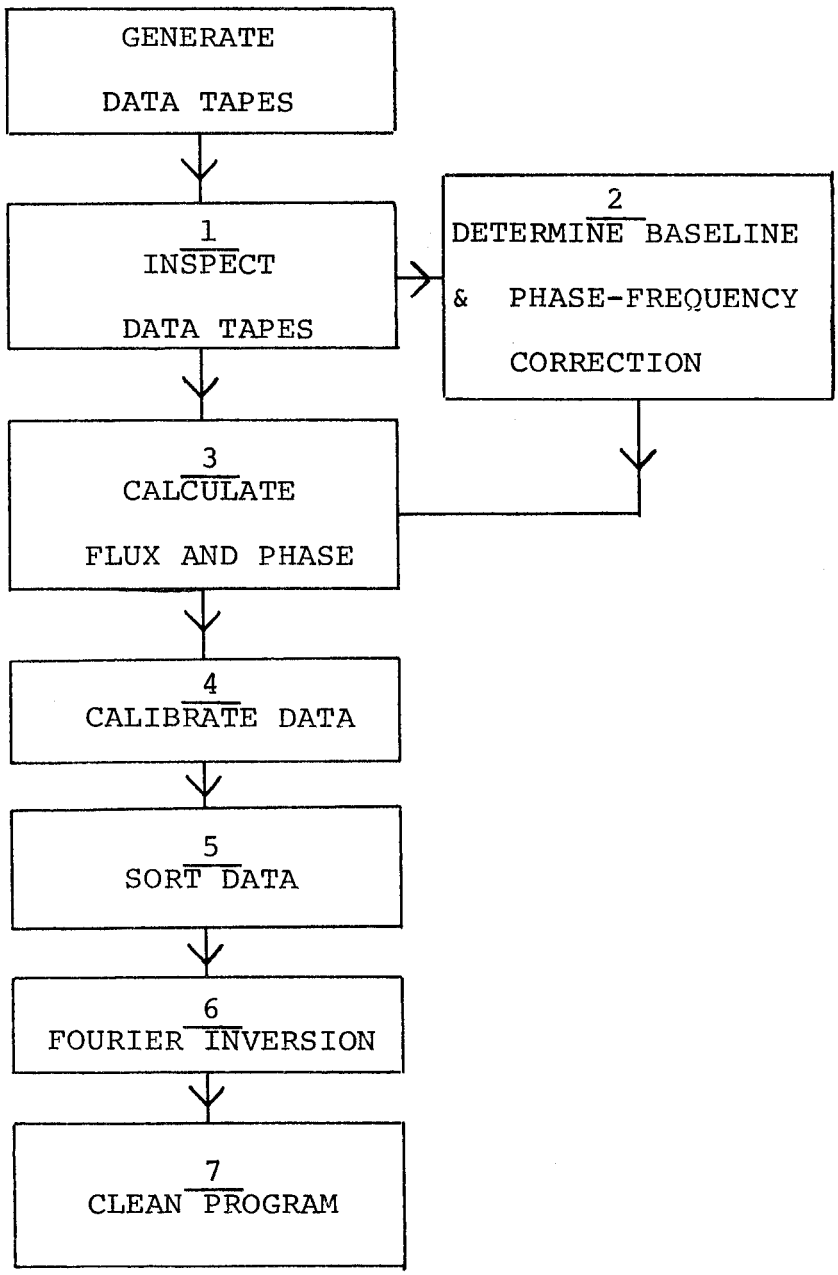

FIGURE 2-7. Block diagram of interferometer data reduction routine. See text for details.

Because calibrators are unresolved sources with known positions and fluxes, their raw flux and phase measurements provide direct instrumental gain and phase calibration.

(4) The calibration is best considered in two parts, calibration of the broadband channel and calibration of the narrowband channels relative to the broadband channel. The broadband channel is easily calibrated from periodic observations of the calibrators. The system gain and phase stability are dependent upon many factors, e.g. the sun rising or setting, temperature stability in the box housing the front end receiver, etc. Over a 24 hour period, the instrumental phase normally did not vary by over 0.1 lobes nor did the gain change by more than 10%. By observing calibrators every hour or so, the phase could be calibrated to within 0.01 lobes and the gain within 2%. These uncertainties are much smaller than the statistical noise in the narrowband channels and have comparatively little effect on the noise level in the final brightness temperature maps.

Narrowband calibration was performed by pointing the two antennas in directions differing by at least two degrees and observing the noise diode. In such a case, the noise diode is the only source of correlated noise. Because the noise diode has a flat spectrum, the narrowband

amplitude may be directly calibrated against the broadband amplitude. The narrowband phases do not necessarily equal the broadband phase since the cables connecting the noise diode to the antennas differ in length and phase-frequency effects may be important. Whenever the noise diode was observed, the total electrical path length from the noise diode to the correlator was equalized between the two interferometer elements. In such a case, narrowband and wideband phases must be equal. The narrowband phase calibration determined by the noise diode observations was checked by observing sources in the sky and no inconsistencies were found.

Unfortunately the narrowband-to-wideband amplitude ratio often differed in a systematic manner between various observations of the noise diode. In the worst case discrepancies up to 15% were observed but 7% was more typical. The problem is demonstrated by the following data. Three noise diode observations were made with antennas skewed but pointing in the same general direction; however, the local oscillator was shifted by -70 kHz for the third observation. In fig. 2-8, dots show the relative narrowband-to-broadband gain as determined by the second noise diode observation relative to the first observation and plus signs show the same information for the third noise

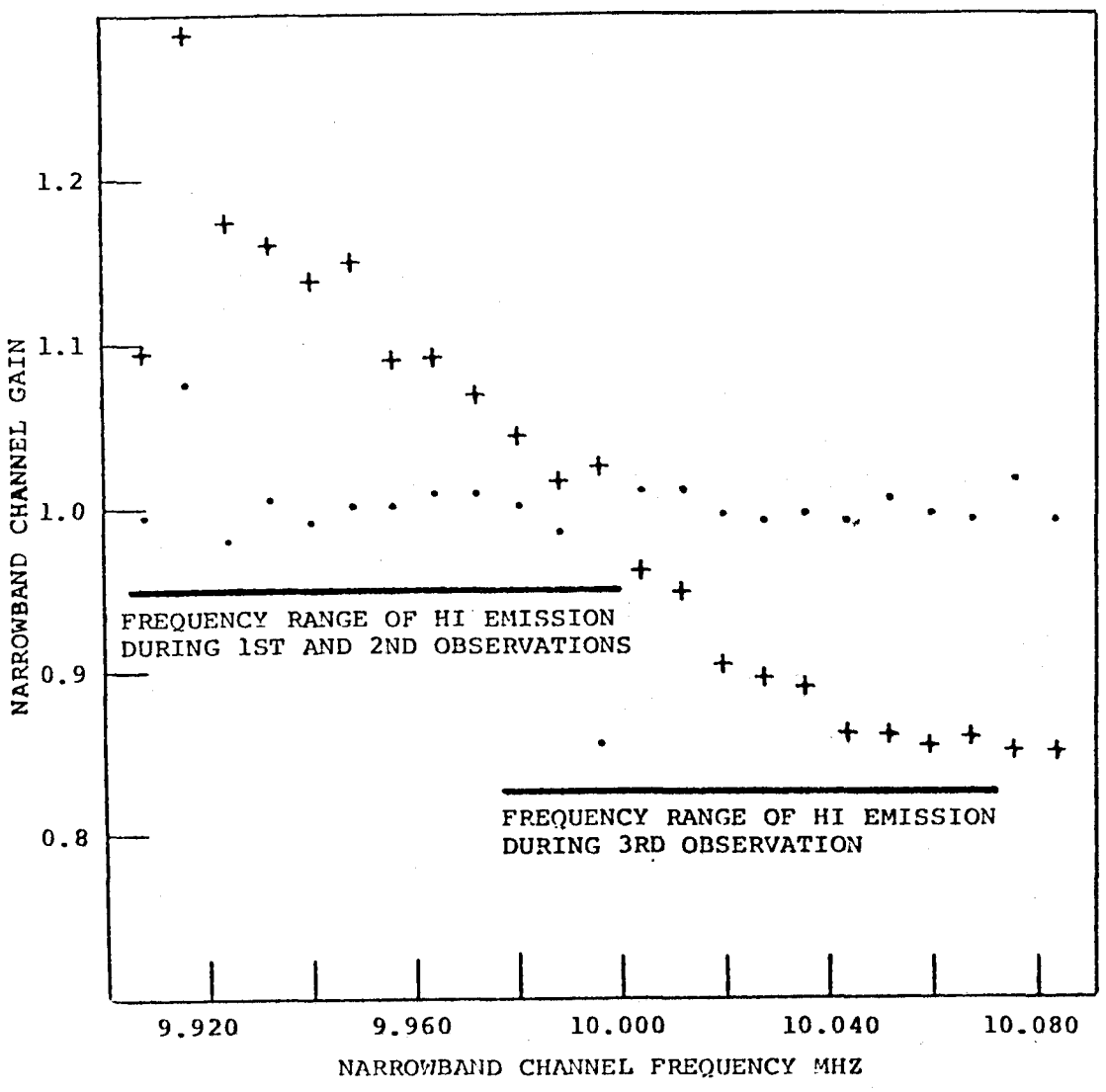

FIGURE 2-8. Influence of HI emission on narrowband channel gain. The data comes from 3 noise diode observations. Ordinate is relative narrowband-to-broadband gain of the 2nd observation (dots) or the 3rd observations (plus signs) divided by relative narrowband-to-broadband gain of the 1st observation.

diode observation relative to the first observation.

Except for two bad channels, the dots indicate that the narrowband to broadband gain remained constant between the first and second observations; the total power from 21 cm emission did not change between the two observations. On the third noise diode observation, a pronounced narrowband gain change has occurred because the HI emission was received in channels different than during the first two observations. Greater total power level in a channel causes a gain decrease. This problem is especially bad when studying HI absorption against continuum sources because channels where absorption would be expected are the same channels where the gain is reduced.

The most likely explanation is as follows. The total power going into the correlator comes from two sources, the receiver and the antenna which contribute T_r and T_a degrees respectively. T_r is frequency independent and around 80° K. T_a comes mainly from 21 cm emission and is frequency dependent and may vary from 0° K to 80° K. It is apparent that the narrowband channels may receive substantially different total powers depending upon the 21 cm emission strength. It has already been noticed that the narrowband channels are not true square law detectors (Bieging 1973). Consequently

one might expect systematic differences in the narrowband calibration dependent upon the 21 cm brightness in the direction at which the antennas were pointed when the noise diode was observed.

Fortunately most of the noise diode observations were performed by driving the two antennas a few degrees apart in opposite directions from the dust cloud being observed. In so far as the HI emission does not change substantially within a few degrees of the dust cloud, the narrowband calibrations will not suffer from systematic errors due to 21 cm emission. By eliminating noise diode observations not taken in the vicinity of the dust cloud being observed, it is believed systematic errors in the narrowband calibration will be insignificant. The final calibrations indicate the relative narrowband to broadband amplitude is calibrated to within 2% and the phase difference to within 0.005 lobes.

(5) The sorting program's major function was to reorder the narrowband data such that all flux and phase measurements at the same velocity are assembled together. All velocities in this paper are with respect to the local standard of rest. At the same time bad channels were eliminated. A narrowband channel was considered bad if

over a few hours time its gain or phase relative to the broadband changed by more than 5% or 0.01 lobes respectively.

(6) Fourier inversion of the visibility was done by a straightforward calculation and the result is called the dirty map. Let A_k and Φ_k be the amplitude and phase measured at (u_k, v_k). The dirty map is equal to

$$\sum_k W_k A_k e^{i\Phi_k} e^{i2\pi(u_k x + v_k y)}$$

where W_k is a weighting factor. Usually the dirty map is hard to interpret due to the sidelobe structure in the dirty beam.

(7) The clean program attempts to eliminate the effects of the dirty beam sidelobes. The dirty map is deconvolved by the dirty beam into a set of point sources. The point sources are then convolved with the clean beam which can be any smooth function about the same size as the dirty beam primary lobe. In this work the clean beams were circular Gaussians. The final map is called the clean map. The appendix gives a more detailed description on how the visibility is transformed into a clean map.

III. L134

L134 GENERAL DESCRIPTION

L134 is an inconspicuous dust cloud situated at a relatively high 35° galactic latitude. Fig. 3-1 is a photograph of L134 taken from the blue Palomar Sky Survey print. The amount of absorption produced by the dust cloud is considerable since no stars are visible through the central part of the dust cloud on the red sensitive print. It is interesting to note that on the red print, L134 appears to be a faint emission nebula (Lynds 1965). The source of this light is not apparent,but van den Berg (1966) speculated that high galactic latitude reflection nebulae may be illuminated by scattered light from the galactic plane.

A direct unambiguous measurement of the distance to L134 is not available; however, there are several indirect arguments which, taken together, provide a rough estimate of the distance. The 35° galactic latitude of L134 is unusually high. A catalogue of dark nebulae compiled by Lynds (1962) has 1802 entries out of which 13 refer to clouds more than 30° from the galactic plane. The important point is that these high galactic latitude dust clouds

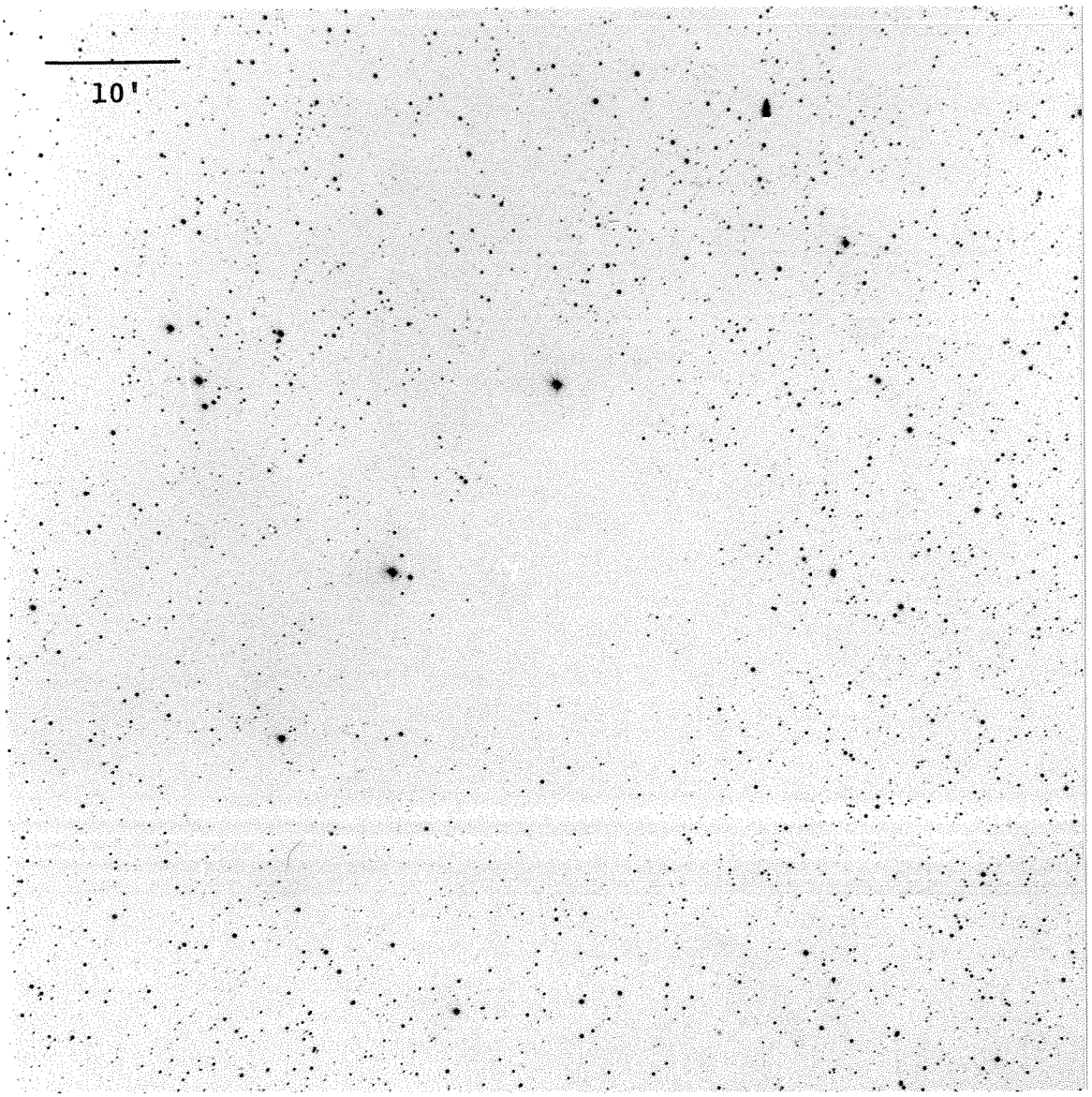

FIGURE 3-1. Photograph of L134 taken from the blue Palomar Sky Survey print. North is on top and east is on the left. Field of view is centered upon the adopted position of L134 given in Table 2-1. Scale is indicated in upper left corner.

do not appear to be randomly distributed in galactic longitude but concentrate toward the two most prominent HI complexes which extend to high positive and negative galactic latitudes, the Scorpius-Ophiuchus complex and the Orion-Taurus-Perseus complex respectively. This suggests that high galactic latitude dust clouds are not nearby objects (a few tens of parsecs) but are more distant objects (around 100 pc) associated with HI complexes that extend well off the galactic plane.

Assuming L134 is associated with the Scorpius-Ophiuchus HI complex, its distance will be about the same as the HI complex. In an early 21 cm survey, Mc Gee et al. (1963) set the distance to this complex as 140 pc based upon a lack of HI emission in the direction of a HII region formed by ξ Ophiuchus. Bok (1956) has studied a large dust cloud near ρ Ophiuchus and gives about the same distance estimate. Finally the Scorpio-Centaurus OB association which lies in the same direction is about 170 pc away (Blaauw 1964). It appears that toward the galactic center there is a large complex of hydrogen, dust and early type stars that extend well above the galactic plane. L134 is probably associated with this complex. Because L134 is seen in absorption against background 21 cm emission, it certainly cannot be more distant than the Scorpio-Ophiuchus

HI complex which is responsible for most of the HI emission. This indicates L134 is around 170 pc or somewhat less.

An alternate estimate of the distance can be obtained by doing star counts. Inspection of the Palomar Sky Survey prints shows that the inner part of L134 is essentially opaque down to the limiting plate magnitude. One can ask the question at what distance could an opaque dust cloud be placed before foreground stars appear in substantial numbers. Define the following quantities:

$N(m,r)$	number of stars per unit solid angle down to apparent magnitude m and within distance r of the sun
$\Phi(M,z)$	number of stars per unit magnitude per unit volume at absolute magnitude M and distance z above the galactic plane
A	magnitudes of absorption per unit distance
b	galactic latitude

$N(m,r)$ can be calculated by the following equation.

$$N(m,r) = \int_0^r dx\, x^2 \int_{-\infty}^{m\, -5\log(x)\, -Ax\, +\, 5} dM\, \Phi(M,\, x \sin b)$$

Data for $\Phi(M,z)$ were taken from Allen (1973) and the above integral was calculated numerically. The expected number of foreground stars in front of L134 as a function of distance was determined. At 170 pc about 30 stars (down

to the 20th magnitude) could be expected within an area $3\ 10^{-5}$ sterad corresponding to the essentially opaque part of L134. Taken at face value, the star count calculation would place L134 not much farther than 100 pc; however, the uncertainties are sufficiently great that a distance up to 170 pc could not really be considered as being inconsistent.

A minimum distance limit could be placed on L134 if a foreground star can be found. HD 141269 lies on the north edge of the dust cloud (see fig. 3-1, bright star 10' north of center). Let us assume a star at that position lying in back of L134 would be absorbed by at least 3 magnitudes. HD 141269, a G0 star, was compared with HD 141247, a F9V star about 1° away. As near as the eye can judge, both stars appear to be equally bright on the red and blue Palomar Sky Survey prints. Any G0 star suffering 3 magnitudes of absorption would appear noticeably brighter on the red print than the blue print; therefore HD 141269 must lie in front of L134. A main sequence G0 star has an absolute magnitude around 4.4. The apparent magnitude of HD 141269 is around 8 so the star must be about 50 pc away and L134 must at least be that far. The foregoing argument is not conclusive but it is consistent with the idea that L134 is associated with the Scorpio-Ophiuchus HI and dust complex. The true distance to L134 is not well known, but an adopted

distance of 170 pc is reasonable.

L134 RESULTS

In this section the basic data on L134 are presented, but interpretation of the observations is deferred to the next section. The interferometer data indicates L134 may consist of two velocity components. Fig. 5-10 (page 102) shows data from the 100 ft. EW spacing. The strongest component at 2.8 km/sec coincides with the velocity at which OH and H_2CO have been detected. Fourier inversion of the visibility for this component produces a clean map which is superposed on a photograph of L134 in fig. 3-2. It is difficult to define very precisely the limits of the dust cloud, but the temperature depression seems to agree well in size and position with the dust cloud. The second component is near 0.7 km/sec, and a clean map of its structure is shown in fig. 3-3.

Figures 3-4 through 3-6 show the 115 GHz transition of CO (J = 1 to J = 0) of CO taken at various positions around L134. The CO observations were provided by N. Scoville. A frequency switching technique was used to calibrate the bandpass shape. The local oscillator was shifted back and forth by 50 MHz and the power from the

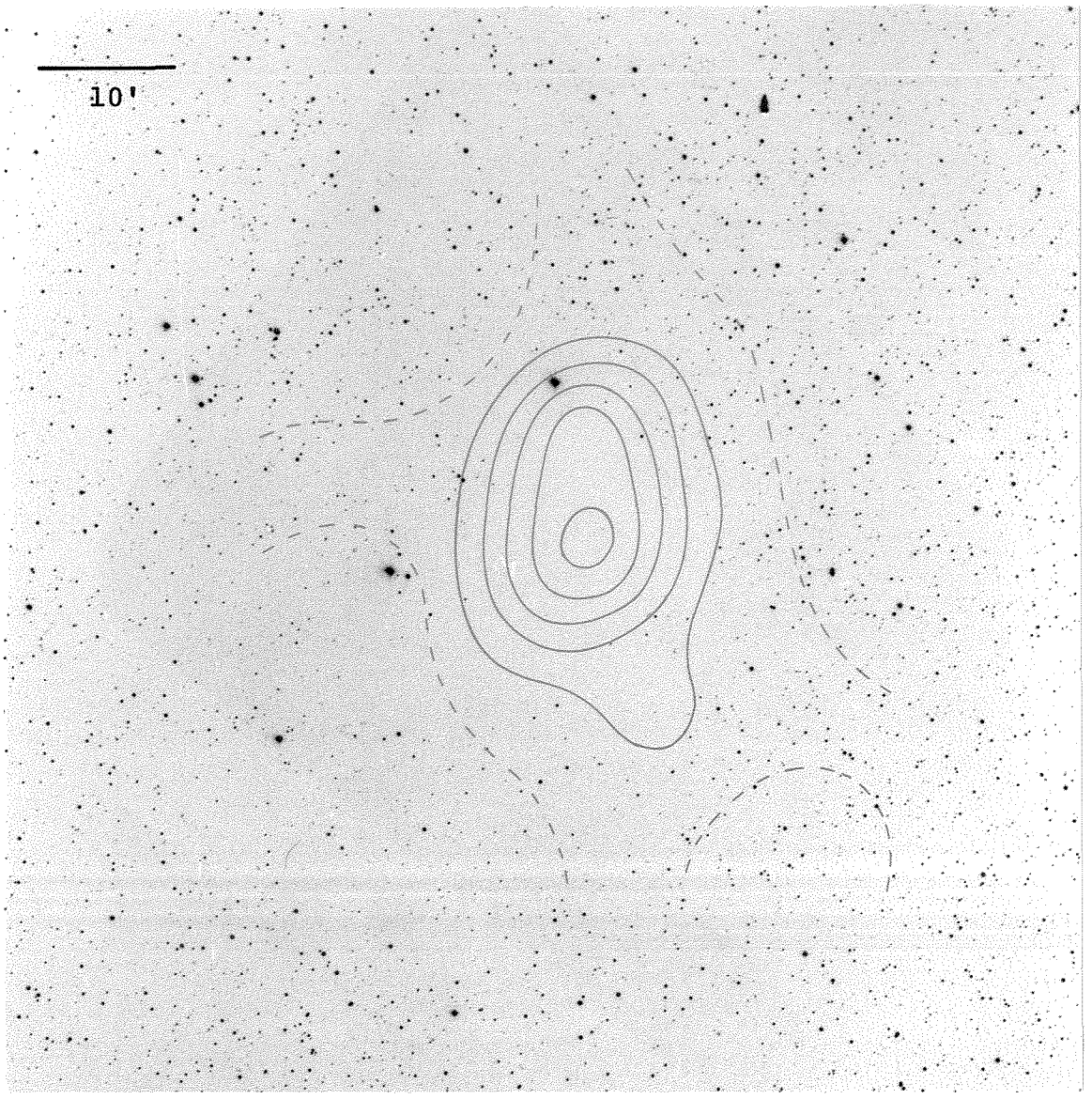

FIGURE 3-2. Contour map of brightness temperature from interferometer observations of L134 at 2.43 km/sec. Contour interval is 4° K and synthesized beam diameter is 7'. Scale is indicated in upper left corner. Zero spacing information is missing; therefore, the dashed contour lines were set at 0° K for reference. The contour lines represent a 20° K drop in brightness temperature. No correction has been made for the antenna beam. Noise level is 1° K.

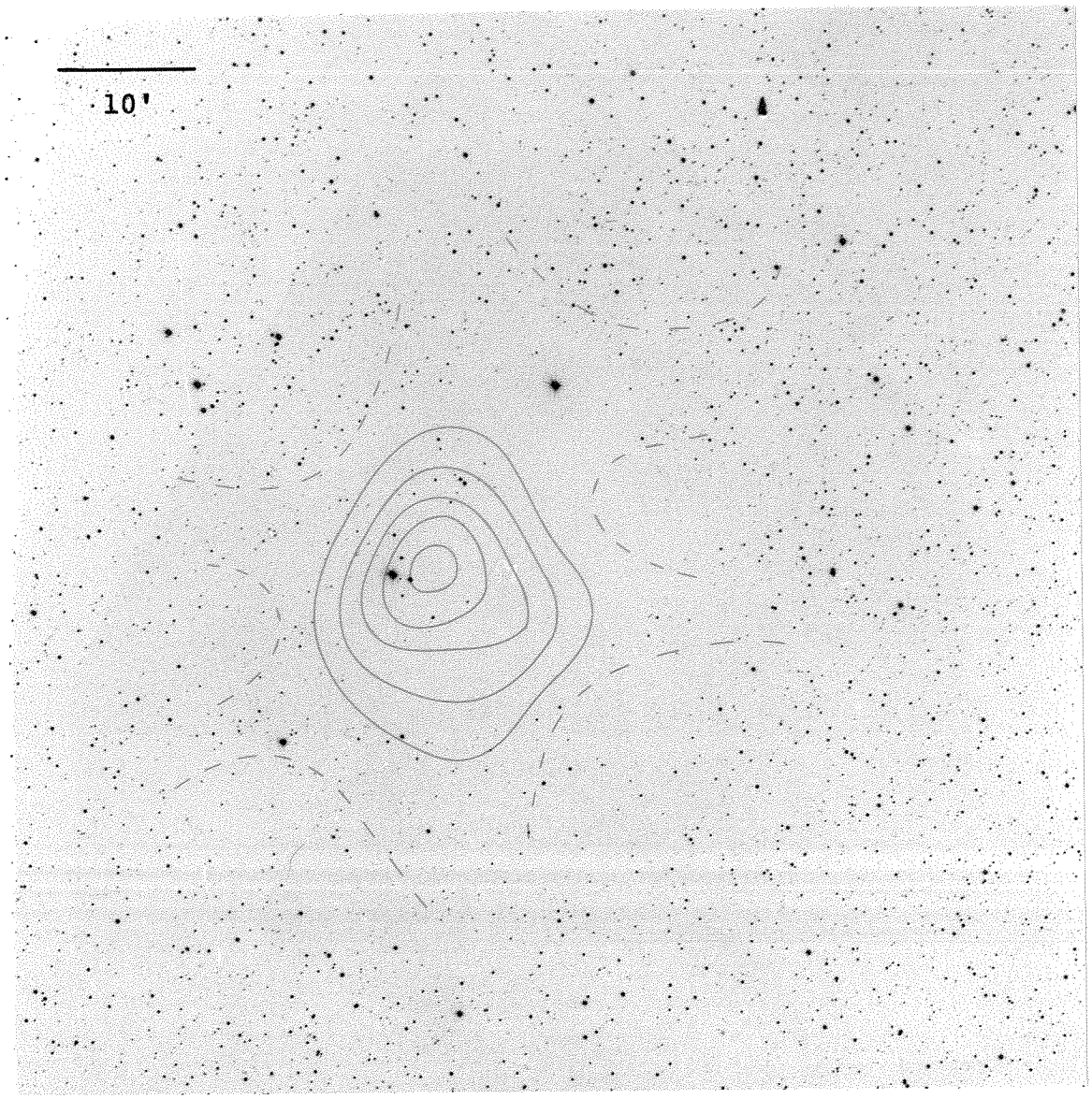

FIGURE 3-3. Contour map of brightness temperature from interferometer observations of L134 at 0.74 km/sec. Contour interval is 2° K and synthesized beam diameter is 7'. Scale is indicated in upper left corner. Zero spacing information is missing; therefore, the dashed contour lines were set at 0° K for reference. The contour lines represent a 10° K drop in the brightness temperature. No correction has been made for the antenna beam. Noise level is 1° K.

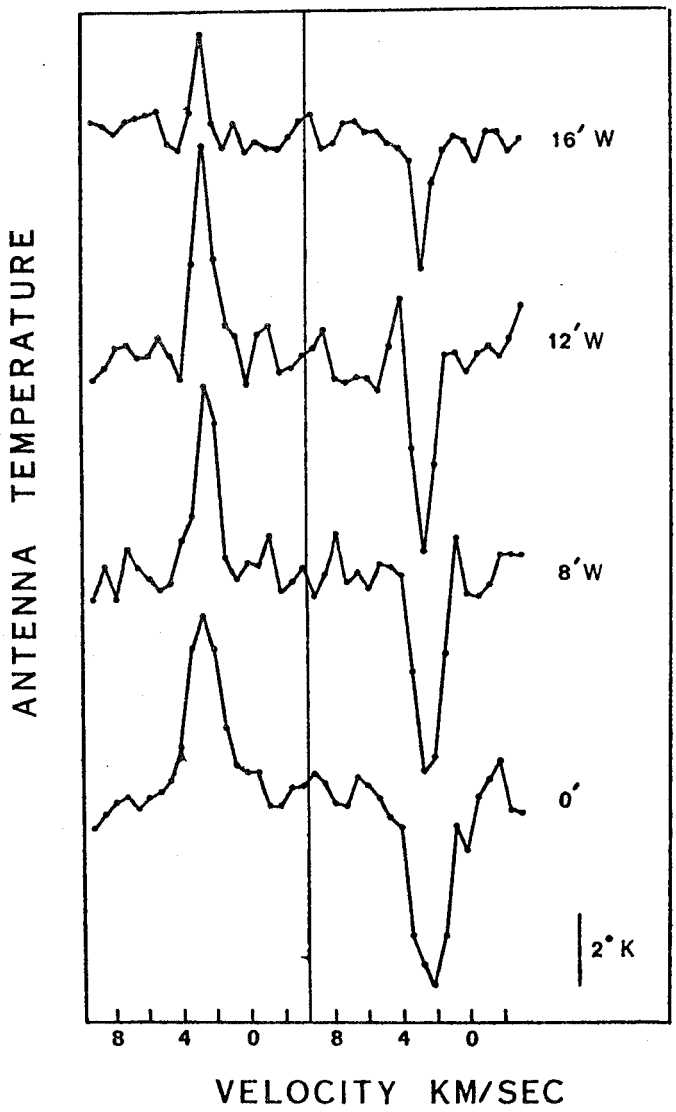

FIGURE 3-4 The CO 115 GHz emission profile at various positions near L134. A frequency switching technique was used so an emission line appears twice in one scan (see text for explanation). Numbers to the right of each scan indicates position in minutes of arc west of L134. Observations were provided by N. Scoville.

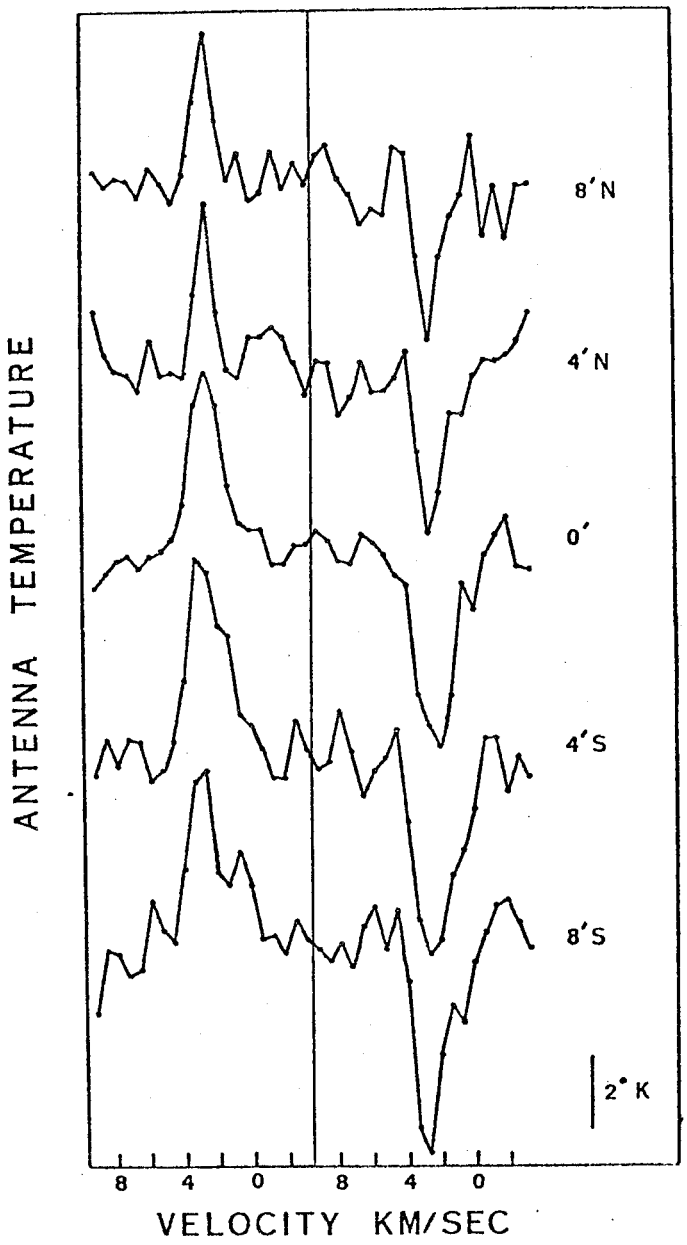

FIGURE 3-5. The CO 115 GHz emission profile at various positions near L134. A frequency switching technique was used so an emission line appears twice in one scan (see text for explanation). Numbers to the right of each scan indicates the position in minutes of arc north and south of L134. Observations were provided by N. Scoville.

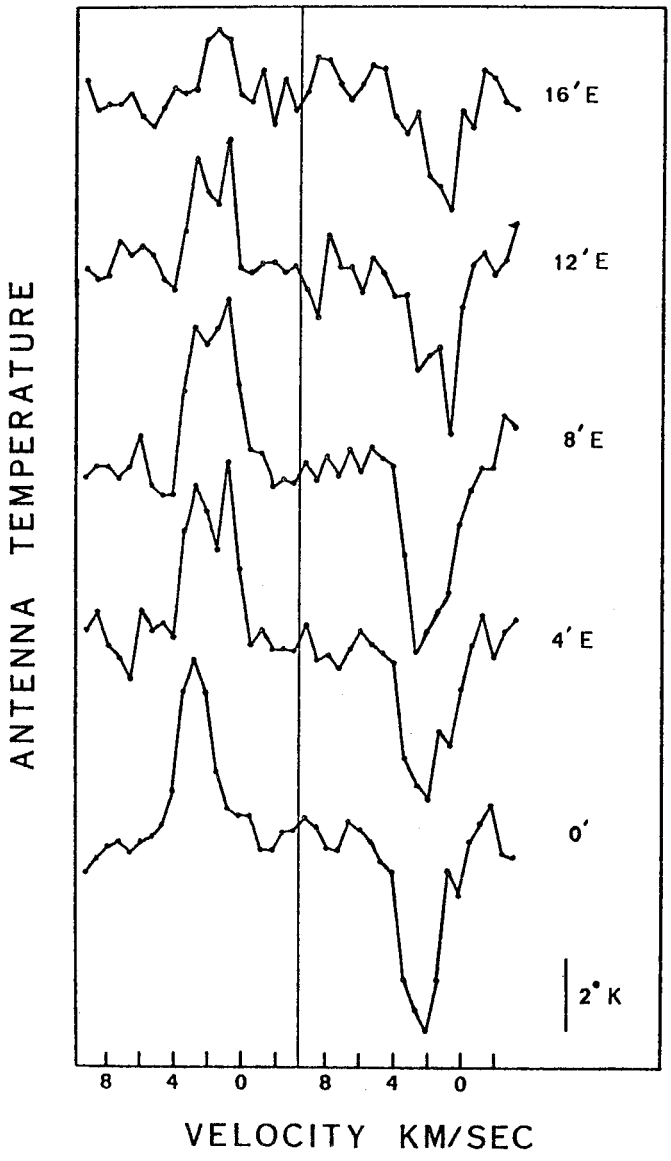

FIGURE 3-6. The CO 115 GHz emission profile at various positions near L134. A frequency switching technique was used so an emission line appears twice in one scan (see text for explanation). Numbers to the right of each scan indicates position in minutes of arc east of L134. Observations were provided by N. Scoville.

filters was differenced. Consequently an emission line appears twice in any scan but with opposite signs.

Single dish observations at 21 cm were made on L134 to determine if there might not exist a larger component which was resolved out by the interferometer. Fig. 3-7 shows the HI emission profile centered on L134. The 21 cm emission profile was also measured on a grid of about 80 points surrounding L134, and fig. 3-8 and 3-9 show the antenna temperature at 0.6 km/sec and 2.8 km/sec measured at the various grid points.

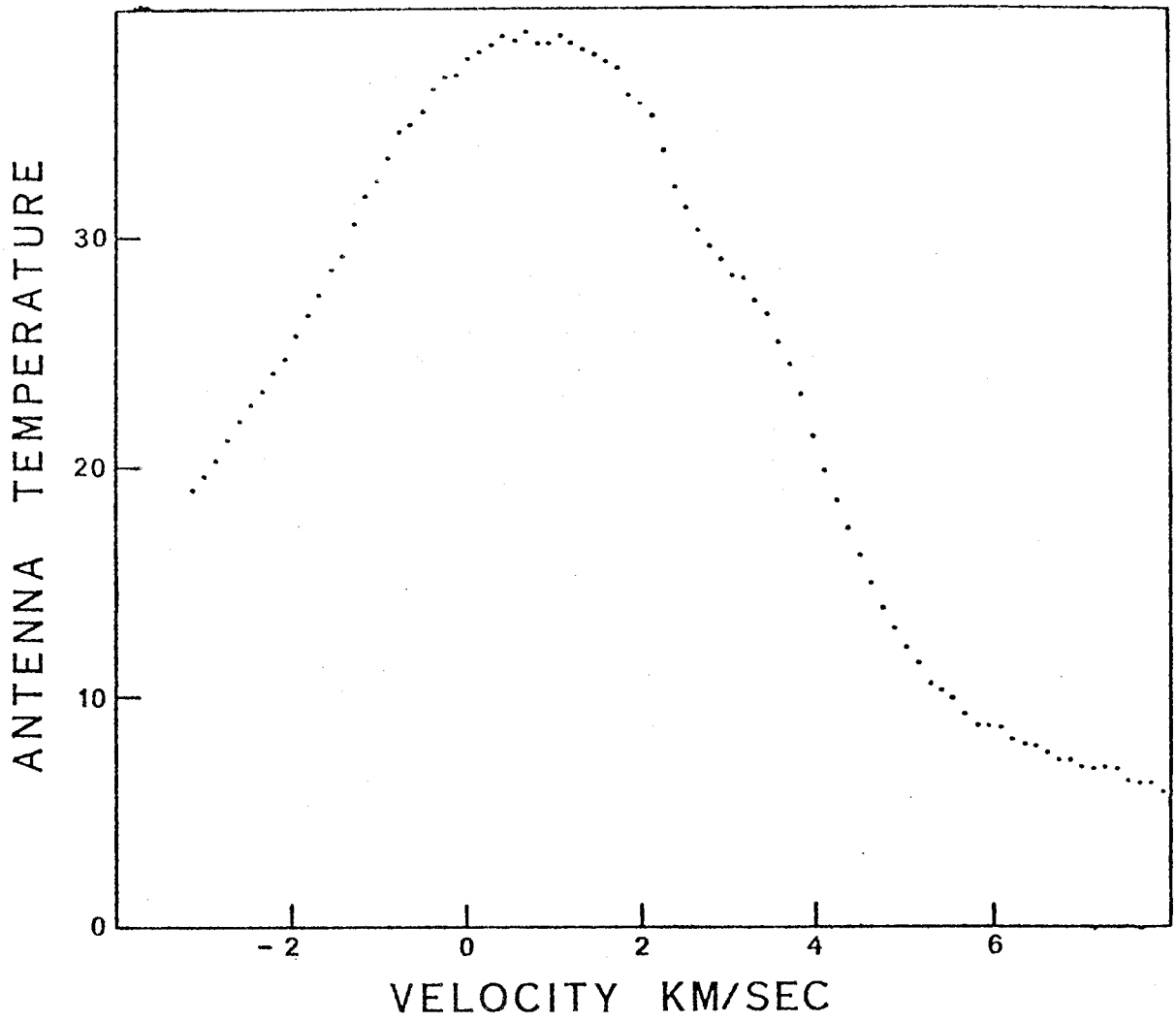

FIGURE 3-7 Hydrogen 21 cm emission profile centered upon L134. Antenna temperature is measured in degrees Kelvin.

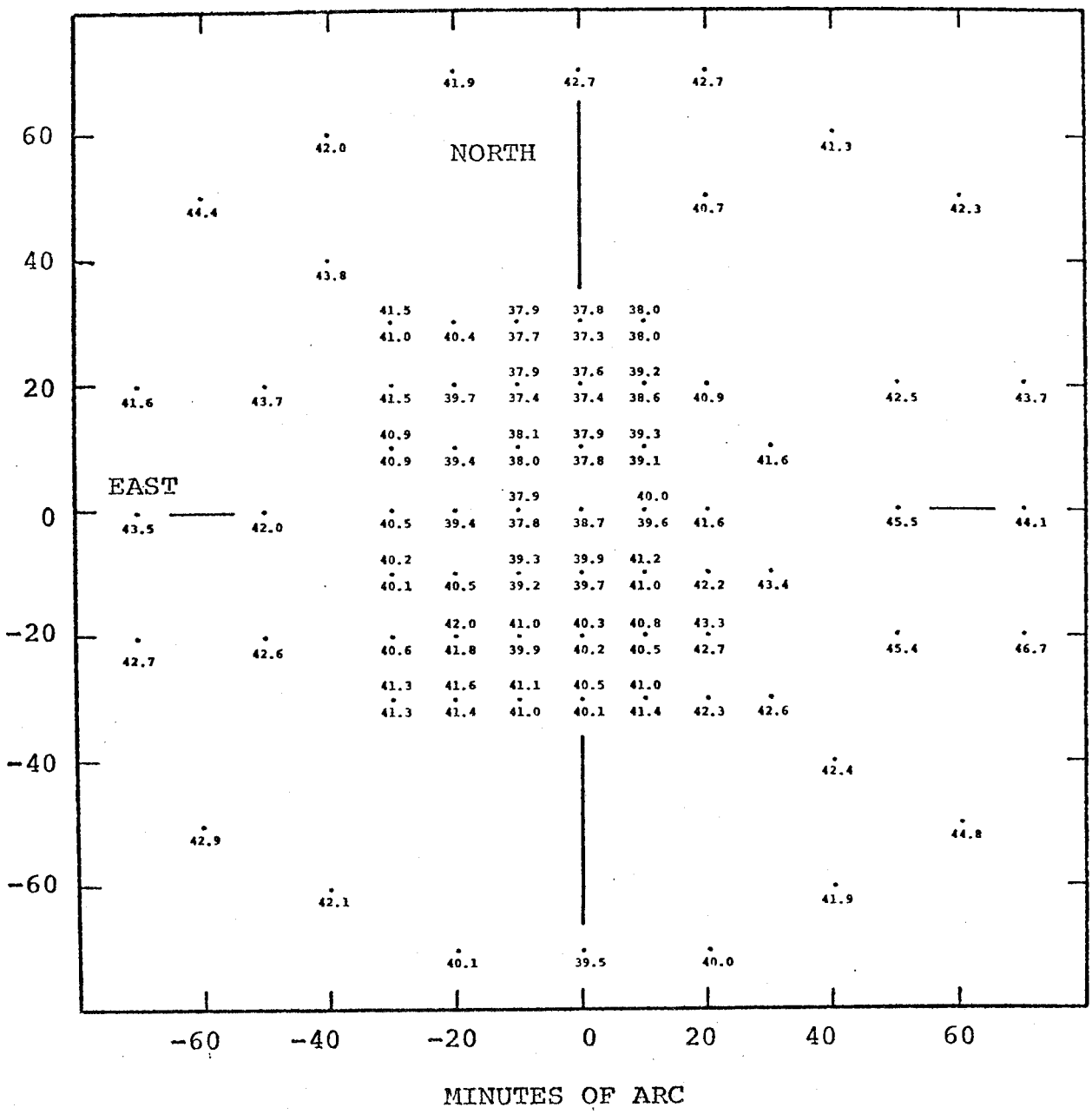

FIGURE 3-8. Antenna temperature as a function of position around L134 at 0.6 km/sec. The number by each dot is the antenna temperature in degrees Kelvin at that position. Two numbers at one position represent two independent measurements. Field of view is centered upon L134.

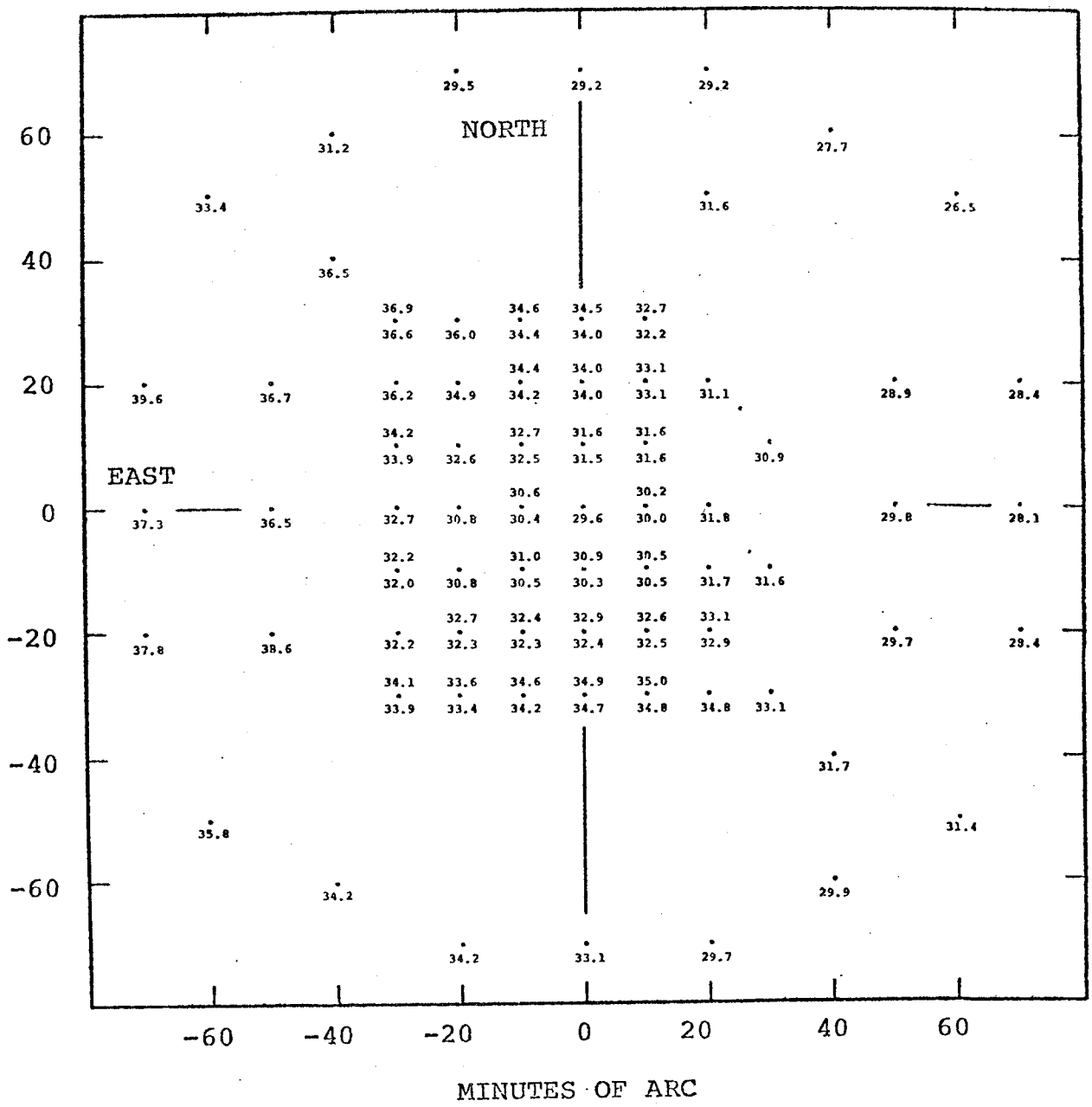

FIGURE 3-9 Antenna temperature as a function of position around L134 at 2.8 km/sec. The number by each dot is the antenna temperature in degrees Kelvin at that position. Two numbers at one position represent two independent measurements. Field of view is centered upon L134.

L134 DISCUSSION

(Dust Cloud Structure)

Prior to any attempt to interpret the data, the compatability of single dish and interferometer observations must be considered. The clean map reveals a brightness temperature depression of 20° K, and the question is what would such a feature look like using single dish observations. The clean map (fig. 3-2) was corrected for the 90 ft. antenna beam and then convolved with a 22' circular Gaussian beam (modeling the 130 ft. antenna beam). The resulting brightness temperature map was multiplied by 0.75 (the main beam efficiency of the 130 ft. antenna) to convert to an antenna temperature map. By subtracting this map from the observed antenna temperatures (fig. 3-9), effects due to the brightness depression in fig. 3-2 are removed. The resulting antenna temperature map is shown in fig. 3-10. Two conclusions may be drawn: (1) Single dish and interferometer observations are compatible. The predicted decrease of antenna temperature (4.6° K at maximum) matches the observed temperature decrease centered on L134 (fig. 3-9). (2) No large scale structure associated with L134 is apparent in fig. 3-10. The temperature fluctuations which remain are probably due to changes in the background brightness unassociated with L134. The evidence indicates that the interferometer observations give a fairly complete

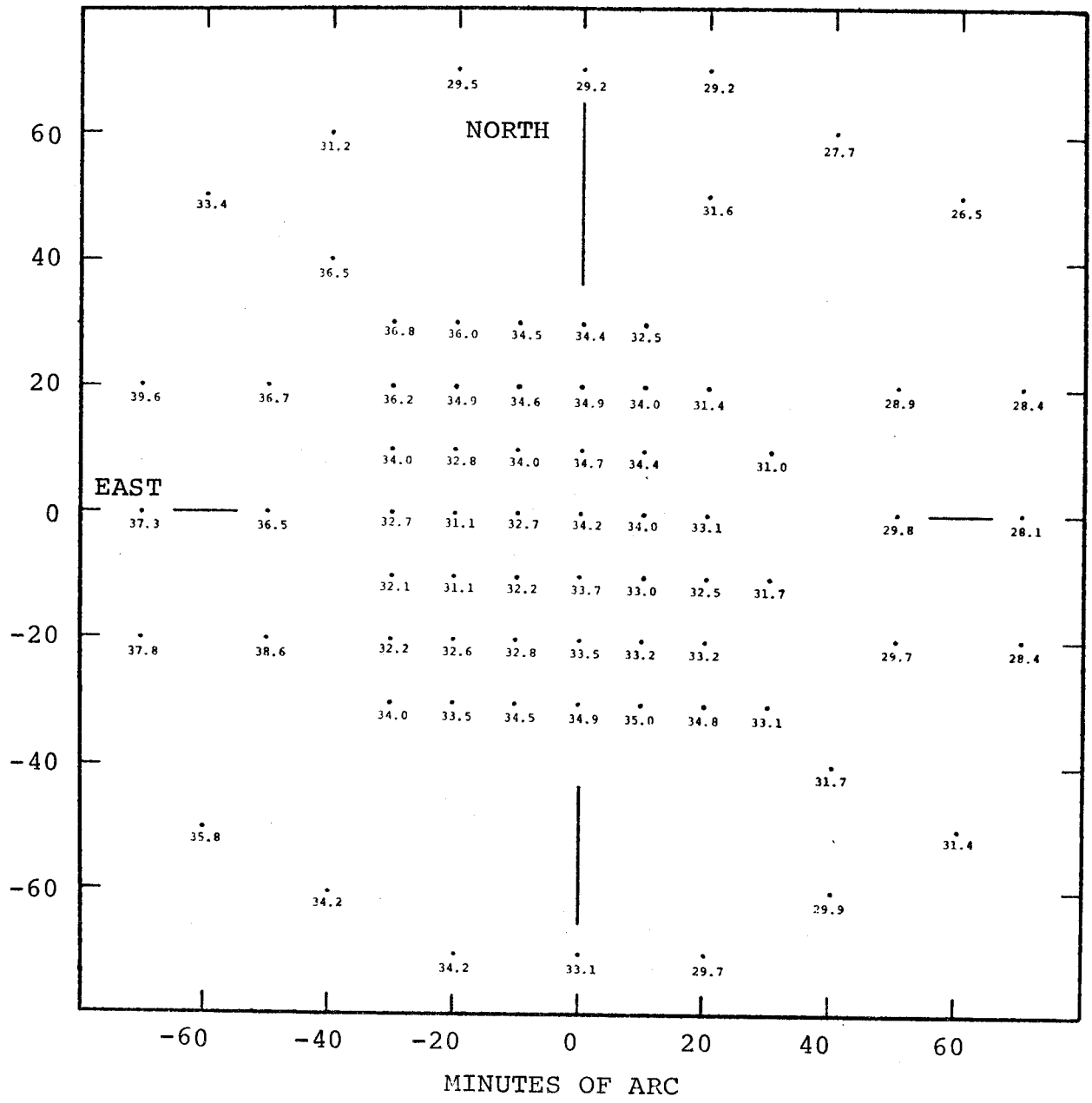

FIGURE 3-10. Corrected antenna temperature as a function of position around L134 at 2.8 km/sec. This map is the same as fig. 3-9 except effects due to the temperature depression in fig. 3-2 have been removed. The number by each dot is the antenna temperature in degrees Kelvin at that position. Field of view is centered upon L134.

picture of L134; or in other words, there is no extended component associated with L134 which would have been resolved out by the interferometer and gone undetected.

The lack of substructure is disappointing in the sense that the observations were partially motivated in the hope of detecting dust cloud fragmentation. It is possible that the two velocity components could be the result of fragmentation, and this will be discussed later. As far as each individual component is concerned, each appears to be a single cloud with no significant substructure. The temperature depression is tightly confined to the region where obscuration by dust is high. Such simple dust clouds are ideal for comparison with theoretical calculations which usually deal with an idealized model.

(Sancisi's Observations)

Extensive HI observations of L134 have been made by Sancisi (1971), and a few comments are needed. The poorer spatial resolution (0.6° HPBW) and poorer velocity resolution (2 km/sec) of Sancisi's observations prevented detection of the HI component reported in this paper. The HI emission minimum reported by Sancisi had a 2 km/sec velocity dispersion and was centered at 0.5 km/sec. These parameters differ substantially from molecular line measurements.

Brightness temperature measurements with the 130 ft. antenna confirm Sancisi's findings (fig. 3-8); there is a temperature depression at 0.6 km/sec. However, the region of lowest temperature is located north of the center of L134. The general hydrogen emission is not uniform and convincing demonstration that the decreased brightness is not chance coincidence has not been made. It is interesting to speculate that perhaps the decreased brightness feature reported by Sancisi represents a depletion of hydrogen over a large volume which eventually condensed to form L134.

(2.8 km/sec Absorption Line)

The narrow velocity range over which the brightness temperature decreases implies that a true absorption line has been detected (see fig. 3-11), since it is highly unlikely such a narrow line can be caused entirely by a lack of atomic hydrogen. The absorption line will be studied using a simple model in which a cold cloud of hydrogen absorbs uniform background radiation. Foreground hydrogen will be neglected. Lyman α observations (Jenkins and Savage 1974) indicate that the hydrogen density varies greatly. The average density is 0.25 cm^{-3} within 100 pc of the sun, and this amount of foreground hydrogen would contribute a maximum 5° K brightness temperature assuming 100° K spin temperature and 3 km/sec velocity dispersion. Knowledge about the amount and

velocity distribution of hydrogen in front of L134 is so highly uncertain that it is best to simplify the analysis and neglect foreground hydrogen. This is a conservative assumption because the effect of foreground hydrogen is to diminish the depth of the absorption line.

Let $T_B(v)$ represent the background brightness temperature assuming it is only a function of velocity. $T_B(v)$ is determined from the 21 cm emission profile (fig. 3-7). Four parameters describe the atomic hydrogen in L134: spin temperature T_c, optical depth τ_c, velocity dispersion σ_c, and velocity v_c. The apparent brightness temperature is

$$T(v) = T_B(v)\, e^{-\tau(v)} + T_c(1 - e^{-\tau(v)})$$

where

$$\tau(v) = \tau_c e^{\frac{-[v - v_c]^2}{2\sigma_c^2}}$$

Because the interferometer completely resolves out the uniform background brightness, the brightness temperature as measured by the interferometer is

$$T'(v) = T(v) - T_B(v).$$

A computer program was used to optimize T_c, τ_c, σ_c, and v_c such that $T'(v)$ gave a least squares fit to the data.

Because T_c and τ_c are highly correlated, the least squares fit program does not converge to a physically acceptable solution when all four parameters are allowed to vary freely, i.e. $T_c \to -\infty$ and $\tau_c \to 0$. To insure a physically acceptable solution, either T_c or τ_c must be held fixed. Fig. 3-11 and 3-12 show the absorption line at the dust cloud center along with some fitted theoretical profiles where either T_c or τ_c have been fixed at various values. Table 3-1 summarizes the results. N_H is the columnar density of atomic hydrogen in the dust cloud.

TABLE 3-1

LEAST SQUARES FIT PARAMETERS FOR L134

T_c °K	τ_c	v_c km/sec	σ_c km/sec	N_H cm^{-2}	STANDARD ERROR
5.00	0.86	2.76	0.50	$9.9\ 10^{18}$	1.5
10.0	1.09	2.77	0.49	$2.5\ 10^{19}$	1.5
20.0	2.60	2.83	0.44	$1.1\ 10^{20}$	1.7
17.7	2.00	2.81	0.45	$7.4\ 10^{19}$	1.6
22.2	5.00	2.86	0.39	$2.0\ 10^{20}$	2.1
23.4	10.0	2.91	0.37	$4.0\ 10^{20}$	2.6

Judging by eye (fig. 3-11 and 3-12) only the curves with τ_c set at 5 and 10 do not appear to give an adequate fit to the data. The absorption line shape is wrong. The

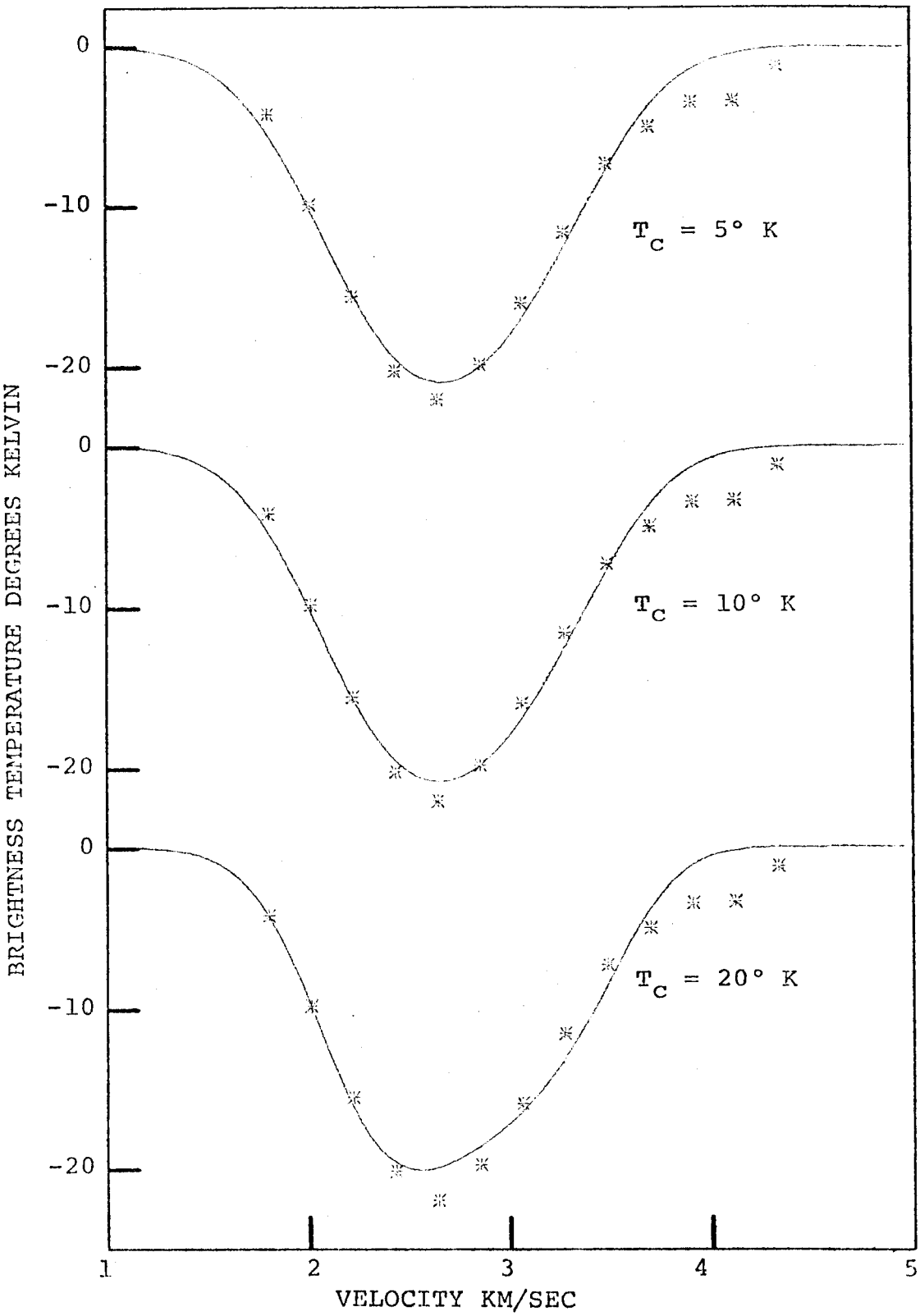

FIGURE 3-11. Absorption line profile at center of L134. Solid lines are the best fitting theoretical profiles where the temperature is fixed at 5° K, 10° K and 20° K.

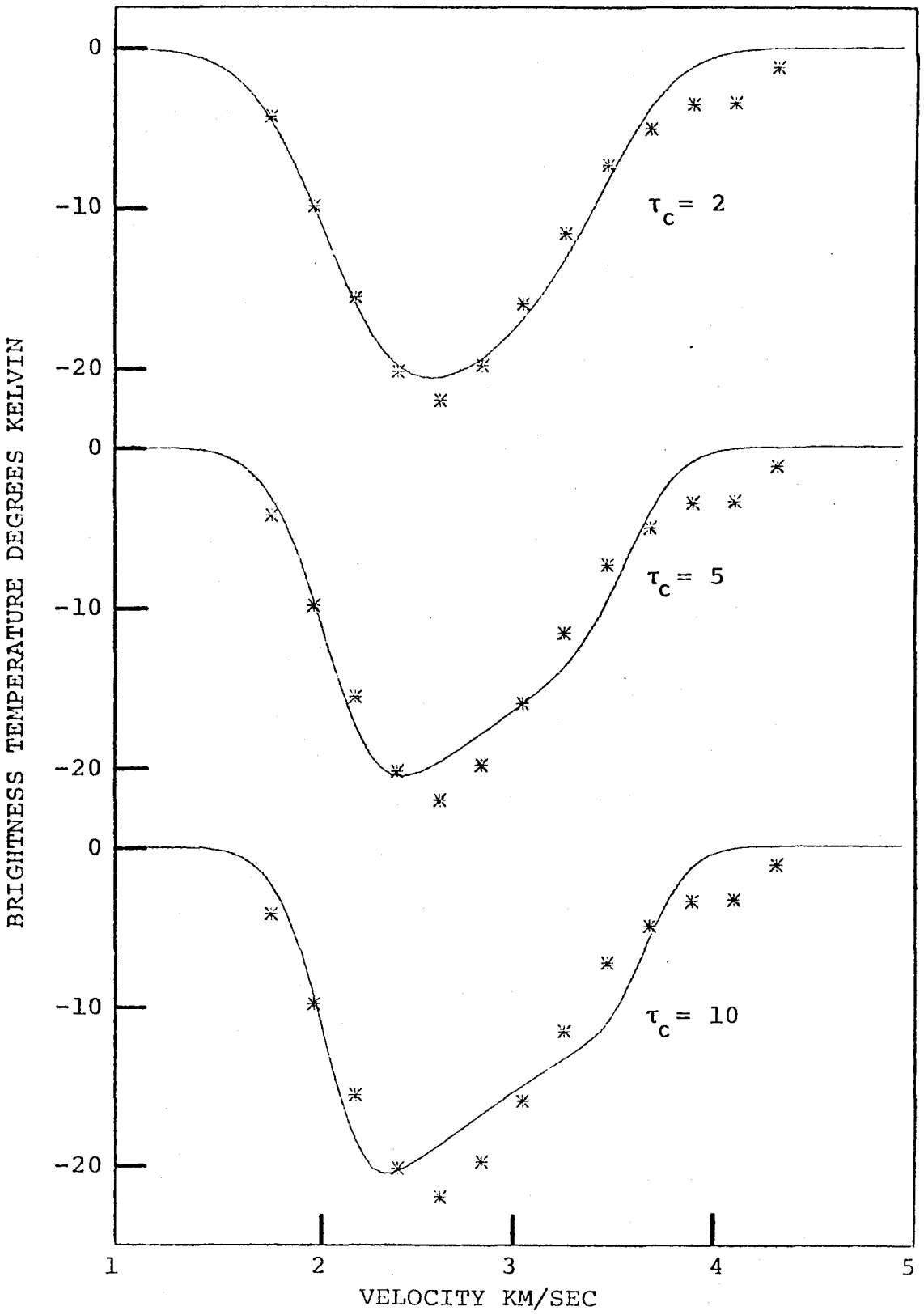

FIGURE 3-12. Absorption line profile at center of L134. Solid lines are best fitting theoretical profiles where the maximum optical depth is fixed at 2, 5 and 10.

goodness of fit with $T_c = 20°$ K is marginal. The following reasonable limits may be placed upon the hydrogen in the dust cloud.

$$0° \text{ K} < T_c \leq 20° \text{ K}$$

$$0.8 \leq \tau_c \leq 2$$

$$10^{19} \text{ cm}^{-2} \leq N_H \leq 10^{20} \text{ cm}^{-2}$$

$$v_c = 2.80 \pm 0.03 \text{ km/sec}$$

$$\sigma_c = 0.47 \pm 0.03 \text{ km/sec}$$

Heiles (1973) has observed the H_2CO 6 cm line in L134 and finds an absorption line at 2.795 ± 0.006 km/sec and a velocity dispersion 0.249 ± 0.008 km/sec. At 10° K the velocity dispersion due purely to thermal motion is 0.05 km/sec for H_2CO; therefore, the observed 0.249 km/sec velocity dispersion must be mainly due to turbulent motion. The synthesized beam for HI observations and the antenna beam used for the H_2CO observations are about the same size. If 0.249 km/sec is used to remove turbulent broadening from the HI absorption line, the residual dispersion is 0.40 km/sec which corresponds to 20° K. If hydrogen has a 20° K spin temperature, the HI optical depth is about 2 and there must be 10^{20} atoms/cm^2 of hydrogen along the line of sight through L134. This result is consistent with the absorption line profiles in fig. 3-11 and 3-12 where $T_c = 20°$ K and $\tau_c = 2$.

(HI Density)

A lower limit to the expected amount of HI can be estimated by taking 8 magnitudes to be a lower limit on the optical absorption. The basis of this estimate is that no stars are visible through L134 on the red Palomar Sky Survey print. Assume extinction is produced with an efficiency of $4.5\ 10^4$ mag cm^2/gm (Bok et al. 1970). Based upon cosmic abundance, hydrogen is 100 times more abundant by mass than the heavy elements that presumably make up the dust. Under these assumptions, the expected columnar hydrogen density is greater than 10^{22} cm^{-2}, 100 times greater than the observed value. To calculate the hydrogen density, the extent of L134 along the line of sight is needed. The angle subtended by 0.75 pc at 170 pc distance is 15', the apparent angular size of L134. If the extent of L134 along the line of sight is 0.75 pc, then the hydrogen density is greater than 4300 cm^{-3}. Hollenbach et al. (1971) have considered the problem of molecular hydrogen formation in dust clouds. For dense dust clouds, they predict most of the hydrogen should be in molecular form. The residual columnar atomic hydrogen density should be

$$N_H = 8.5\ 10^{22}\ n^{-1}\ \ cm^{-2}$$

where n is the total hydrogen density per cm^3. With $n = 4300\ cm^{-3}$, $N_H = 2.0\ 10^{19}\ cm^{-2}$. This value falls within the range of N_H given in Table 3-1, but it is smaller than

the value of N_H suggested by using the H_2CO line width to deduce a 20° K spin temperature for hydrogen.

(Velocity and Velocity Dispersion Maps)

Hollenbach et al. (1971) predict that atomic hydrogen in dense dust clouds like L134 is located in a thin shell lying at the dust cloud edge. Unfortunately τ_c cannot be measured as a function of position with sufficient accuracy to confirm or reject a shell-like distribution for atomic hydrogen. The resolution of the synthesized beam is inadequate for such a measurement. On the other hand, v_c and σ_c are less sensitive than τ_c to uncertainties generated by poor angular resolution. Fig. 3-13 and 3-14 are contour maps showing how v_c and σ_c change across the face of the dust cloud. Using a rectangular grid of points spaced 2' apart, a least squares fit to the absorption line profile was obtained at each position with T_c always fixed at 10° K. The region examined (outlined by the dashed line in fig. 3-13 and 3-14) was confined to the area where the absorption line was at least 10° K deep. It is difficult to fit absorption lines less than 10° K deep to the model. Fig. 3-15 shows a representative sample of absorption line profiles along a north-south line through L134, and Table 3-2 tabulates the various parameters.

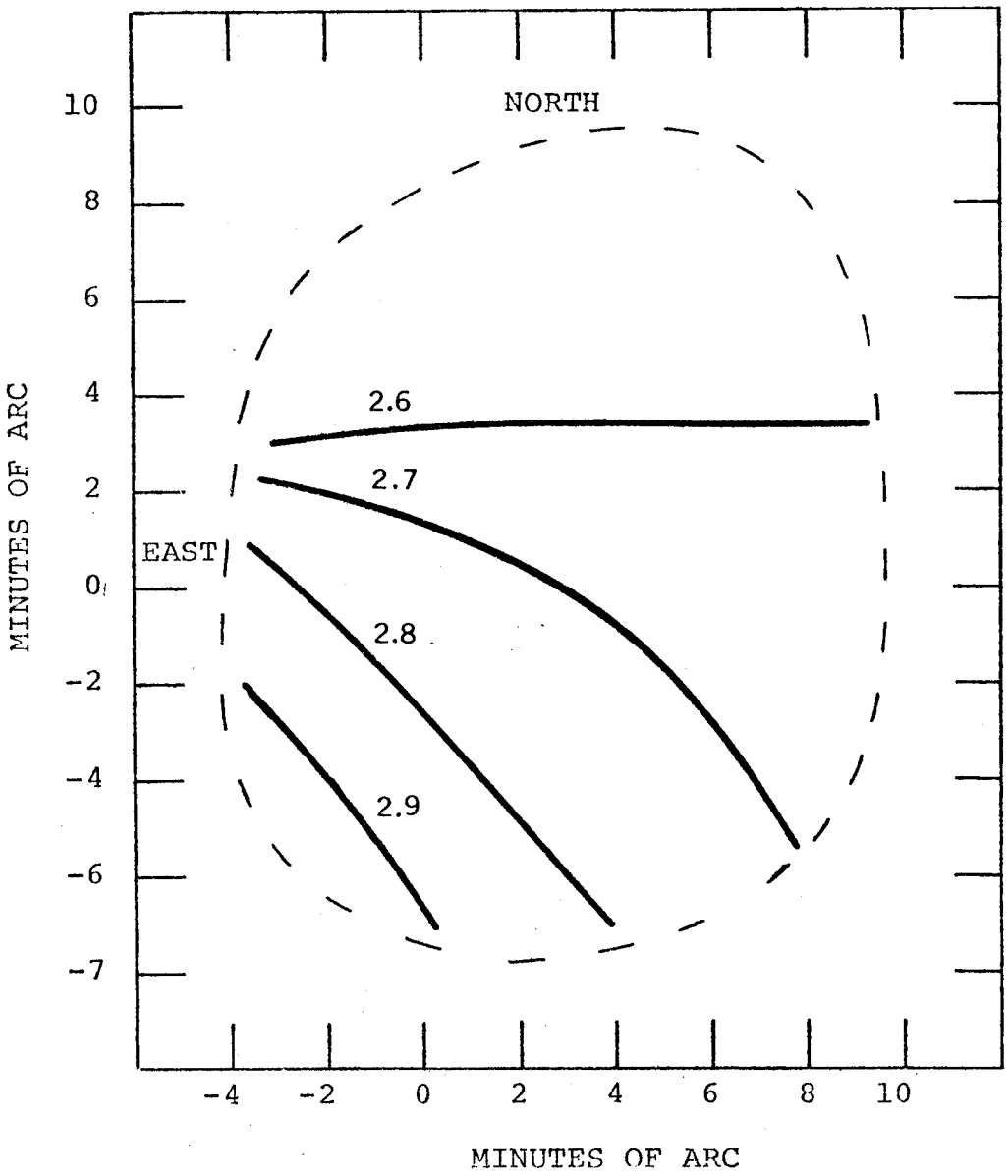

FIGURE 3-13. Velocity contour map of L134. Numbers by solid contour lines indicate the velocity in km/sec. Dashed line outlines the region over which the velocity was measured. The (0,0) position corresponds to the position of L134 given in Table 2-1.

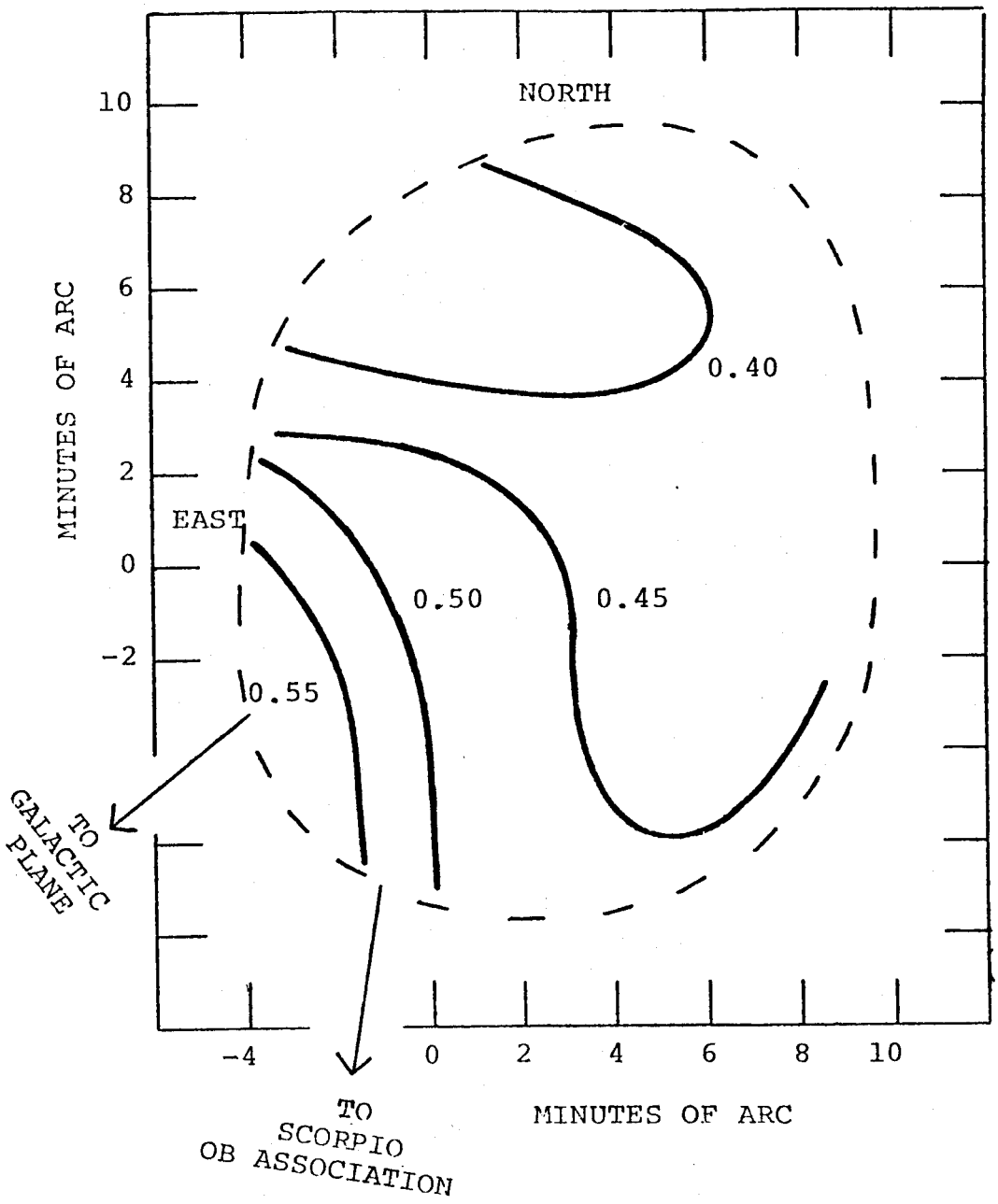

FIGURE 3-14. Contour map of absorption line width for L134. Numbers by solid contour lines indicate the velocity dispersion, σ_c , in km/sec. Dashed line outlines the region over which the velocity dispersion was measured. The (0,0) position corresponds to the position of L134 given in Table 2-1. The direction to the galactic plane and the Scorpio OB association are indicated.

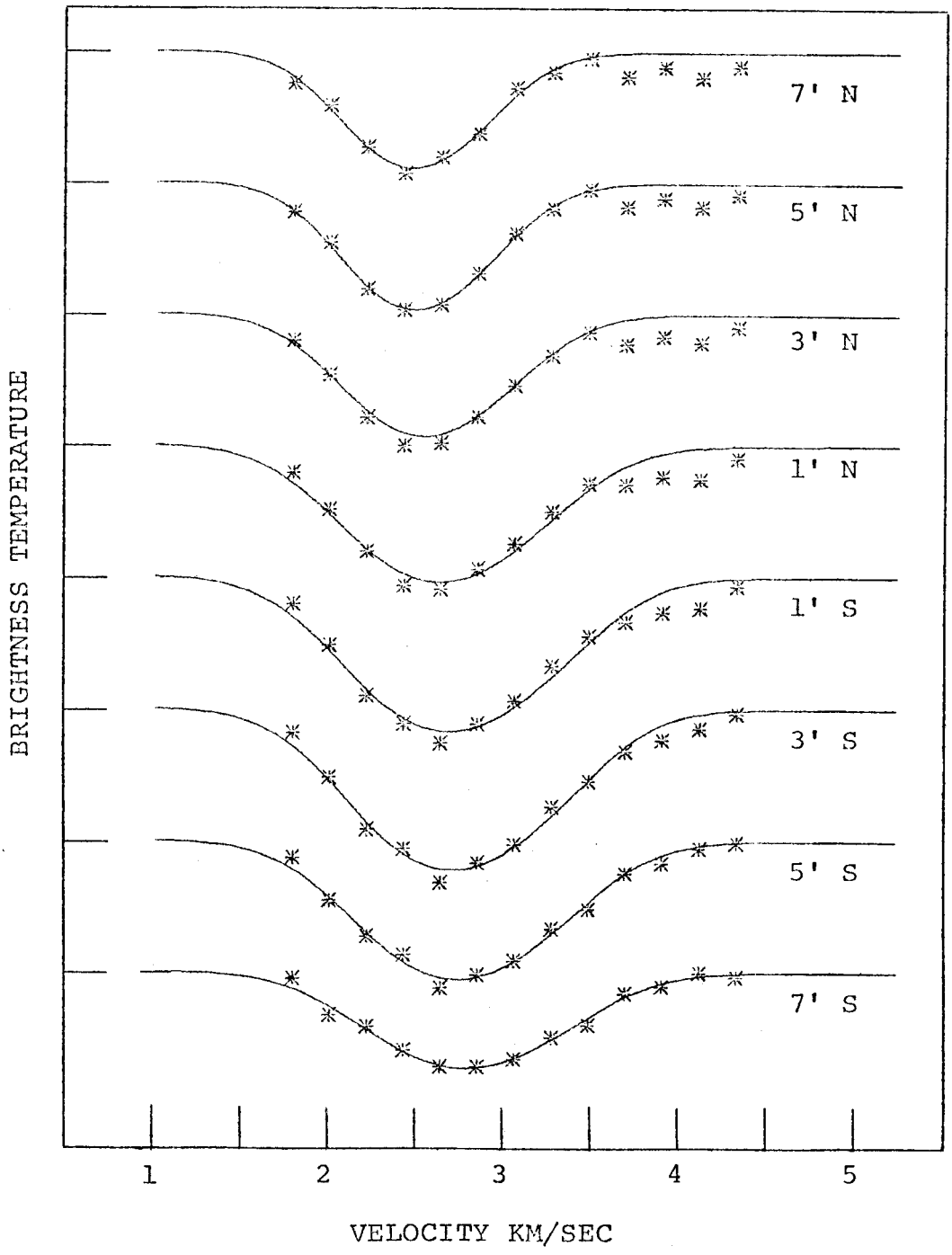

FIGURE 3-15. 21 cm absorption line as a function of position in L134. Position with respect to the adopted position of L134 is given to the right of each absorption line. Profiles are displaced from one and another by 15° K brightness temperature. Solid line is the fitted profile whose parameters are given in Table 5-2.

TABLE 3-2

LEAST SQUARES FIT PARAMETERS FOR L134

AS A FUNCTION OF POSITION

POSITION FROM CENTER	T_c °K	τ_c	v_c km/sec	σ_c km/sec
7' NORTH	10.0	0.73	2.54	0.37
5' NORTH	10.0	0.80	2.57	0.38
3' NORTH	10.0	0.83	2.64	0.43
1' NORTH	10.0	0.94	2.73	0.48
1' SOUTH	10.0	1.09	2.77	0.49
3' SOUTH	10.0	1.06	2.79	0.47
5' SOUTH	10.0	0.77	2.80	0.47
7' SOUTH	10.0	0.45	2.84	0.47

Apparently a 0.3 km/sec velocity gradient exists across the dust cloud, but exactly how the velocity contour map should be interpreted in terms of the dust cloud kinematics is not clear. It is somewhat peculiar that the velocity contour lines tend to converge on the east side of the dust cloud. Perhaps a rotation-like motion is present. In any case, an estimate is needed on how large a velocity is dynamically important. Following Bok et al. (1970) the minimum mass (in solar masses) of dust which is required to produce Δm magnitudes of absorption in a cloud with radius R (pc) is

$$M_d = 0.22\ R^2 \Delta m$$

For L134 R = 0.4 pc and $\Delta m \geq 8$ which implies $M_d \geq 0.28\ M_\odot$. The total mass M should be about 100 M_d or $M \geq 28\ M_\odot$. The condition for stability can be crudely approximated by equating the total kinetic energy to the gravitational binding energy,

$$\frac{kT}{u} + v^2 = \frac{GM}{R}$$

where u is the mean mass per particle and v is the turbulent velocity. Taking T = 10° K, u = $1.7\ 10^{-24}$ gm, kT/u equals 0.08 km^2/sec^2. Based upon the velocity contour map, v = 0.3 km/sec or $v^2 = 0.09\ km^2/sec^2$ which is very close to kT/u. Using R = 0.4 pc and M = 28 $M_\odot$, then GM/R is 0.3 km^2/sec^2. Assuming GM/R has not been seriously underestimated, L134 is close to equilibrium or slightly bound.

Fig. 3-14 indicates that the absorption line is wider in the southeast part of L134 than elsewhere. In searching for an explanation for the asymmetry, the ultraviolet radiation field is an obvious factor to consider for two reasons: (1) Radiation near 1000 Å is the dominant mechanism for disassociating molecular hydrogen into atomic hydrogen; (2) The UV radiation field should be anisotropic at the position of L134. Habing (1968) has estimated the average interstellar radiation density at 1000 Å. The only significant sources of radiation at 1000 Å are O stars and

early B stars. In addition if the albedo of dust grains is high (0.9) at 1000 Å, scattered light from dust grains may be comparable to direct radiation from the stars. In any case, B stars and dust are tightly confined to the galactic plane. Clearly if L134 is 100 pc north of the galactic plane, it must receive considerably more radiation from the galactic plane direction than the galactic pole. Another factor to be considered is the proximity of L134 to the Scorpius OB association. Habing estimated that within 67 pc, direct radiation from the Scorpius OB association will produce a UV energy density comparable to the average interstellar density. L134 is approximately 60 pc from the Scorpius OB association. Arrows in fig. 3-14 point in the direction of the galactic plane and the Scorpius OB association.

The theory used by Hollenbach et al. (1971) assumes that the rates at which molecular hydrogen is formed and destroyed are equal. Increasing the UV radiation will produce a proportional increase in the columnar atomic hydrogen density. The absorption lines were examined to determine if the optical depth is greater in that part of L134 facing the galactic plane and the Scorpius OB association than the opposite side, but there is no hard evidence that such is the case. The broad absorption lines on the

southeast side of L134 are best fitted by simply increasing the velocity dispersion of the hydrogen. Also it should be noted that all the absorption lines have a fairly symmetric shape (fig. 3-15) and not the flattened shape predicted for lines of large optical depth (fig. 3-12). It cannot be determined whether or not the optical depth might systematically change by a factor of 2 or 3 from one side to another side of L134; however, the data does indicate that the contrast in optical depth is not greater than a factor of 10. More high latitude dust clouds need to be examined to see if they exhibit asymmetries similar to L134.

(0.7 km/sec Absorption Line)

Attention will now be focussed on the 0.7 km/sec component of L134. It is shown in fig. 3-3 and lies off to the southeast of the 2.8 km/sec component. Without independent evidence it cannot be determined if the 0.7 km/sec component is connected with the dust cloud or represents a random brightness fluctuation in the 21 cm emission. Fortunately carbon monoxide observations provide an important clue. Fig. 3-16 shows the contour maps of the two L134 components superposed along with marks indicating positions where the CO observations were made. If CO line profiles (fig. 3-4 through 3-6) are compared with their positions (fig. 3-16), it is apparent that the

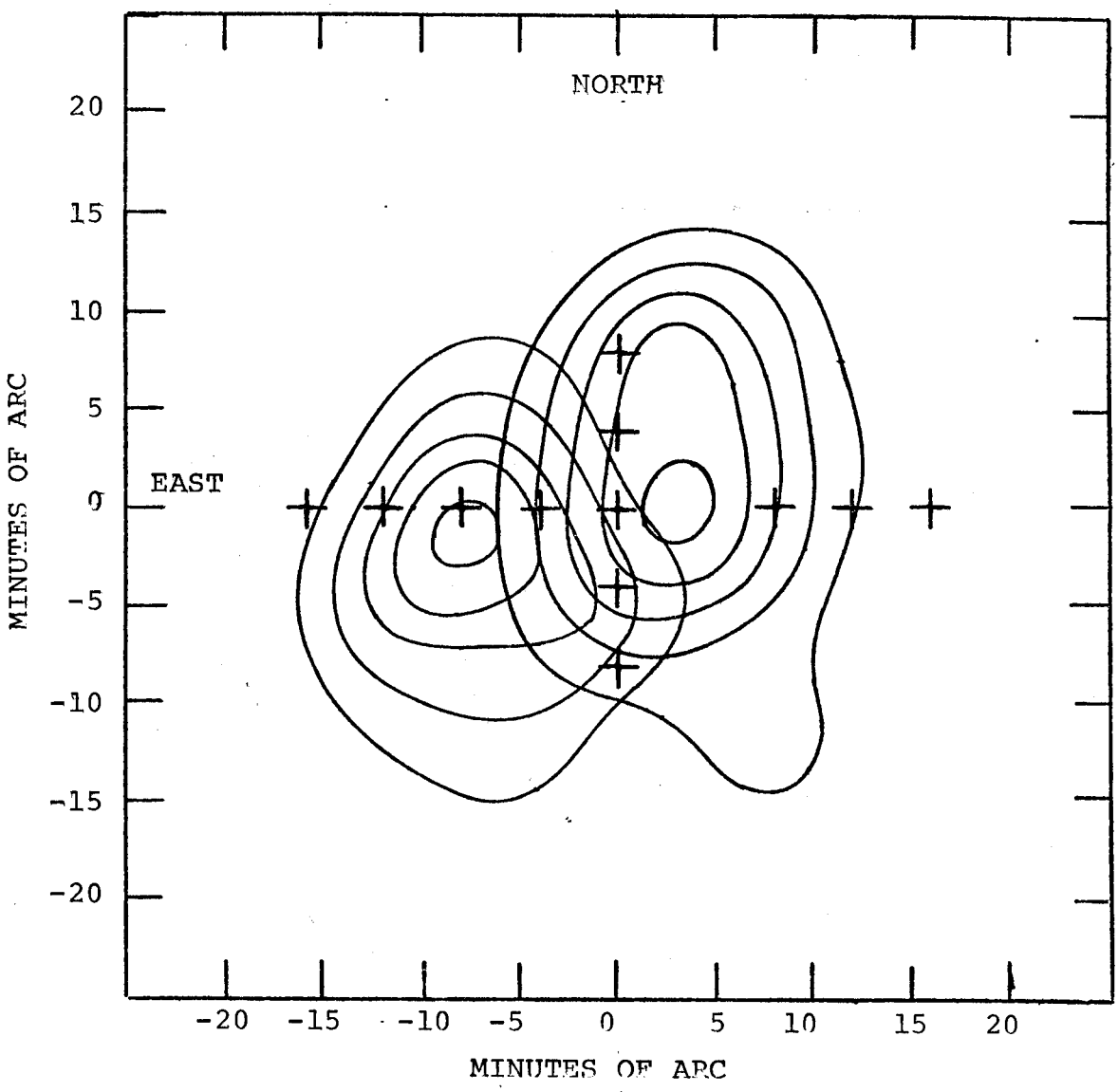

FIGURE 3-16. Positions of CO observations. Crosses indicate the positions at which the CO emission lines in fig. 3-4 through 3-6 were measured. Contour lines are the two 21 cm sources shown in fig. 3-2 and 3-3.

CO emission line is split in the region where the two L134 HI components overlap. The CO velocities are 2.8 $\pm$ 0.2 km/sec and 0.8 $\pm$ 0.3 km/sec. The corresponding HI absorption line velocities are 2.80 $\pm$ 0.03 km/sec and 0.65 $\pm$ 0.05 km/sec. The excellent velocity and position agreement between the CO and HI observations makes unlikely the possibility that the 0.7 km/sec component is a chance fluctuation of the background emission and is unrelated to dust clouds.

The HI absorption line for the low velocity component was analyzed in the same manner as the 2.8 km/sec line. Fig. 3-17 shows the best fitting line profiles; the top profile shows the best fit with all four parameters allowed to vary and the remaining curves have the spin temperature fixed at various values. Table 3-3 tabulates the results. The best fit solution allowing all 4 parameters to vary is physically unacceptable. With a spin temperature at 41° K, the absorption line must have a velocity dispersion greater than 0.58 km/sec. The remaining solutions listed in Table 3-3 are physically reasonable.

(Relationship Of The Two Components)

The data indicate that there are two dust clouds separated by about 2 km/sec, but the relationship of these

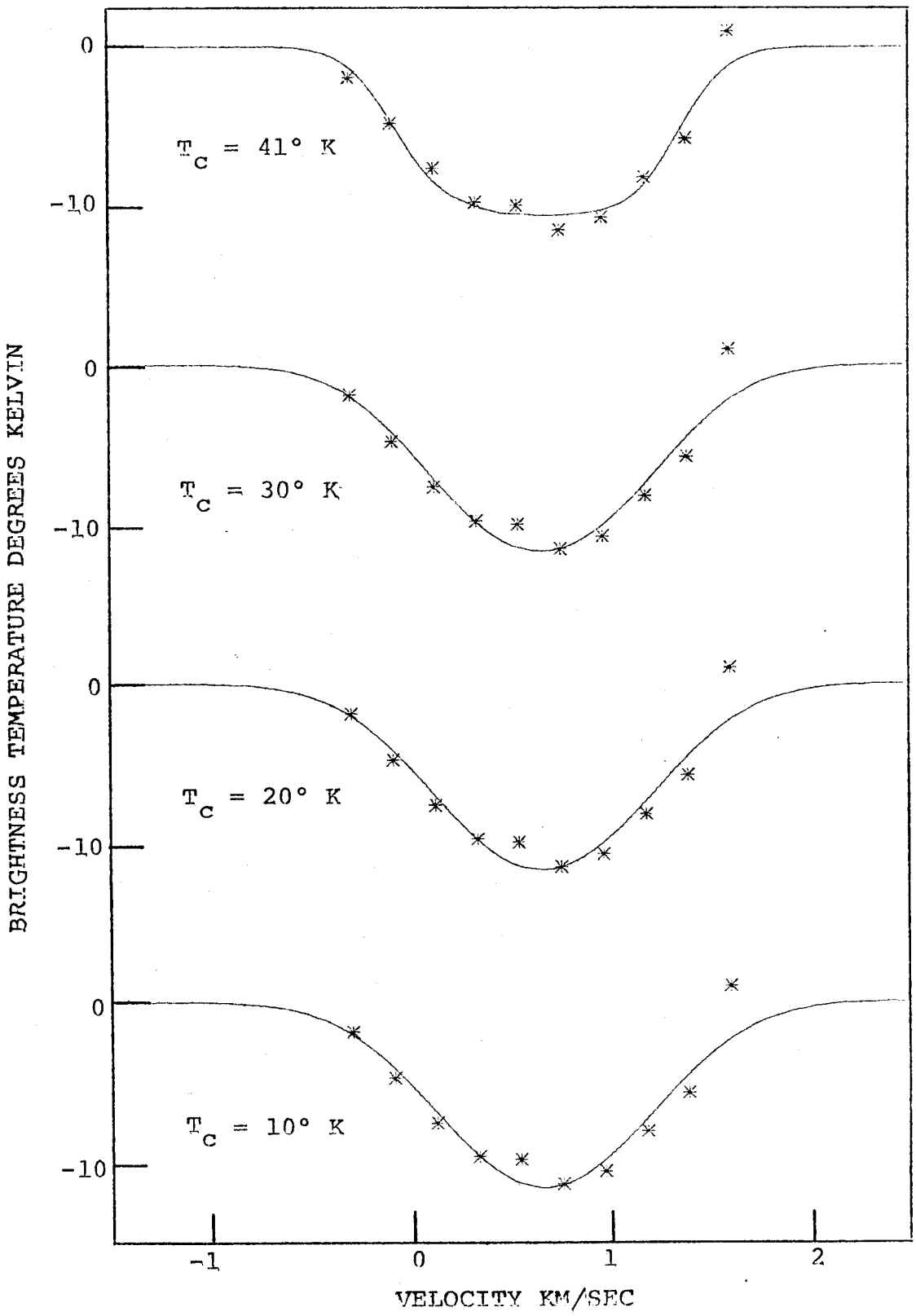

FIGURE 3-17. Absorption line profile in L134. Solid lines are best fitting theoretical profiles assuming various values for the spin temperature.

two dust clouds is not apparent. Larson (1973) has suggested that the collapse of a rotating cloud might produce two smaller condensations orbiting around each other. For L134 $\sqrt{GM/R}$ is greater than 0.5 km/sec, and this is not far from the 2 km/sec velocity difference between the two components. The 0.7 km/sec cloud is smaller than the other cloud and is probably denser as well. This would be consistent with the smaller columnar atomic hydrogen density in the 0.7 km/sec cloud. The evidence for two dust clouds in orbit is meager. Since the radii of the dust clouds are comparable to their projected separation, such an orbiting model may not be stable. More dust clouds should be carefully examined for multiple velocity components. After this is done, the significance of the two velocity components in L134 may be better evaluated.

TABLE 3-3

LEAST SQUARES FIT PARAMETERS FOR L134

T_c °K	τ_c	v_c km/sec	σ_c km/sec	N_H cm^{-2}	STANDARD ERROR
41.0	6.30	0.61	0.35		1.2
30.0	0.78	0.63	0.49	$5.3\ 10^{19}$	1.5
20.0	0.47	0.64	0.50	$2.2\ 10^{19}$	1.5
10.0	0.33	0.64	0.51	$7.8\ 10^{18}$	1.5

IV. L1495

L1495 GENERAL DESCRIPTION

In contrast to the other two dust clouds studied, L1495 is not an isolated compact object but seems to be part of a dust complex extending over several degrees. Fig. 4-1 is a photograph of L1495 centered upon the direction in which the interferometer antennas were pointed.

Determination of the distance to L1495 is an inexact process at the best. A kinematic distance based upon galactic rotation is not available because the galactic longitude is too close to 180°. Several statistical methods based upon star counts can be used; however, for highly obscured regions, such techniques do not work well. The simplest distance estimate is made by assuming L1495 is at the distance determined for the Taurus dust complex. Based upon photometric and spectroscopic observations, Racine (1968) has estimated distances of stars illuminating reflection nebulae in the Taurus region. The closest and farthest stars among 11 stars observed in the Taurus region were estimated to be at 95 pc and 165 pc. Accordingly an adopted distance of 130 pc for L1495 would be reasonable and is probably not in error by more than 25%.

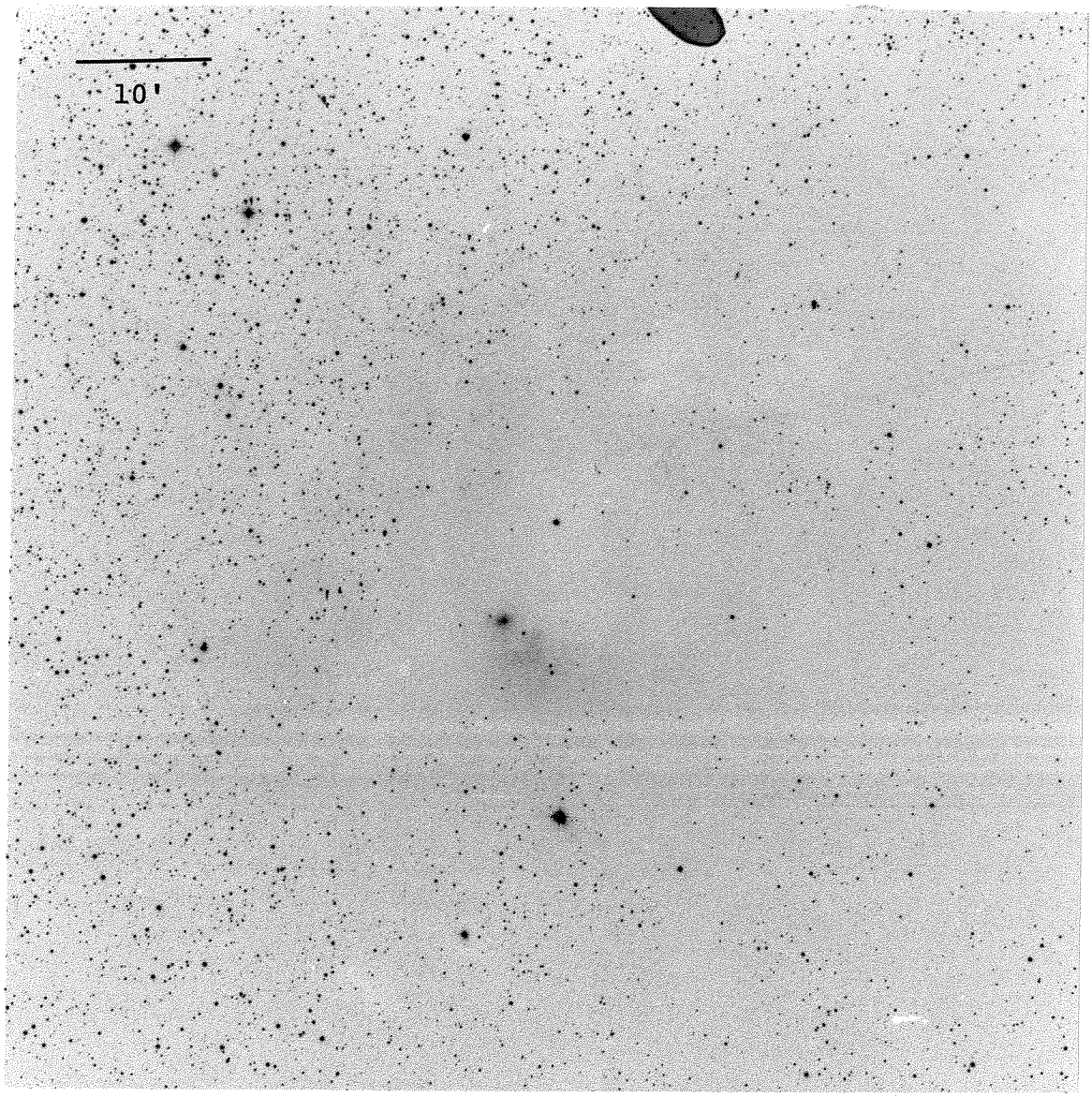

FIGURE 4-1. Photograph of L1495 taken from the red Palomar Sky Survey print. North is on top and east is on the left. Field of view is centered upon the position of L1495 given in Table 2-1. Scale is indicated in upper left corner.

L1495 RESULTS

In L1495 there is good evidence for the existence of cold HI associated with the dust cloud. The single dish observations will be considered first. Cudaback and Heiles (1969) reported detecting OH emission at 7.2 km/sec. Fig. 4-2 through 4-4 show the HI emission profiles for a series of positions which progressively move from less obscured regions toward the central part of the dust cloud. One feature which clearly stands out is the development of a shoulder-like dip as one moves into the dust cloud. It is significant that this feature occurs at 7 km/sec.

In fig. 4-5 emission profiles can be compared directly. Interpreting the line profile would be facilitated if all off-cloud profiles were approximately the same; however, the situation is not so simple. Nevertheless, at 7 km/sec the on-cloud profile suffers a prominent temperature dip as compared to the three off-cloud positions north, east and south of L1495. The exception is the profile 30' west of the adopted position of L1495, but this is an area of high obscuration as can be seen in fig. 4-1. Contour maps of the antenna temperature were made using data from a grid of about 60 observation points. The contour map at 7 km/sec is shown superposed on a photograph of L1495 in fig. 4-6.

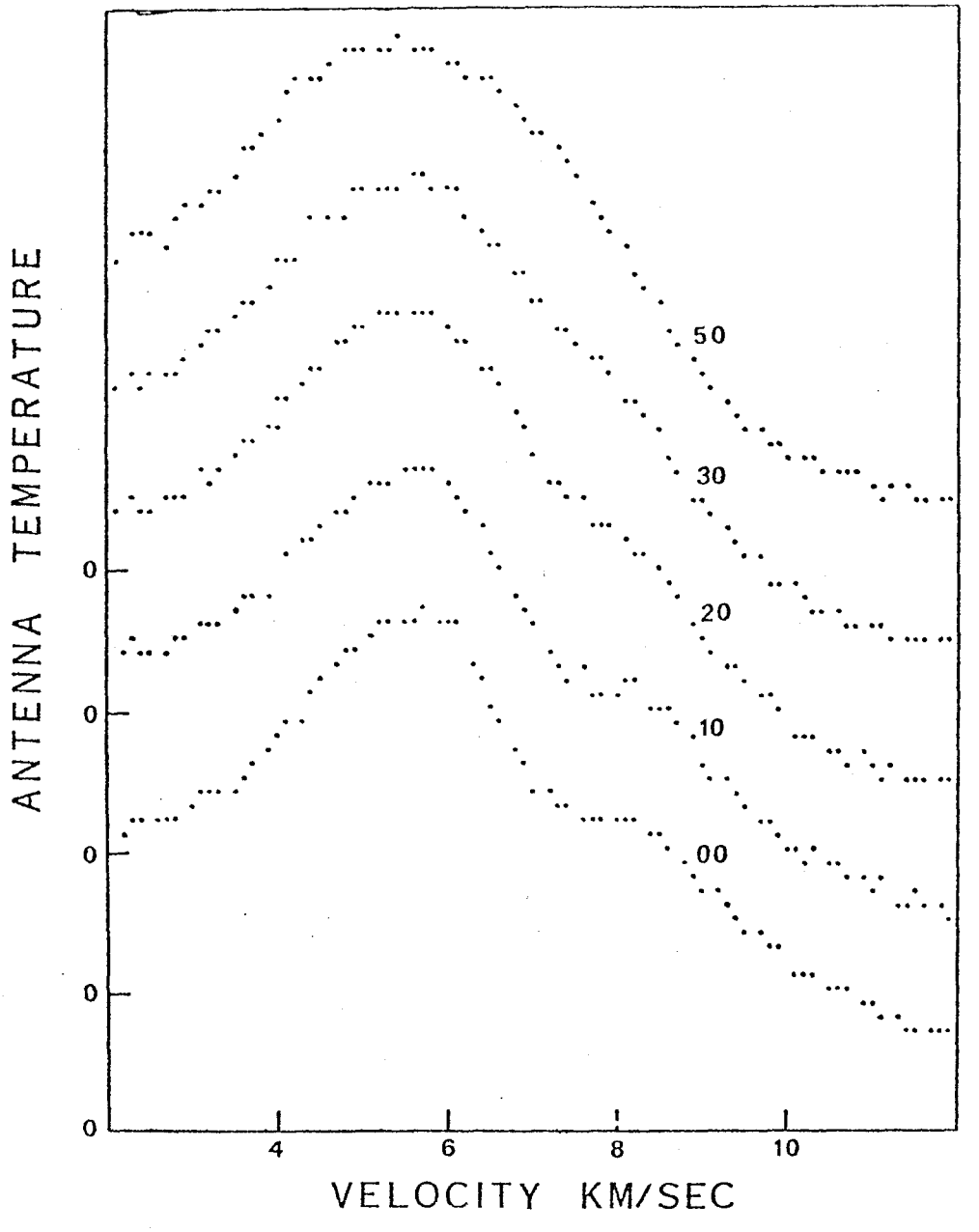

FIGURE 4-2. Hydrogen 21 cm line emission profiles measured at positions north of L1495. Each profile is labeled by a number giving the position in minutes of arc north of L1495. Profiles are displaced from each other by 10° K antenna temperature and the zero point for each profile is indicated.

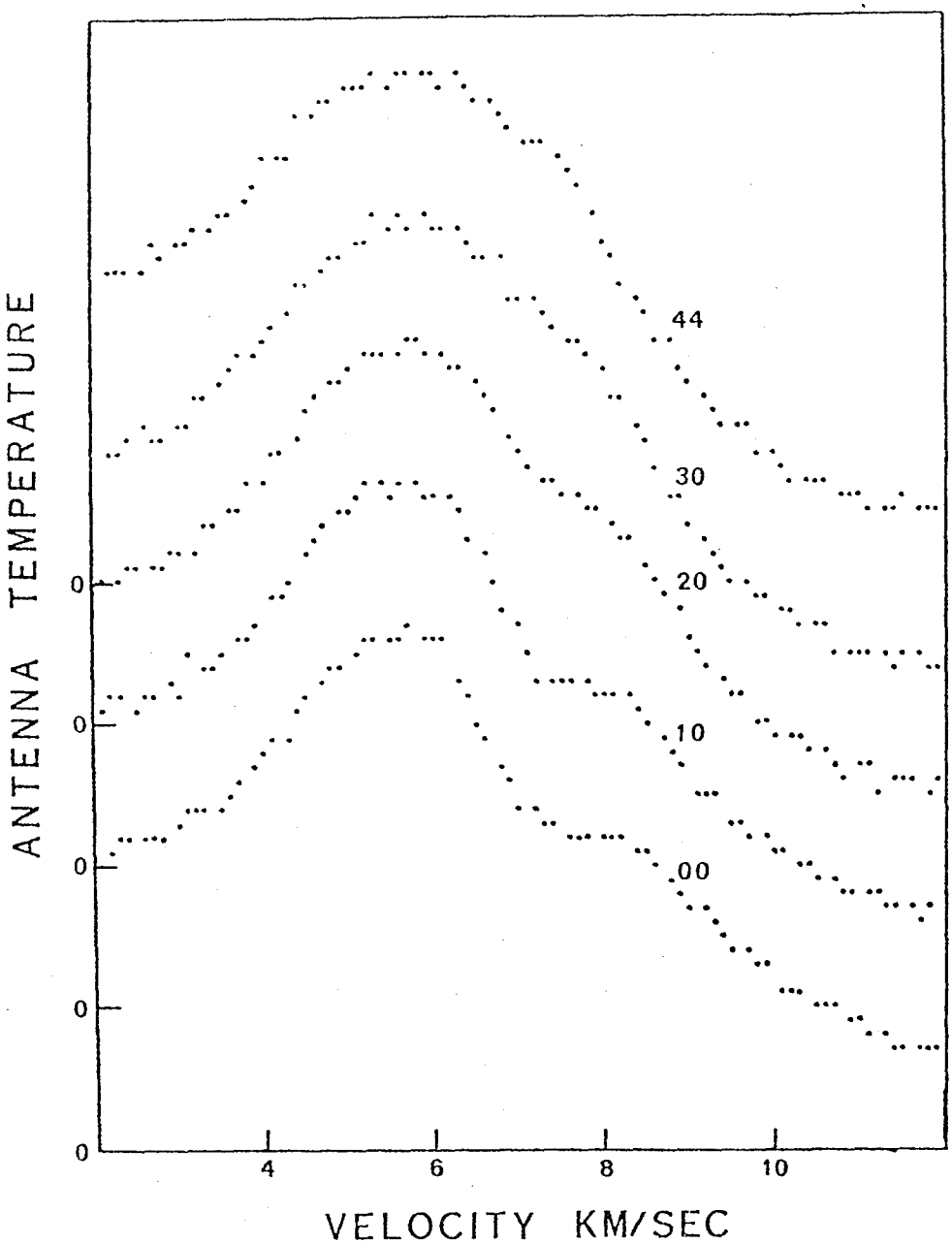

FIGURE 4-3. Hydrogen 21 cm line emission profiles measured at positions east of L1495. Each profile is labeled by a number giving the position in minutes of arc east of L1495. Profiles are displaced from each other by 10° K antenna temperature and the zero point for each profile is indicated.

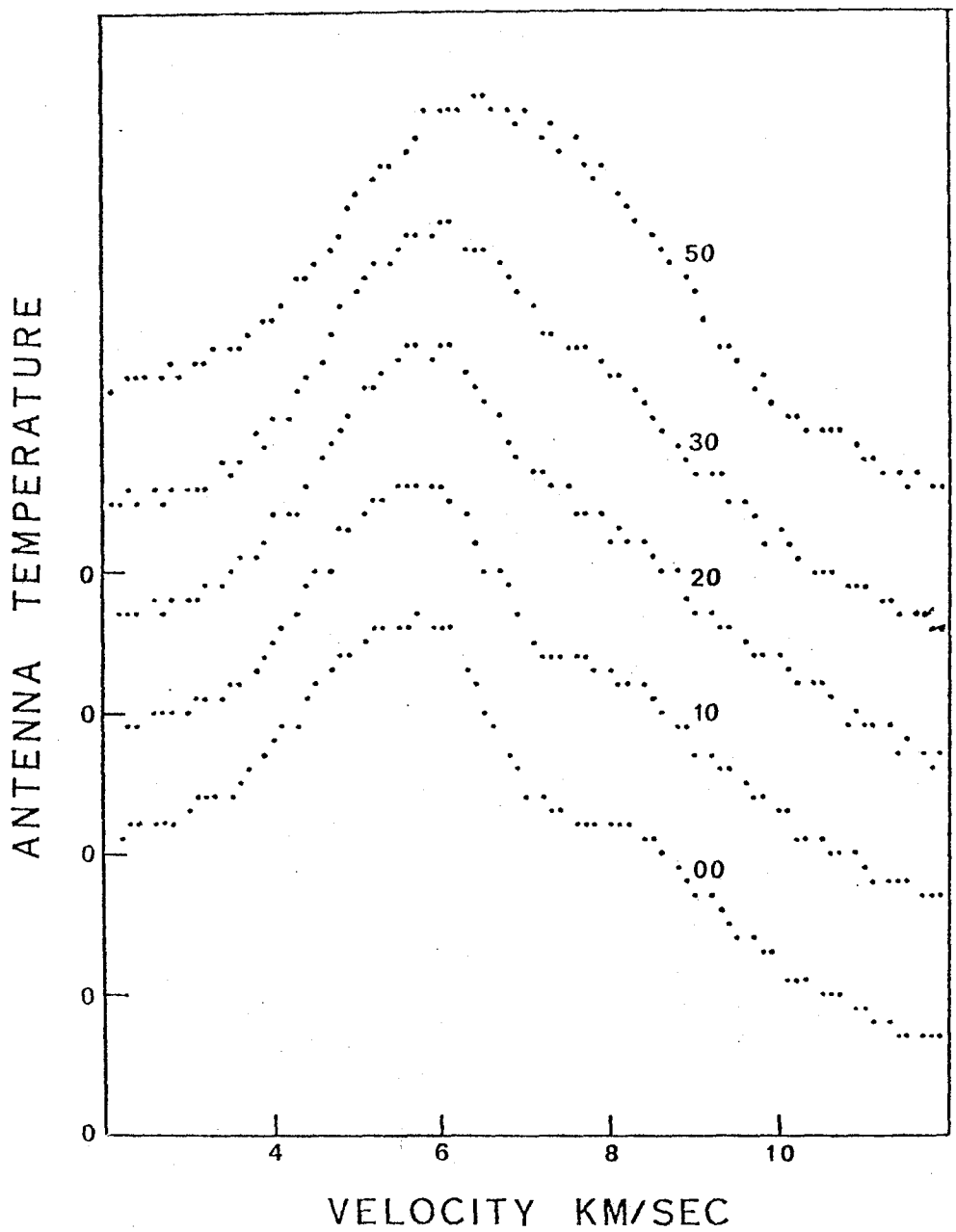

FIGURE 4-4. Hydrogen 21 cm line emission profiles measured at positions south of L1495. Each profile is labeled by a number giving the position in minutes of arc south of L1495. Profiles are displaced from each other by 10° K antenna temperature and the zero point for each profile is indicated.

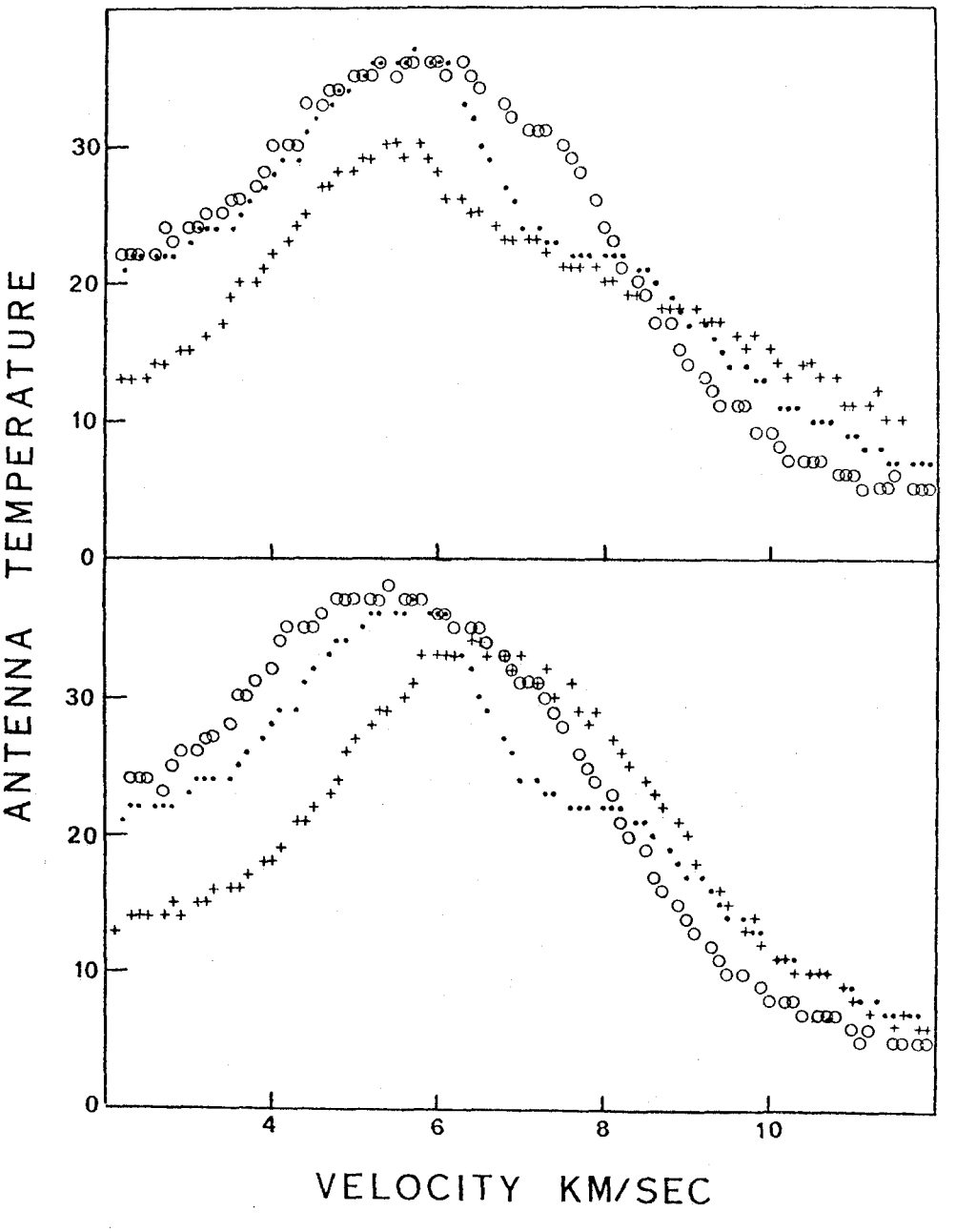

FIGURE 4-5 Comparison between off-cloud and on-cloud 21 cm emission profiles for L1495. Dotted profile upper and lower graph is on-cloud profile. Open circle profile upper graph is 30' east and lower graph 30' north of L1495. Plus profile upper graph is 30' west and lower graph 30' south of L1495. Antenna temperature is in degrees Kelvin.

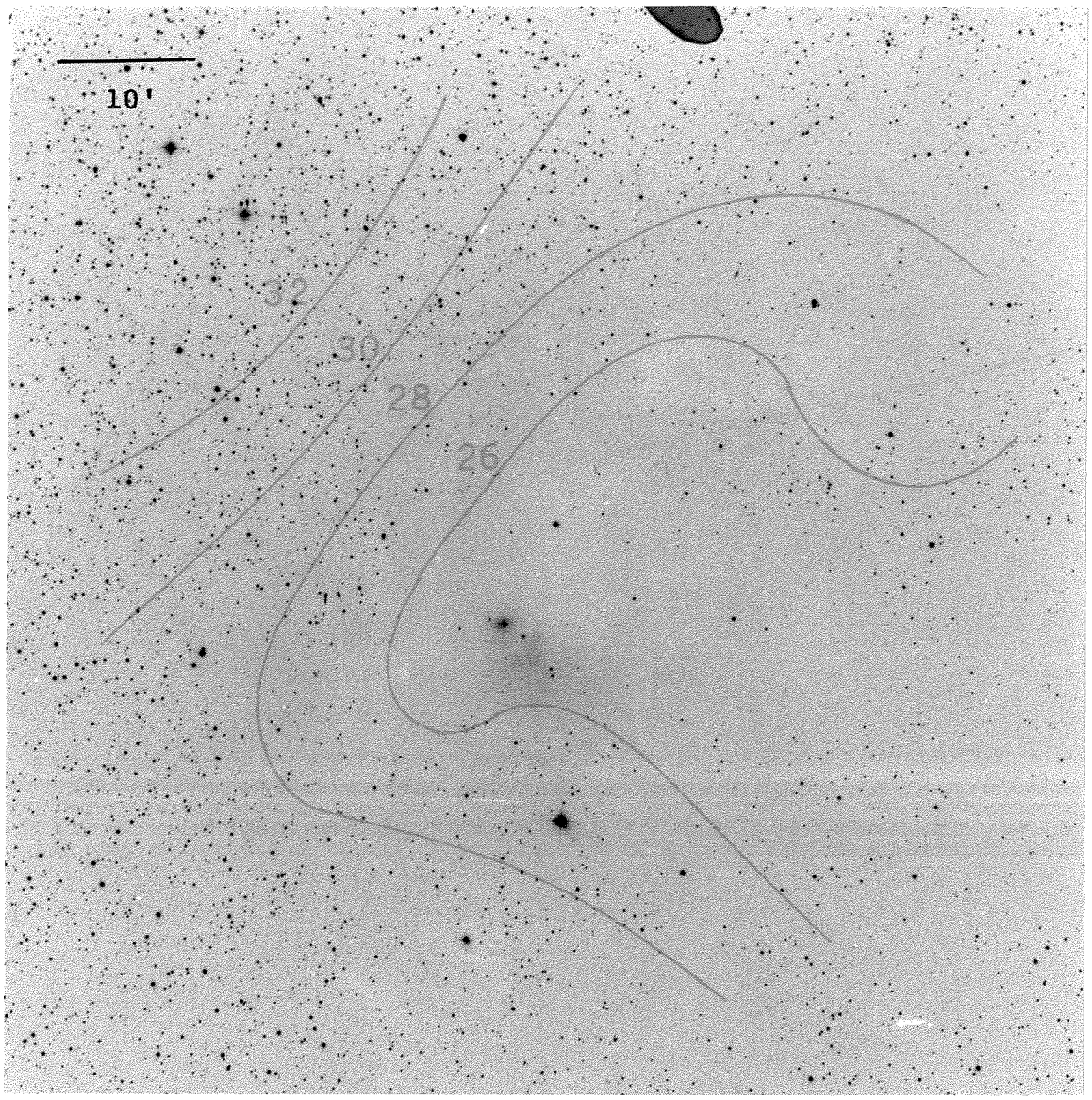

FIGURE 4-6. Contour map of antenna temperature at 7 km/sec. Observations were made with a 22' beam. Scale is indicated in upper left corner. Noise level is about 0.5° K antenna temperature.

The antenna temperature contour lines and the star density are well correlated. If other contour maps at various velocities are made, similar looking maps are obtained over roughly a 1 km/sec velocity range centered at 7 km/sec. Outside this velocity range, the contour maps do not appear to be as closely related to the dust distribution. These data provide convincing evidence that L1495 affects the 21 cm brightness temperature at a velocity coincident with the OH velocity.

The interferometer cannot discern the overall structure of this large dust cloud, but observations were made to see what substructure might exist. Fig. 4-7 shows a plot of a quantity approximating the average visibility amplitude versus velocity at a 100 ft. NS spacing. Coincident with the OH velocity, there appears a rather prominent feature. Fig. 4-8 shows a clean map produced by Fourier transforming the visibility at 7.07 km/sec. Besides the feature at 7 km/sec, fig. 4-7 indicates some sort of feature at 3 km/sec. The visibility at this velocity was transformed, and the resulting clean map consists of contour lines with positive brightness temperature, i.e. the feature had a higher brightness temperature than the background. Contour maps from single dish observations at 3 km/sec do not correspond well to the dust distribution.

The interferometer feature at 3 km/sec probably is due to a background brightness fluctuation unrelated to L1495.

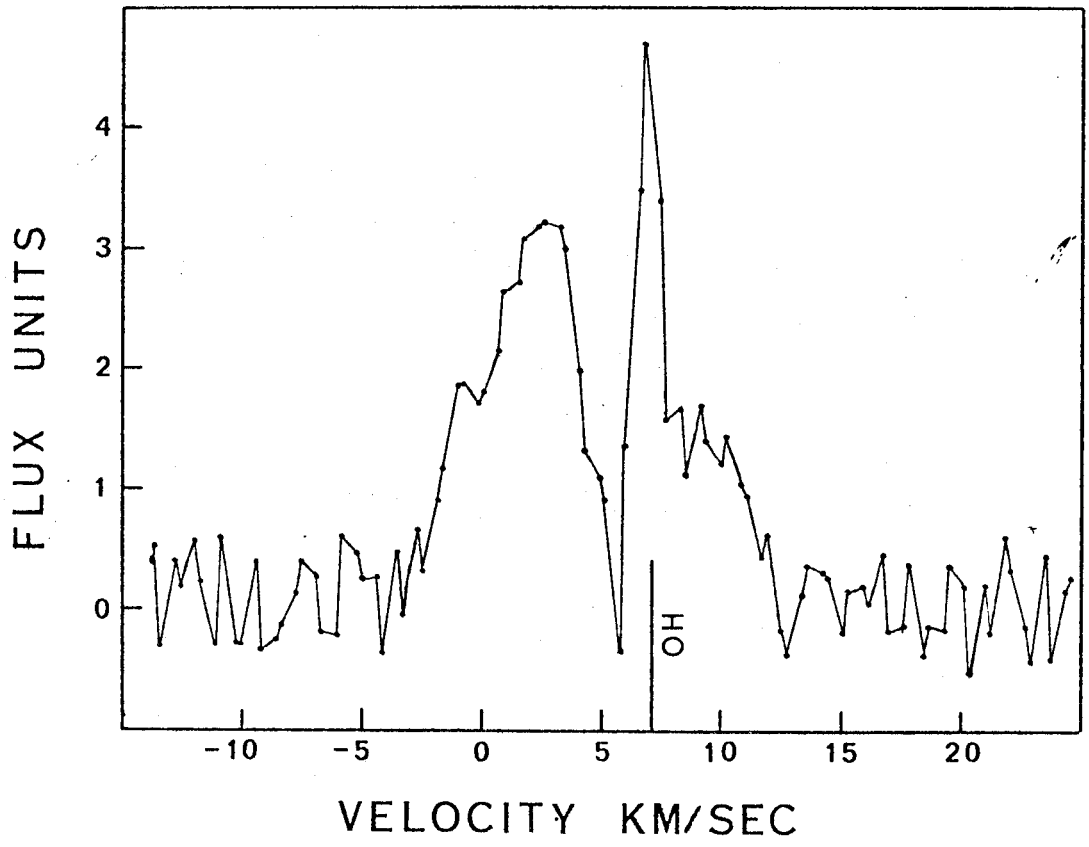

FIGURE 4-7. Plot of a quantity approximating the average visibility amplitude at a 100 ft north-south spacing versus velocity. The velocity at which OH has been detected in L1495 is indicated.

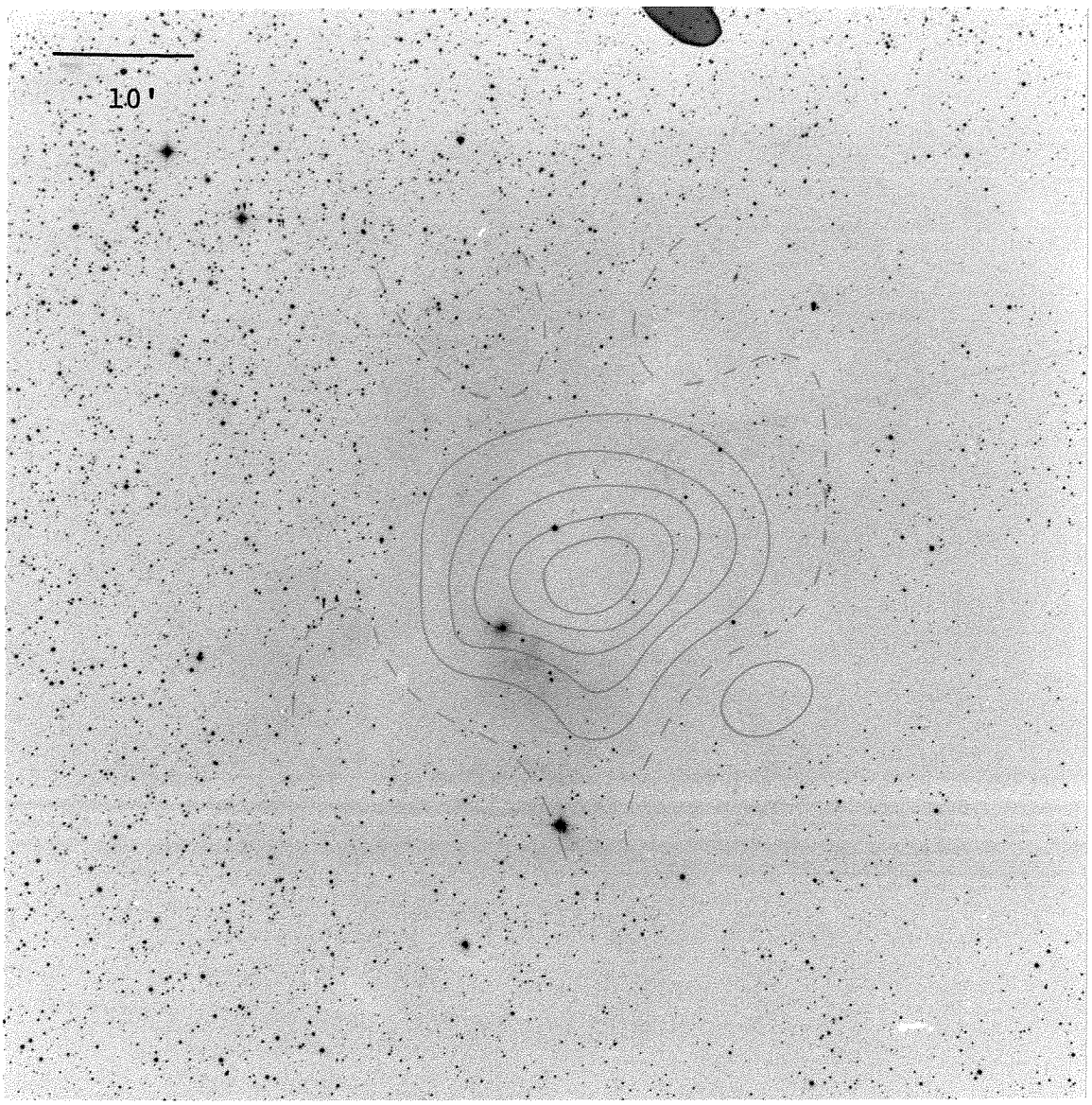

FIGURE 4-8 Brightness temperature contour map of L1495 from interferometer observations at 7.07 km/sec. Contour interval is 2° K and synthesized beam diameter is 7'. Scale is indicated in upper left corner. Zero spacing information is missing; therefore, the dashed contour lines were set at 0°K for reference. The main feature represents a 10° K drop in the brightness temperature. No correction has been made for the antenna beam. Noise level is 1° K.

L1495 DISCUSSION

A strong correlation exists between low brightness temperature and heavy optical obscuration (fig. 4-6). The 21 cm emission decreases at a velocity coincident with the OH velocity (fig. 4-7). These observations leave little doubt that physical conditions in L1495 have caused changes in the 21 cm emission. An earlier observation of L1495 (Heiles 1969) is consistent with these findings. Hopefully physical conditions in L1495 may be deduced by analyzing the 21 cm emission profile.

To explain the decreased 21 cm emission, at least one of the following two conditions must be true: (1) lower spin temperature inside the dust cloud than outside the dust cloud; (2) less hydrogen inside the dust cloud than outside the dust cloud. The narrow velocity range over which the brightness temperature decreases provides good evidence that cold hydrogen absorbing background radiation is present. If the decreased brightness temperature is produced only by a lack of hydrogen, i.e. no absorption is taking place, then the velocity range over which the temperature decreases must equal the velocity dispersion of the missing gas. The hydrogen responsible for most of the 21 cm emission is assumed to come from clouds with a 100° K

spin temperature. The velocity dispersion at 100° K is 0.9 km/sec ($\sqrt{kT/m}$) and turbulent motion will cause additional broadening. The observed velocity dispersion of the absorption line is less than 0.6 km/sec. This evidence suggests that the 21 cm emission decrease is a true absorption feature due to cold hydrogen in L1495.

To determine the characteristics of the absorption line, the single dish and interferometer observations must both be considered. Observational selection has divided the 21 cm structure of L1495 into two components: (1) A large area with decreased emission extending out to the dust cloud edge is detected by single dish observations but resolved out by the interferometer. (2) A smaller region with decreased emission is detected by the interferometer but mostly undetected by single dish observations due to insufficient angular resolution. Ideally a procedure similar to that described in the appendix should be used to combine single dish and interferometer maps into a single brightness temperature map. Unfortunately such a procedure is not practical because the 130 ft. antenna has insufficient resolution to measure the visibility out to 130 λ, the shortest available interferometer baselines. A simpler method will be used to combine the interferometer and single dish results. The only constraint is that the

final brightness temperature map must be consistent with all observations.

A brightness temperature map produced from single dish observations is the true brightness distribution smoothed by the 130 ft. antenna beam pattern. The beam can be approximated as a circular Gaussian 22' wide at the half-power points. Convolving the true brightness distribution with a 22' Gaussian will reduce the true visibility amplitude by 0.085 at 130 λ. The visibility is measured only to 10% at 130 λ due to noise. Consequently a map produced by simply adding the single dish map and interferometer map will be consistent with the interferometer measurements; in other words, in the region of the (u,v) plane measured by the interferometer, the visibility of the single dish map is negligible.

On the other hand, a map produced by merely adding the interferometer map and single dish map will not be consistent with single dish observations because the interferometer map has significant visibility near zero spacing. To insure that the final map is consistent with single dish observations, the following procedure was used. First, the interferometer map is corrected for the antenna beam. Next the corrected interferometer map is convolved

with a 22' circular Gaussian thereby approximating smoothing by the 130 ft. antenna. The smoothed map is then subtracted out of the single dish map, and the resulting map and the corrected interferometer map are added directly. The procedure is repeated over the velocity range covered by the absorption line.

The resulting 21 cm absorption line profile at the center of L1495 is shown in fig. 4-9 and 4-10. In order to provide a quantitative description of the absorption line, a model was fitted to the data. Foreground hydrogen was neglected and the background brightness temperature as a function of velocity T(v) was described as a Gaussian.

$$T(v) = T_B \exp\left(-(v-v_B)^2/(2\sigma_B^2)\right)$$

The optical depth of hydrogen in L1495 was given by

$$\tau(v) = \tau_c \exp\left(-(v-v_c)^2/(2\sigma_c^2)\right)$$

Assuming the spin temperature T_c in the dust cloud is constant, then the observed 21 cm brightness must be

$$T(v)e^{-\tau(v)} + T_c(1 - e^{-\tau(v)}).$$

A computer program (provided by R. Crutcher) calculated a least squares fit to the data where possible parameters to be adjusted were T_c, v_c, τ_c, σ_c, T_B, v_B, and σ_B.

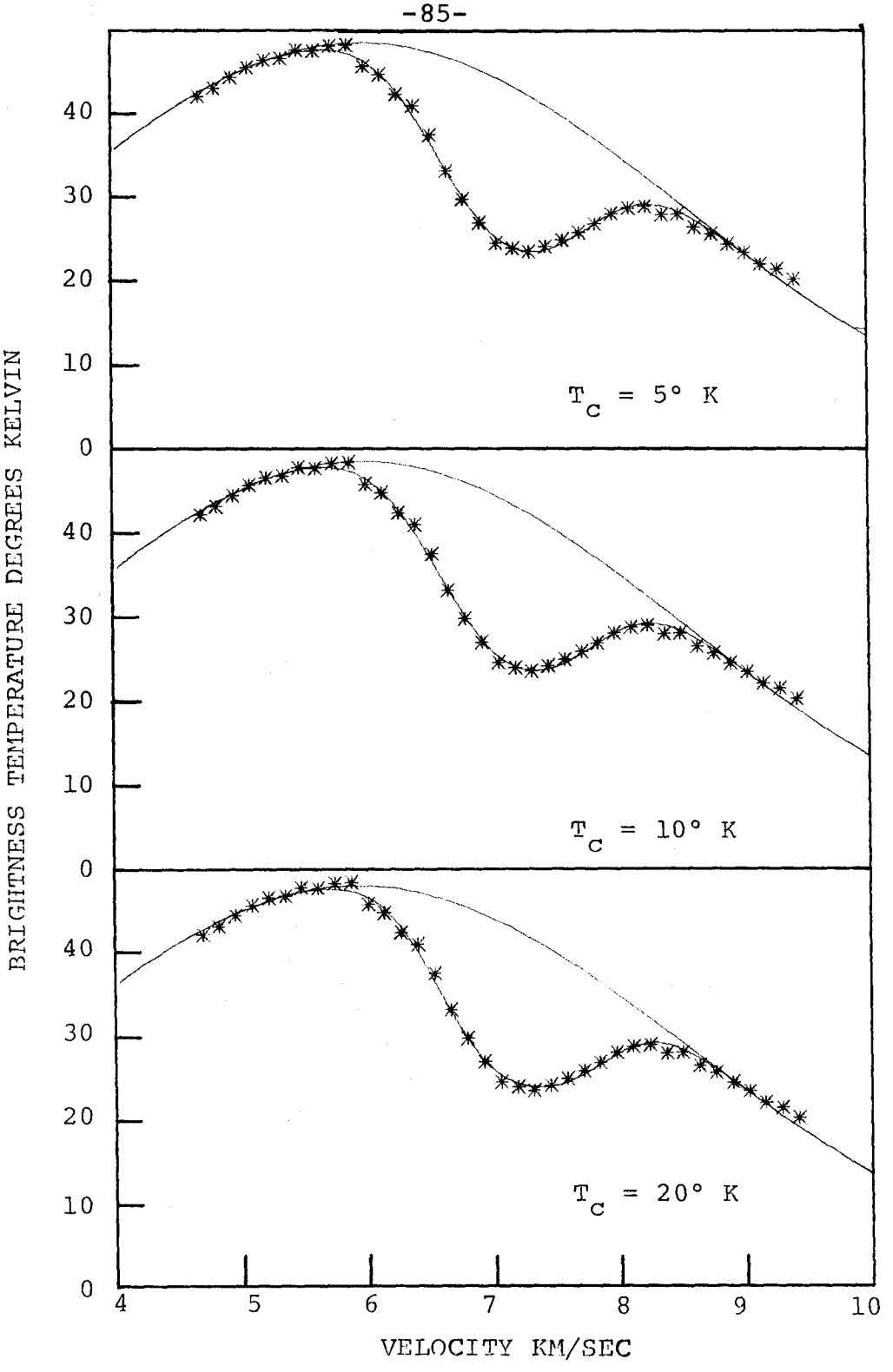

FIGURE 4-9. 21 cm absorption line at center of L1495. The line going through the data points is the best fit possible with T_c, the dust cloud temperature, fixed at the indicated values. The other line shows the background brightness temperature used in calculating the best fit.

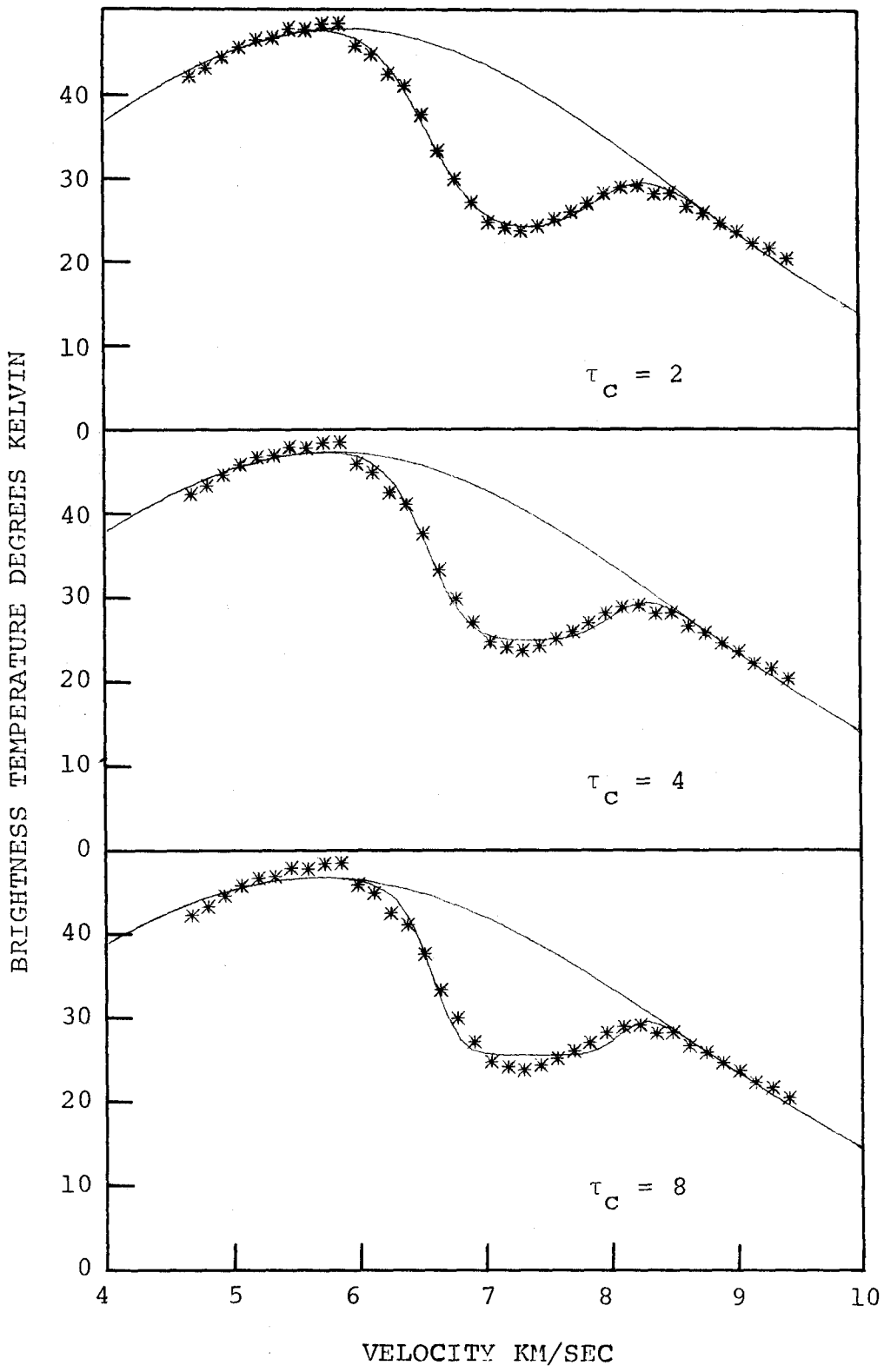

FIGURE 4-10. 21 cm absorption line at center of L1495. The line going through the data points is the best fit possible with τ_c, the optical depth, fixed at the indicated values. The other line shows the background brightness temperature used in calculating the best fit.

If all parameters are allowed to vary, the least squares program is divergent with $T_c \to -\infty$ and $\tau_c \to 0$. Either T_c or τ_c needs to be held fixed. Fig. 4-9 shows three best fits with T_c constrained to be 5, 10, and 20 degrees Kelvin, and in fig. 4-10 τ_c was constrained to be 2, 4, and 8. Table 4-1 tabulates results from the various fits where N_H is the columnar atomic hydrogen density.

One point becomes immediately obvious. T_c and τ_c are correlated. Within a certain range, it is not possible to distinguish between larger optical depth with hotter hydrogen and smaller optical depth with cooler hydrogen. A satisfactory fit is possible with the following limits:

$$0° \text{ K} < T_c \leq 20° \text{ K}$$

$$0.6 \leq \tau_c \leq 2$$

$$v_c = 7.27 \pm 0.04 \text{ km/sec}$$

$$\sigma_c = 0.51 \pm 0.04 \text{ km/sec}$$

$$10^{19} \text{ cm}^{-2} \leq N_H \leq 10^{20} \text{ cm}^{-2}$$

The expected columnar hydrogen density is greater than 10^{22} cm^{-2} so most of the hydrogen must be molecular and the residual atomic hydrogen is cold. Except for the velocity, the parameters which characterize the atomic hydrogen in L134 and L1495 are nearly identical. Apparently physical conditions in the two dust clouds are similar.

TABLE 4-1

LEAST SQUARES FIT PARAMETERS FOR L1495

T_C	τ_C	v_C	σ_C	T_B	v_B	σ_B	N_H	STANDARD ERROR
5.0	0.69	7.23	0.544	49.2	5.98	2.54	$8.7\ 10^{18}$	0.58
10.0	0.84	7.25	0.534	49.1	5.97	2.55	$2.1\ 10^{19}$	0.59
20.0	1.59	7.29	0.493	48.6	5.92	2.60	$7.3\ 10^{19}$	0.63
22.0	2.00	7.31	0.474	48.4	5.89	2.63	$9.7\ 10^{19}$	0.67
25.1	4.00	7.35	0.412	47.7	5.81	2.72	$1.9\ 10^{20}$	0.88
26.0	8.00	7.37	0.354	47.2	5.70	2.83	$3.4\ 10^{20}$	1.18

V. L1517

L1517 GENERAL DESCRIPTION

Fig. 5-1 is a photograph of L1517 centered upon the adopted position given in Table 2-1. It can be seen that L1517 does not appear to be a single homogeneous dust cloud but consists of 4 subcondensations. There is no evidence to indicate that L1517 is a faint emission nebula. The position of L1517 places it in the Taurus dust complex for which Racine (1968) has estimated a distance of 130 pc. Lack of foreground stars only indicates the dust cloud is not much further than about 300 pc.

AB Aurigae (HD 31293) is a 7th magnitude star situated on the southeast edge of L1517. Herbig (1960) has described this peculiar emission line star and estimated its distance to be 175 pc, but Racine (1968) gives 120 pc to the same star. CO observations of AB Aurigae and L1517 suggest the two objects are physically associated (Loren et al. 1973). The 6.0 km/sec velocity reported for CO agrees well with OH at 5.7 km/sec (Crutcher 1973) and H_2CO at 5.9 km/sec (Dieter 1973). A distance of 130 pc to L1517 will be adopted with the realization it may be in error by several tens of parsecs.

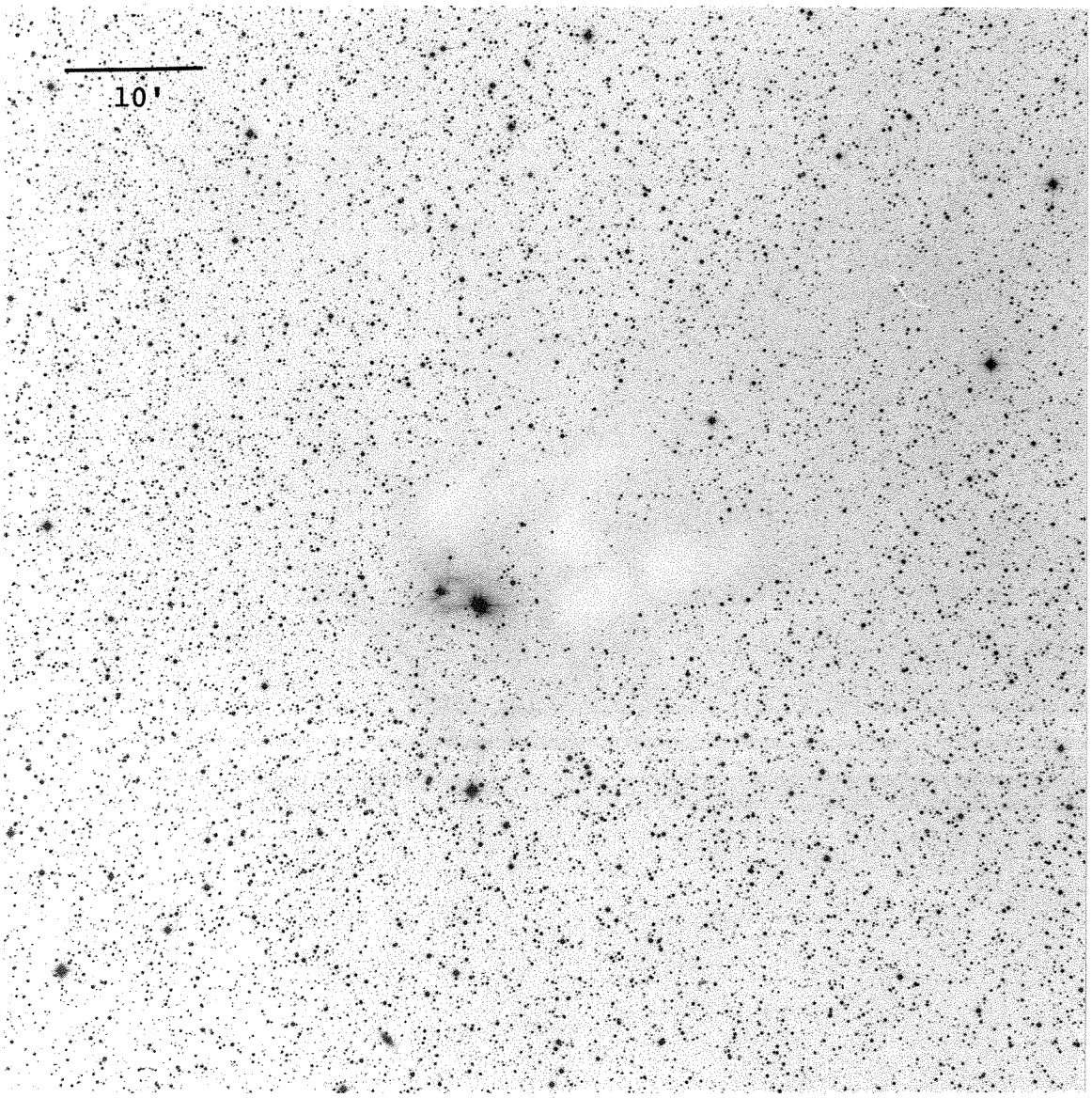

FIGURE 5-1. Photograph of L1517 taken from the red Palomar Sky Survey print. North is on top and east is on the left. Field of view is centered upon the position of L1517 given in Table 2-1. Scale is indicated in upper left corner.

L1517 RESULTS

In contrast to L134 and L1495, L1517 produces no readily apparent effect on the 21 cm brightness temperature as measured by the interferometer or single dish observations. Figure 5-2 through 5-6 are representative samples of low velocity resolution (2 km/sec) HI emission profiles. In total about 80 positions were observed over a grid of points centered on L1517. Comparison between the on-cloud profile (fig. 5-2) and the 8 positions off cloud (fig. 5-3 to 5-6) shows no obvious feature which can be attributed to the presence of L1517. There is a prominent dip (perhaps self-absorption) in the emission profile at about 0 km/sec; however, this feature appears in both on-cloud and off-cloud line profiles and it is not at the OH and H_2CO velocities. The on-cloud 21 cm profile has no unusual feature which can be attributed to the dust cloud.

A comment is needed here about the technique of subtracting on-cloud profiles from off-cloud profiles. In the case of L1517, the HI line emission profile changes in a complicated manner (probably unrelated to the dust cloud) over a scale length comparable to the dust cloud diameter. Consequently the difference between an on-cloud and off-cloud profile is in large part produced by

physical circumstances unrelated to the presence of the dust cloud. Generalizing from this particular case, any claim attributing differences between on-cloud and off-cloud profiles to the dust cloud must be viewed with caution especially if there is no independent corroborative evidence.

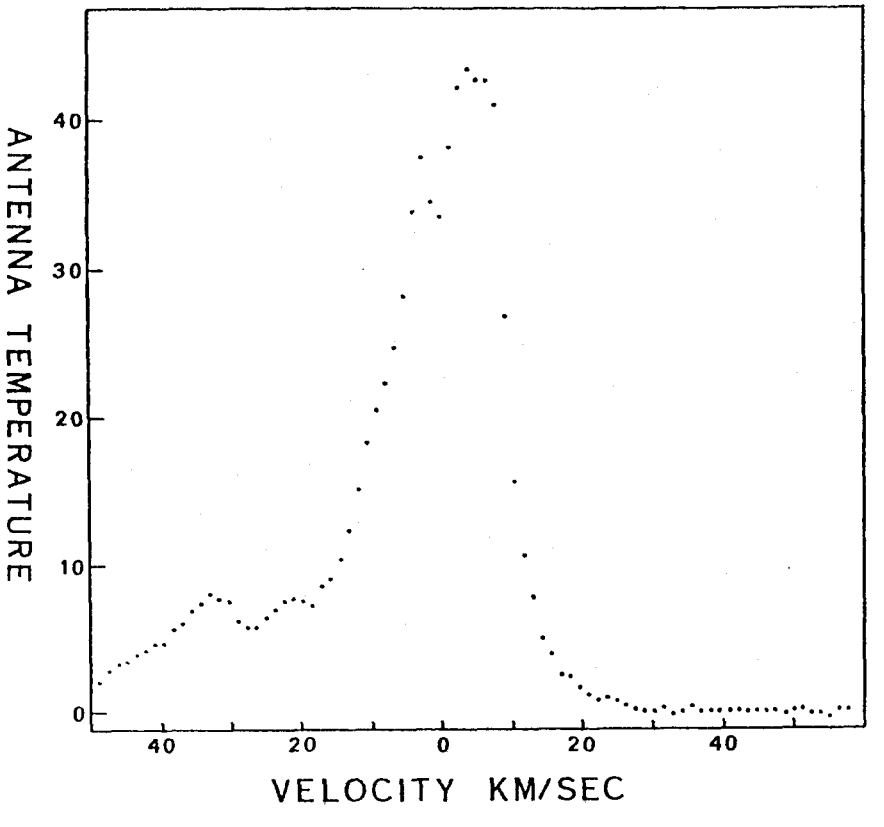

FIGURE 5-2. Hydrogen 21 cm line emission profile measured with antenna centered on L1517. Ordinate is antenna temperature in degrees Kelvin and abscissa is velocity with respect to the local standard of rest.

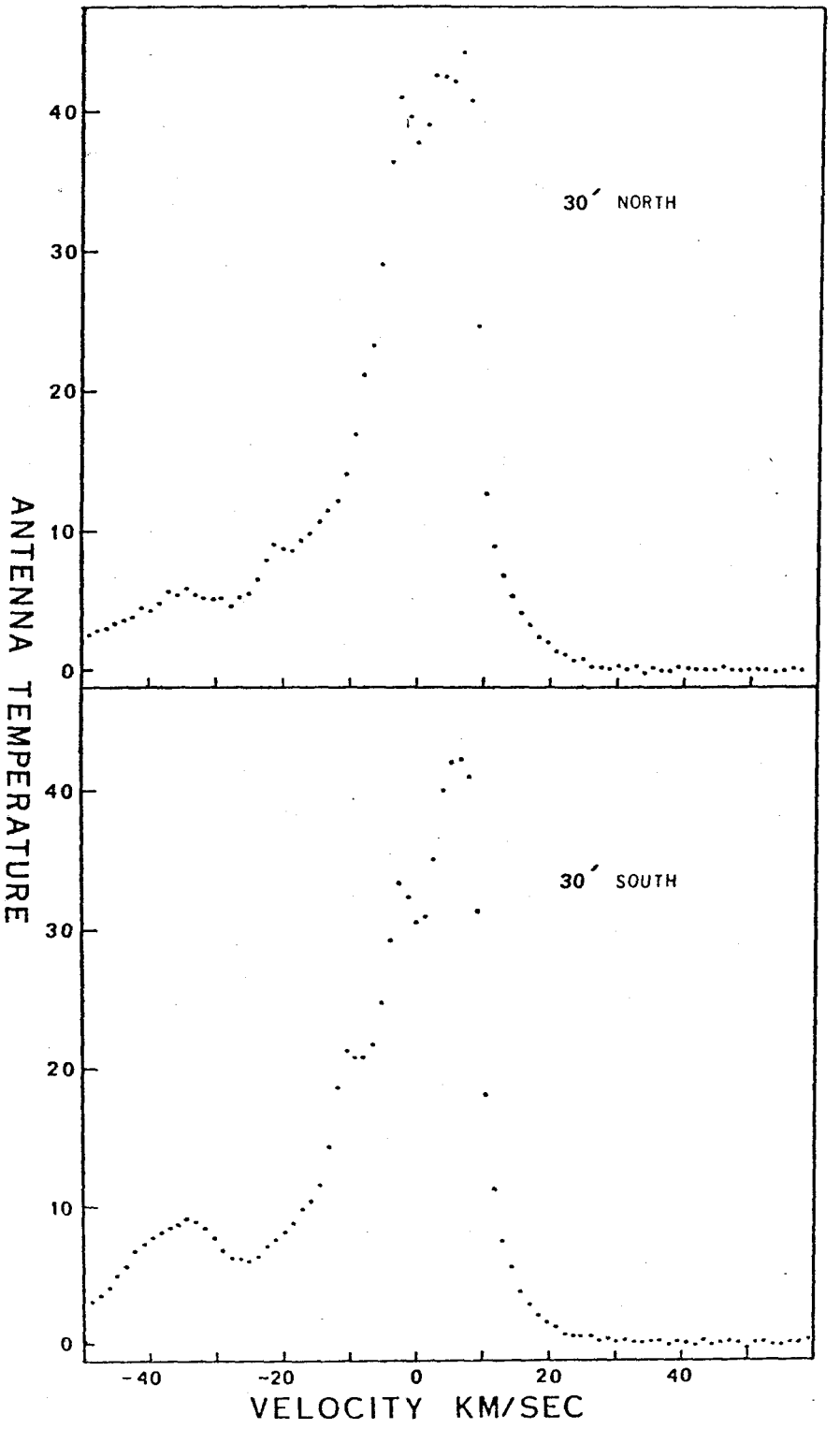

FIGURE 5-3. Hydrogen 21 cm line emission profiles measured at two positions 30' north and south of L1517. Ordinate is antenna temperature in degrees Kelvin and abscissa is velocity with respect to local standard of rest.

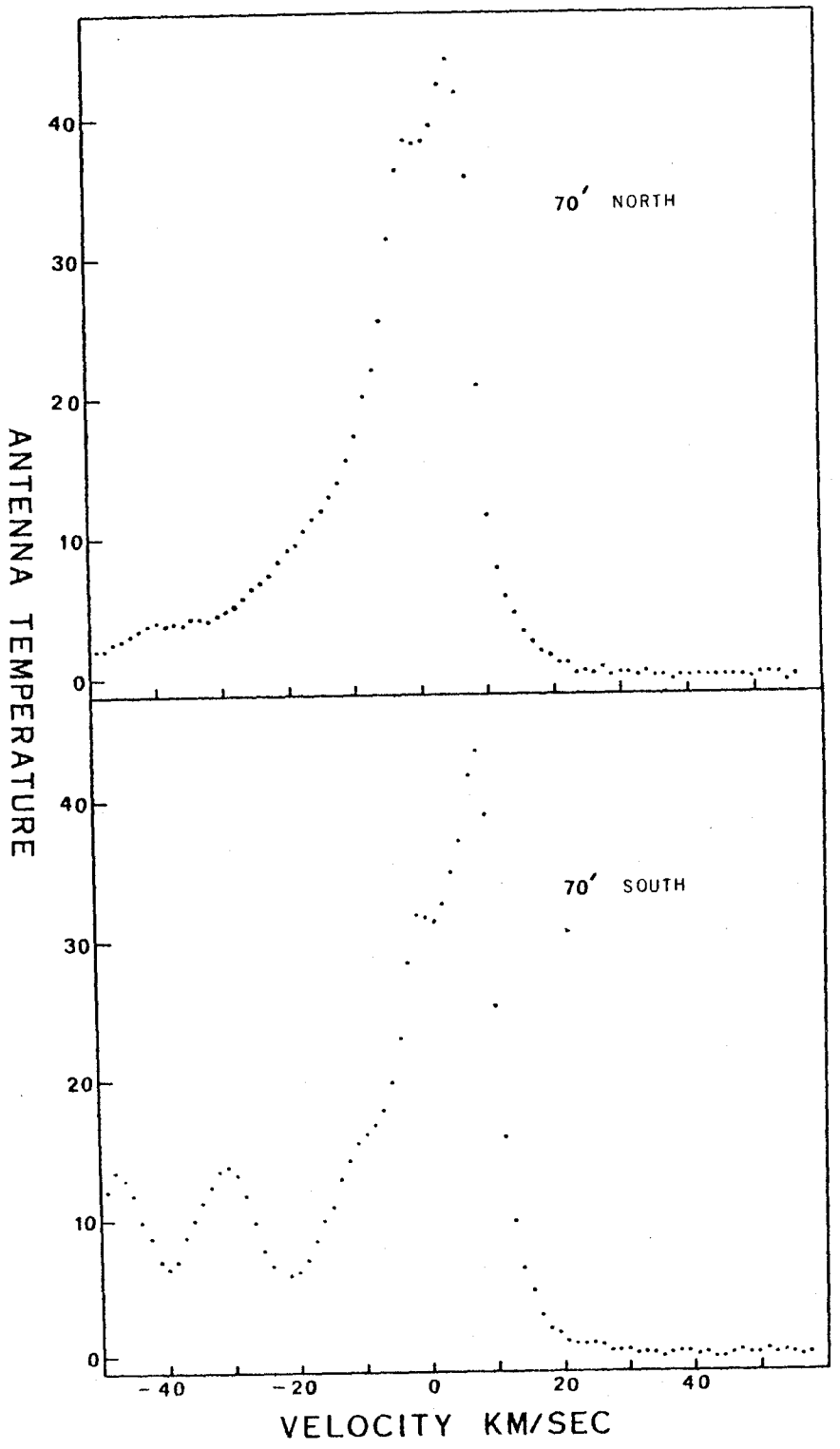

FIGURE 5-4. Hydrogen 21 cm line emission profiles measured at two positions 70' north and south of L1517. Ordinate is antenna temperature in degrees Kelvin and abscissa is velocity with respect to local standard of rest.

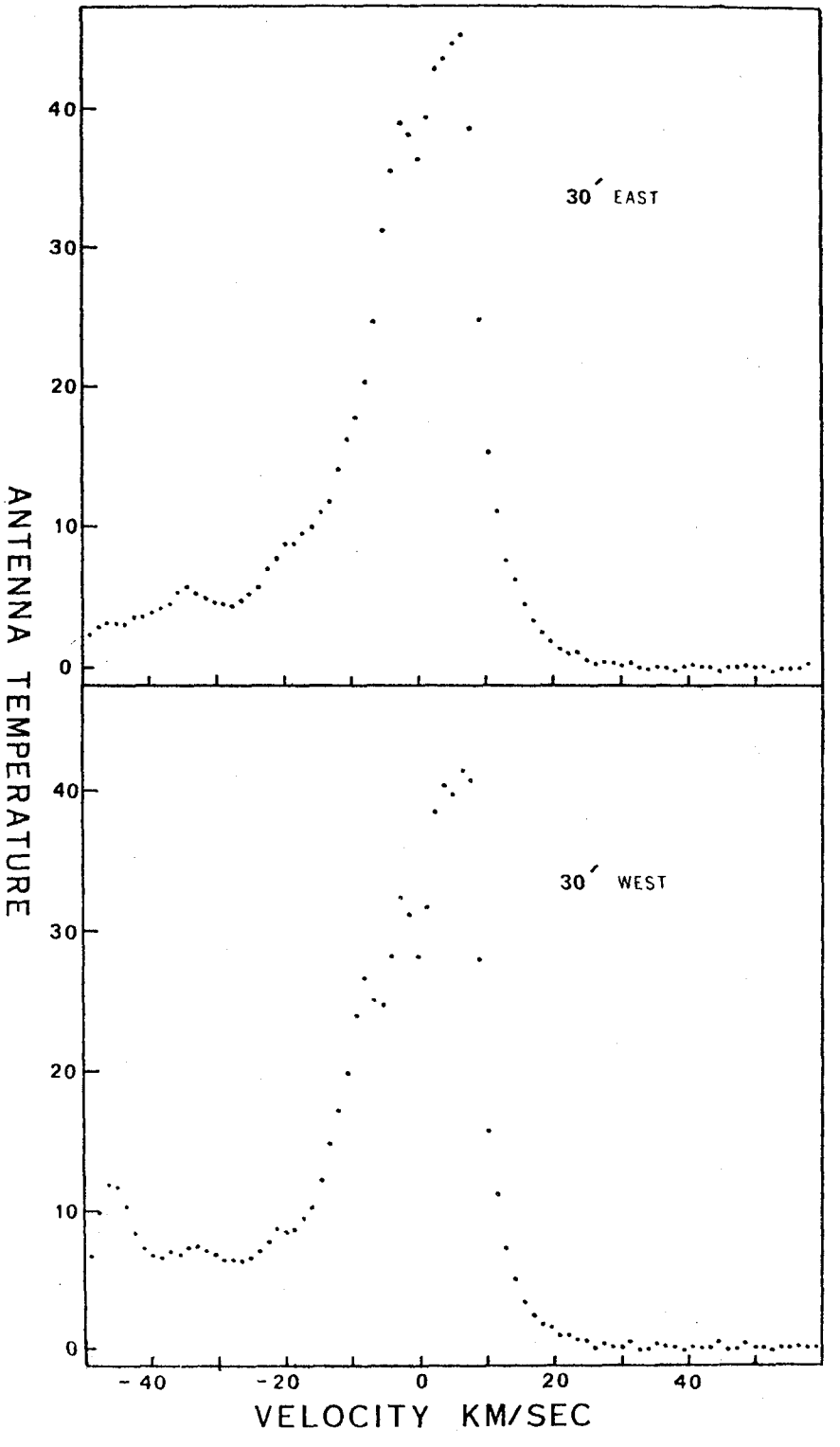

FIGURE 5-5. Hydrogen 21 cm line emission profiles measured at two positions 30' east and west of L1517. Ordinate is antenna temperature in degrees Kelvin and abscissa is velocity with respect to local standard of rest.

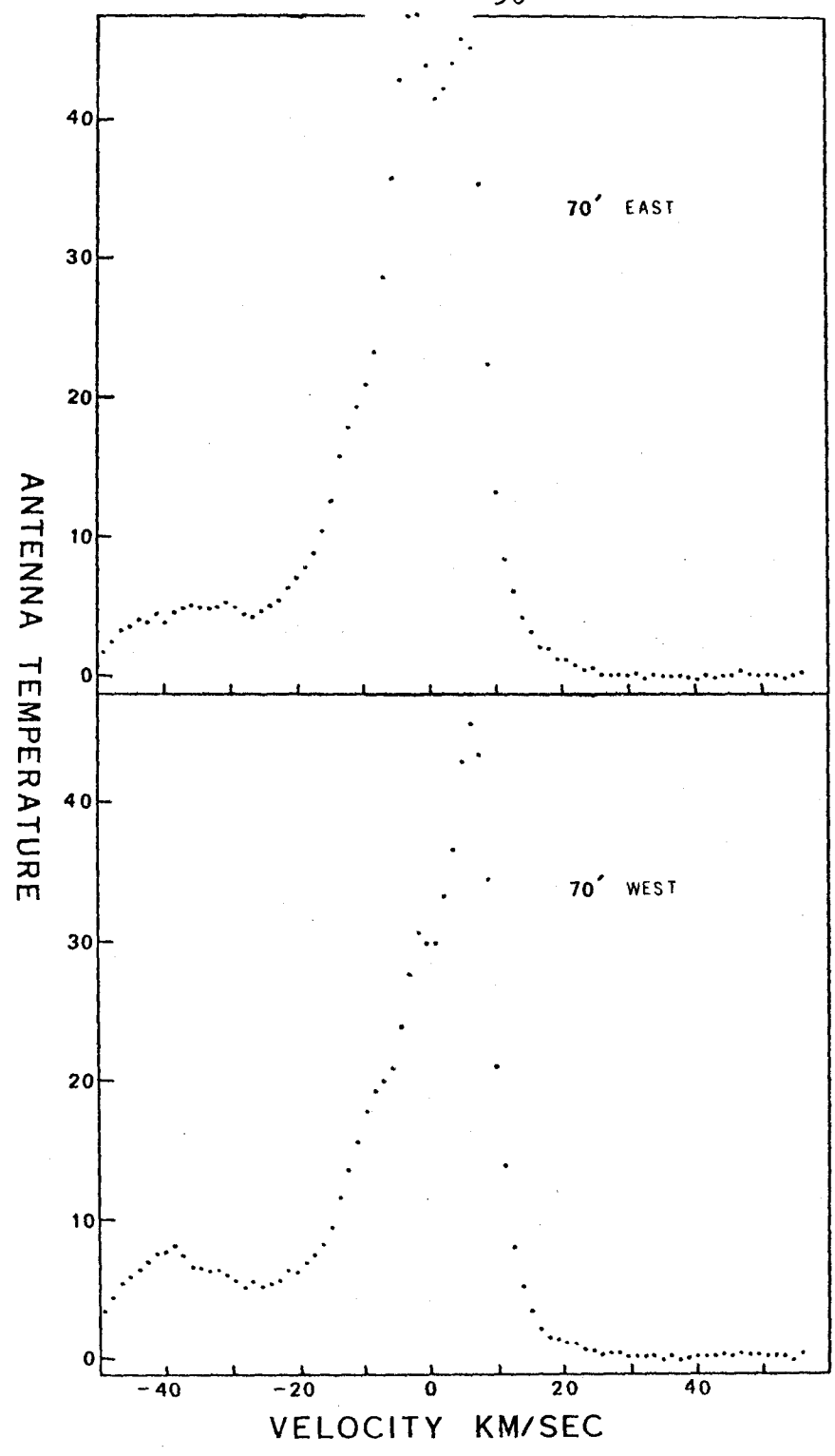

FIGURE 5-6. Hydrogen 21 cm line emission profiles measured at two positions 70' east and west of L1517. Ordinate is antenna temperature in degrees Kelvin and abscissa is velocity with respect to local standard of rest.

Detection of molecular line radiation determines a velocity at which HI in the dust cloud might be expected assuming HI and the molecules are at the same velocity. OH was detected in L1517 at 5.7 km/sec; therefore, single dish observations with a high velocity resolution (0.2 km/sec) were made centered on 6 km/sec. The on-cloud HI profile is shown in fig. 5-7 where data from three separate observations is plotted. A line fitted by eye is drawn and this on-cloud profile has been superposed

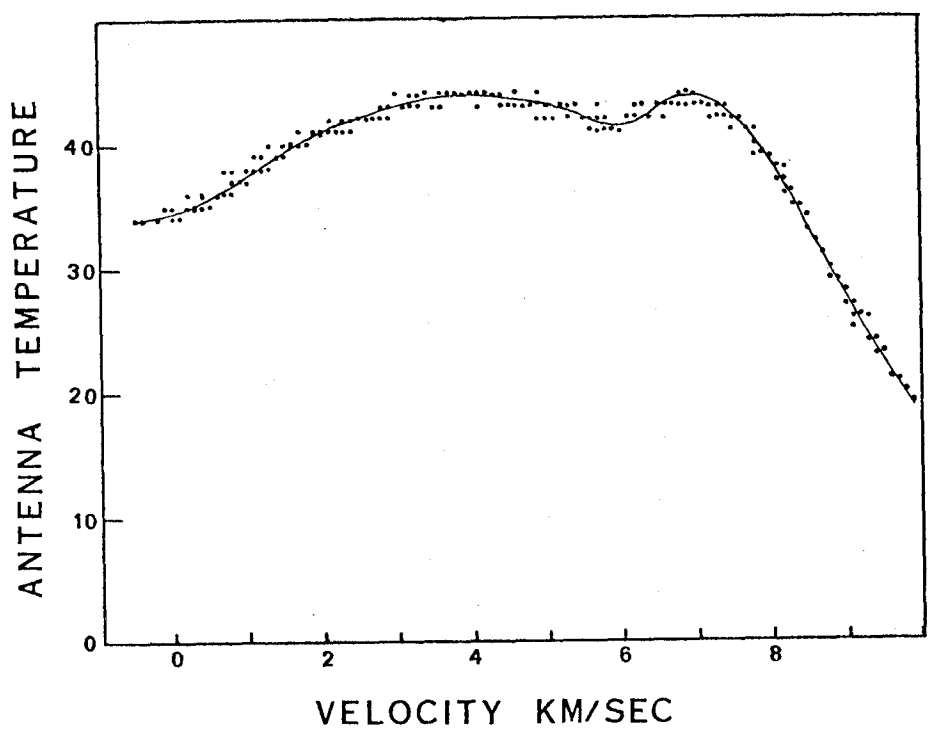

FIGURE 5-7. Hydrogen 21 cm line emission profile measured with antenna centered on L1517. Ordinate is antenna temperature in degrees Kelvin and abscissa is velocity with respect to local standard of rest.

upon the off-cloud data (fig. 5-8 and 5-9) in order that comparisons may be more readily made. The emission profile dip at 6 km/sec (fig. 5-2) might be due to hydrogen in the dust cloud, but the decrease in temperature is too small to make any definite conclusion.

As with single dish observations, the interferometer data indicates no detectable 21 cm feature which may be attributed to L1517. At this point a few remarks need to be made upon how the interferometer data were examined for significant signals. Due to the excessive computer time required, the visibility was not inverted at every velocity where data were available. A priori, the source structure was unknown; therefore, the visibility could not be simply averaged to find those velocities at which the signal was above the noise. The following procedure was used instead. Let $[V_j]$ be a chronologically ordered set of visibility measurements at a given spacing and velocity (V_j is a complex number and V_j^* is its complex conjugate). For all possible pairs of successive measurements, V_j and V_{j+1}, determine if V_j and V_{j+1} were measured within some time interval Δt. If not, disregard the pair, but if so, determine the quantity

$$S_j = \frac{(V_j + V_{j+1})\ (V_j + V_{j+1})^* - V_jV_j^* - V_{j+1}V_{j+1}^*}{2}$$

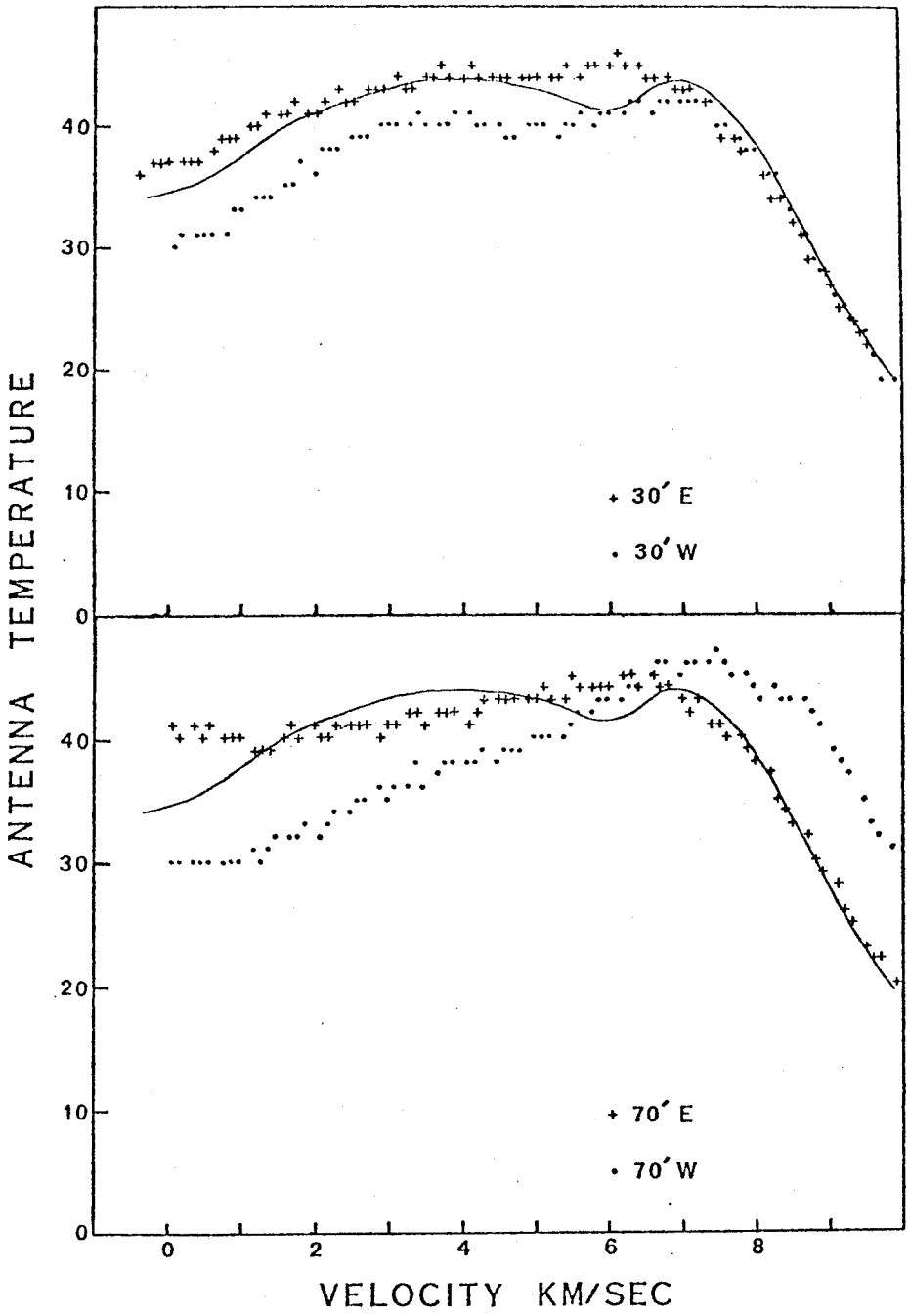

FIGURE 5-8. Hydrogen 21 cm line emission profile centered on L1517 (solid line) compared with line profiles at positions east and west of L1517. Ordinate is antenna temperature in degrees Kelvin and abscissa is velocity with respect to local standard of rest.

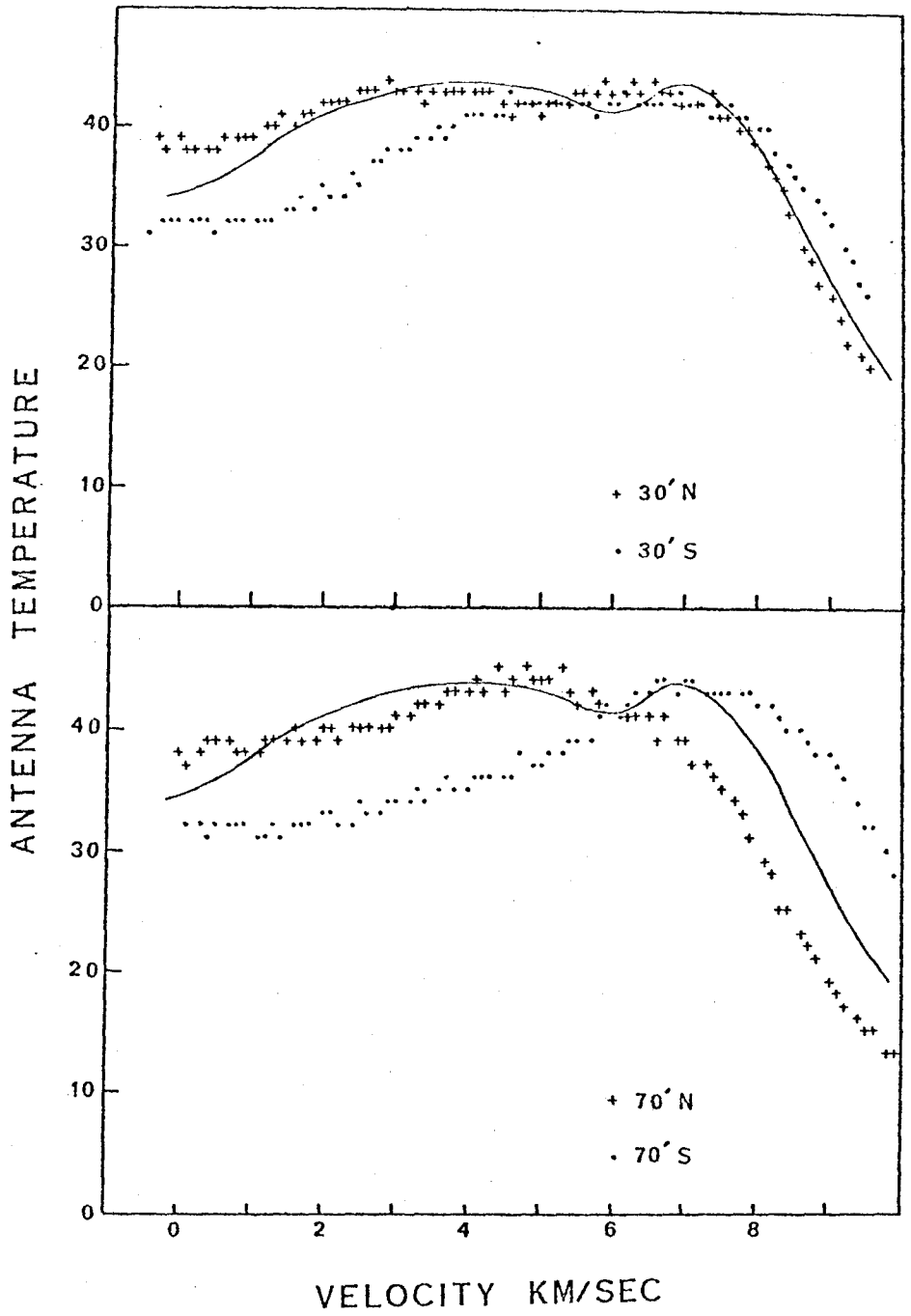

FIGURE 5-9. Hydrogen 21 cm line emission profile centered on L1517 (solid line) compared with line profiles at positions north and south of L1517. Ordinate is antenna temperature in degrees Kelvin and abscissa is velocity with respect to local standard of rest.

Finally calculate $\frac{1}{N}\sum_j S_j$ where N is the total number of terms in the summation. If there is only noise, the phases of successive pairs of measurements must be uncorrelated and in the limit $N \to \infty$, the above summation must approach zero. On the other hand, if there is a source present and Δt is sufficiently short (V_j and V_{j+1} are sampled sufficiently close together in the (u,v) plane), the phases of V_j and V_{j+1} will be about the same and the above summation will be close to the average of the visibility amplitude squared.

In fig. 5-10 the quantity $\pm\sqrt{\frac{1}{N}\left|\sum_j S_j\right|}$ versus velocity is plotted for L1517 and L134 where the sign is the same as for the summation of S_j. It can be seen that the visibility amplitude is greatest at around -8 km/sec, but at 5.7 km/sec there is nothing much above the noise or anything unusual. The graph for L134 has been included to demonstrate the usefulness of this procedure as a purely empirical method to find the important velocities. Based mainly upon the velocity discrepancy, it can be concluded that the large visibility amplitude at -8 km/sec is not caused by the dust cloud which presumably is at 5.7 km/sec OH velocity (Crutcher 1973). Nevertheless, the data at -8 km/sec was Fourier transformed and the resulting brightness temperature contour map is superposed on a photograph of L1517 in fig. 5-11. There is poor correlation between the contour map and the visible dust.

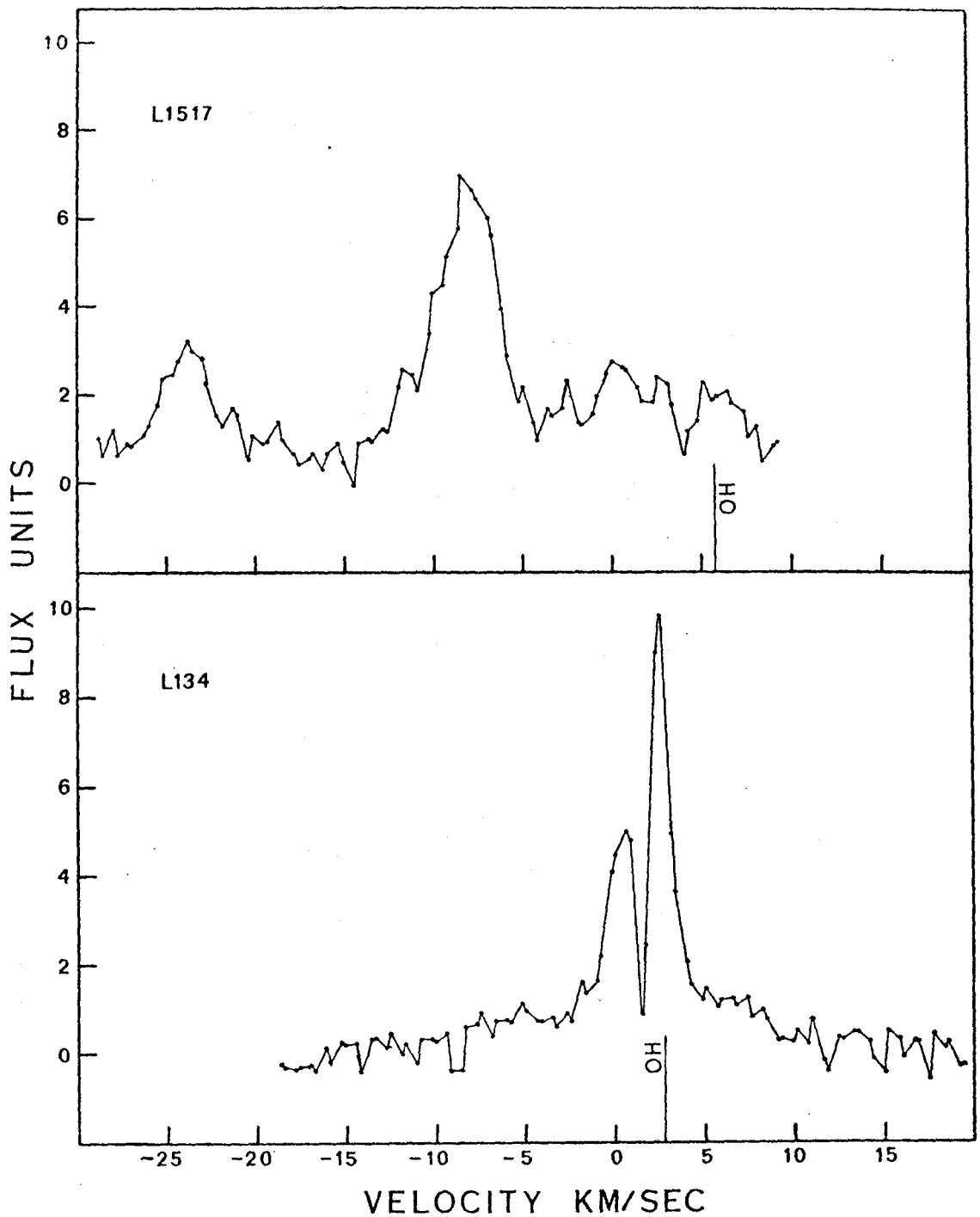

FIGURE 5-10. Plot of a quantity approximating the average fringe amplitude (see text for more precise definition) at the 100 ft. east-west baseline versus velocity for L1517 and L134. Velocity at which OH emission has been detected is indicated.

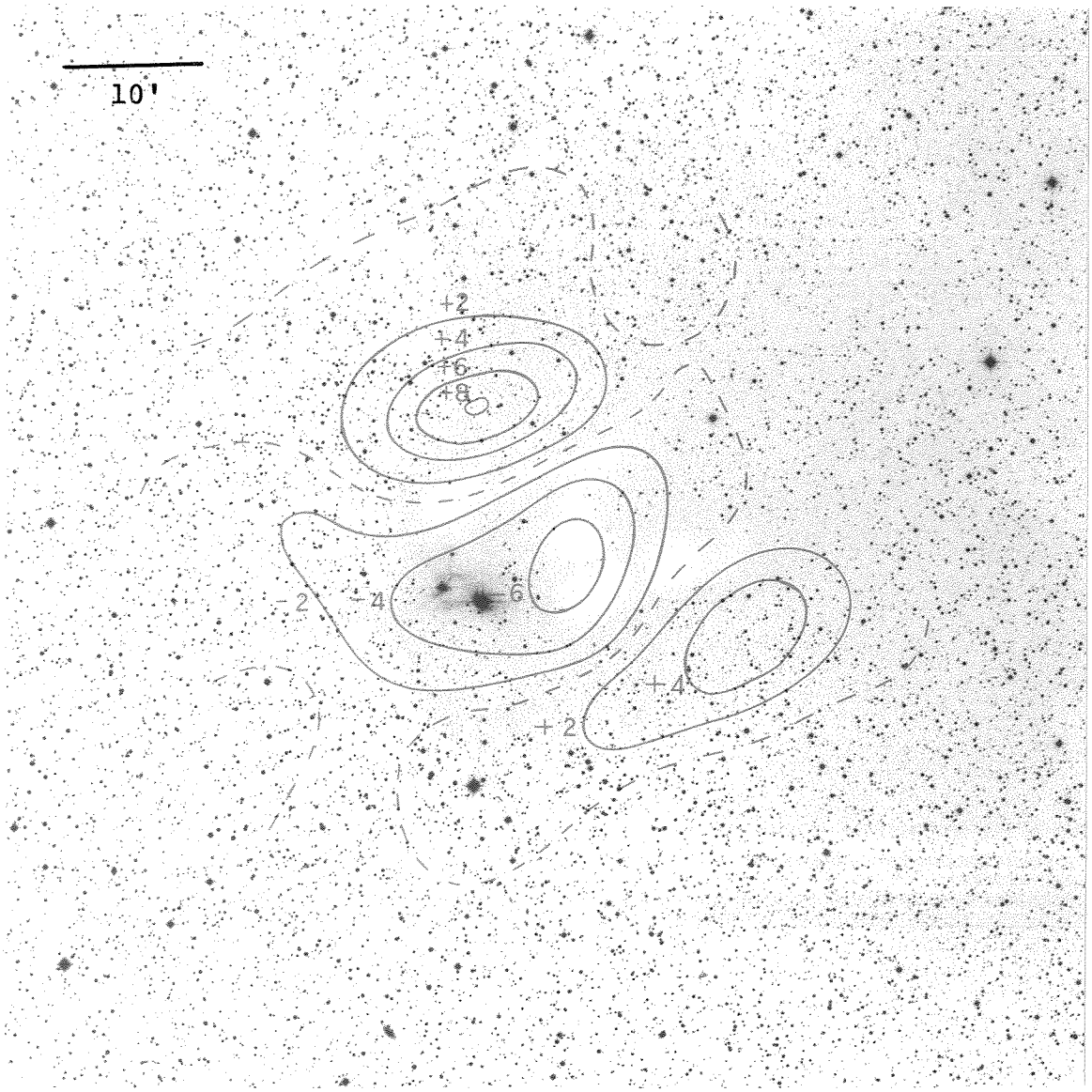

FIGURE 5-11. Brightness temperature contour map of L1517 from interferometer observations at -7.7 km/sec. Contour interval is 2° K and synthesized beam diameter is 7'. Scale is indicated in upper left corner. Zero spacing information is missing; therefore, the dashed contour lines were set at 0° K for reference. No correction has been made for the antenna beam. Noise level is 1° K.

L1517 DISCUSSION

Failure to detect L1517 at 21 cm agrees with negative results obtained by Heiles (1969) for most of the 48 dust clouds observed in a survey. It is doubtful further observations with higher sensitivity or greater angular resolution will detect L1517. The observations are not limited by instrumental noise but by background brightness fluctuations which are as great or greater than any effect produced by L1517. Because of such background fluctuations, it is not possible to ascertain whether or not the emission profile dip at 6 km/sec is due to hydrogen in the dust cloud.

Although the 21 cm emmision line has been studied for over two decades, details about the hydrogen spatial distribution and temperature are not well determined. The evidence available indicates a complex situation; variations of temperature and density are large. To detect and study HI in dust clouds, an unambiguous means of distinguishing the dust cloud structure from background fluctuations must be available. Detection of molecular lines is an important aid because hydrogen will presumably be around the same velocity. OH at 5.7 km/sec has been detected in L1517 (Crutcher 1973). H_2CO observations are ambiguous. Dieter (1973) detected H_2CO at 5.9 km/sec in L1517 but at 1.5 km/sec in

L1519.* Positions given by Lynds (1962) for L1517 and L1519 differ by 6.5'. The antenna used to make the H_2CO observations had a 10' HPBW. Unless the existence of a large velocity gradient is confirmed, 5.9 km/sec should be the accepted H_2CO velocity since this agrees with OH observations. L1517 produces no change in the 21 cm brightness temperature greater than about 5° K at 5.9 km/sec. The failure to detect L1517 may be explained by a number of factors.

The amount of foreground hydrogen will influence the detection of the dust clouds. Based upon the sparsity of foreground stars, none of the dust clouds can be more than a few hundred parsecs away. The amount of atomic hydrogen within a few hundred parsecs of the sun has been measured by observing interstellar Lyman α absorption lines. Jenkins and Savage (1974) estimate the average hydrogen density in the solar neighborhood to be 0.25 cm^{-3}; however, the density varies considerably from the average, from values greater than 2 cm^{-3} to less than 0.1 cm^{-3} depending upon the direction

* There is an unavoidable ambiguity in naming dust clouds due to the arbitrary nature by which a given obscuration may be divided into dust clouds. For example, in fig. 5-1 a region of heavy obscuration is located at the center of the photograph. In this paper L1517 was chosen to refer to the entire area of heavy obscuration (about 20' by 20') as a matter of convenience. Lynds (1962) breaks this region into several dust clouds with different names. As a consequence, L1519 and L1517 refer to different parts of what is considered one dust cloud in this paper.

of observation. The possibility that a denser than average hydrogen cloud lies in front of L1517 cannot be precluded; such a situation could explain the failure to detect L1517 at 21 cm. On the other hand, if the average hydrogen density is 0.25 cm^{-3} or less, then foreground hydrogen will not have an important effect. For example, over a 100 pc path length, spin temperature 100° K, density 0.25 cm^{-3}, velocity dispersion 3 km/sec, the resulting optical depth is about 0.05 at maximum.

If the temperature in the cloud equals the background brightness temperature, the dust cloud will not be detected. Assuming such an hypothesis, a large amount of hydrogen in the dust cloud could go undetected. At 6 km/sec the brightness temperature toward L1517 is 55° K (see fig. 5-7; dividing the antenna temperature by 0.75, the beam efficiency, gives the brightness temperature). HI observations indicate the spin temperature in L134 and L1495 is less than 20° K. A 55° K spin temperature in L1517 seems unlikely unless a source of energy is present in L1517 which is lacking in the other dust clouds. AB Aurigae is the 7th magnitude A0ep star just off the southeast edge of L1517. The possibility that L1517 could receive appreciable UV photons from AB Aurigae capable of disassociating H_2 was considered. The star would have to be within 0.2 pc of the dust cloud to produce a flux

typical of interstellar space at 1000 A (Habing 1968). It does not seem likely that AB Aurigae is a significant source of energy for L1517.

Two possible explanations for not detecting atomic hydrogen in L1517 have been discussed. (1) A large amount of foreground hydrogen could explain the data. This is an ad hoc assumption but,nevertheless, plausible. With such an assumption, nothing can be deduced about L1517. (2) The hydrogen spin temperature in L1517 is about the same as the background brightness temperature, 55° K. The main weakness of this argument is that there is no apparent reason why hydrogen in L1517 should be hotter than the upper limit of 20° K found for hydrogen in L134 and L1495. A third possibility is that hydrogen in L1517 has about the same temperature and velocity dispersion as L1495 and L134, but the hydrogen is undected because the amount of atomic hydrogen is smaller. A temperature depression of 5° K covering the area of L1517 would have been detected by the interferometer. Assume the atomic hydrogen in L1517 has a 20° K spin temperature and the velocity dispersion σ is 0.5 km/sec. Foreground hydrogen will be neglected. The interferometer is sensitive to the difference between the brightness in the cloud and the background; therefore

$$(T_C - T_B)(1 - e^{-\tau}) \leq 5° \text{ K}$$

where T_C is the spin temperature in the dust cloud, T_B is the background brightness temperature and τ is the maximum optical depth of hydrogen in the dust cloud. The columnar atomic hydrogen density cannot exceed $7\ 10^{18}\ cm^{-2}$ without producing a 5° K absorption line. The expected amount of hydrogen can be estimated using the relation on page 2; in such a case, $N \geq 10^{22}\ cm^{-2}$. Hollenbach et al. (1971) predict that the columnar atomic hydrogen density N_H is related to the total hydrogen density n by

$$N_H \simeq 8.5\ 10^{22} n^{-1}\ \ cm^{-2}$$

If N_H is less than $7\ 10^{18}\ cm^{-2}$, then n is greater than $10^4 cm^{-2}$. The accuracy of the above equation at very high densities is doubtful because the model used to make the calculations is highly idealized and because destruction mechanisms other than UV photons may become important at very high densities (Solomon and Werner 1971). Nevertheless on a qualitative basis, if L1517 is a considerably denser dust cloud than L134 and L1495 (Jean's length is inversely proportional to the square root of the density; photographs of L1517 suggest fragmentation into small globules), the residual amount of atomic hydrogen might be sufficiently small to explain the 21 cm observations.

VI. CONCLUDING REMARKS AND SUMMARY

The observations have demonstrated that aperture synthesis is a useful technique for studying compact dust clouds. The major results may be summarized as follows: (1) The contrast between the background and dust cloud 21 cm brightness varies considerably. Some dust clouds (e.g. L134) are easily detected, but others (e.g. L1517) produce no change in the 21 cm emission greater than the typical background fluctuations. (2) In dust clouds where atomic hydrogen is detected, the hydrogen is cold (less than 20° K) and is confined to the region where obscuration by dust is great. The amount of atomic hydrogen is at least 100 times less than the expected hydrogen content based upon the magnitude of optical extinction. (3) No substructure was detected in the three dust clouds that were studied.

Factors extraneous to the dust clouds (e.g. foreground hydrogen) are partially responsible for the variation in the visibility of dust clouds. On the other hand, physical conditions in dust clouds undoubtedly change from cloud to cloud and can influence the ease with which the dust cloud is detected. The optical appearance of L1517 suggests that it is composed of several subcondensations, and

perhaps the subcondensations are sufficiently dense that the amount of atomic hydrogen is too small to detect. A study seeking a correlation between dust cloud size and the amount of atomic hydrogen could help confirm or reject this conjecture.

In the two dust clouds where a 21 cm absorption line is detected, the atomic hydrogen has similar properties (see page 56 and 87). The temperature is less than 20° K; the columnar atomic hydrogen density is between 10^{19} and 10^{20} cm^{-2}; the velocity dispersion is 0.5 km/sec. The usual explanation for the lack of atomic hydrogen is that most of the hydrogen in dense dust clouds is molecular. The observations are consistent with a theory proposed by Hollenbach et al. (1971) which assumes equilibrium between molecular hydrogen formation on grains and destruction by UV photons.

One interesting result is the detection of two velocity components in L134 and its possible interpretation. The evidence either in favor of or against a collapsing dust cloud is not strong. The free fall velocity for L134 is about 0.5 km/sec, but the actual collapse velocity could be substantially different. The observed velocity difference is 2 km/sec and is sufficiently close to 0.5 km/sec

that collapse cannot be precluded. An alternative explanation is that the two components in L134 have arisen as a result of fragmentation thereby leaving two smaller condensations orbiting around each other. The evidence is insufficient at the present time for any conclusions to be made. The failure to detect L1517 is disappointing since its optical appearance suggests some sort of fragmentation. In L134 where the dust cloud is detected, there is no evidence of substructure within either velocity component. If dust clouds of several hundred solar masses are to form stars, at some stage they must fragment. Perhaps 21 cm observations will not detect fragmentation if atomic hydrogen is confined to a shell surrounding the overall dust cloud. In any case more detailed 21 cm observations of a larger sample of dust clouds would help elucidate their structure and kinematics.

The transformation of the interstellar medium into stars involves a density increase by 24 orders of magnitude. Much observational and theoretical work needs to be done to understand this transformation. The dust clouds almost certainly play some role in the birth of stars, but our knowledge about them is far from complete. Dust clouds come in all sizes and shapes, and all of them need to be studied. However, isolated roundish globules far from

HI regions are of special importance because these clouds have the simplest structure and are in the simplest interstellar environment possible. Surely the highly idealized theoretical models come closer to describing reality in the case of isolated globules than other types of dust clouds which in photographs often show very intricate structure. The possibility of making meaningful comparisons between observations and theoretical models seems best for the isolated globules. For future work more detailed observations of large globules are needed. The narrow absorption line in L134 may provide a good opportunity to observe Zeeman splitting. A measurement of the magnetic field would be very interesting. The total obscuration through very dense dust clouds needs to be determined; perhaps infared observations may be useful in this respect. After the data on simple dust clouds can be understood, one is in a better position to understand dust clouds of all types.

APPENDIX

BRIGHTNESS TEMPERATURE MAPS

The purpose of this section is to provide a description about the relation between the actual brightness temperature distribution in the sky and the clean maps produced by the reduction program used in this paper. In addition the problem of combining single dish observations with interferometer data to form one map is considered. The visibility is a hermitian function because the brightness temperature is a real function. Capital letters will designate functions in the (x,y) space and the corresponding small letters are their Fourier transforms. The symbol "*" indicates a convolution operation, i.e.

$$y(x) * z(x) = \int_{-\infty}^{\infty} y(x-x')\, z(x')\, dx'$$

The interferometer observes a portion of the celestial sphere sufficiently small that the brightness temperature $T(x,y)$ can be represented as a flat surface where x and y are angles measured in two orthogonal directions from the center of the field. $t(u,v)$ is not measured directly by the interferometer because the interferometer responds to $T(x,y)P(x,y)$ where $P(x,y)$ is the power pattern of the antenna (also called the primary beam). Consequently the visibility measured by the interferometer is not the true

visibility $t(u,v)$ but rather $t(u,v)*p(u,v)$.

In practice one does not continuously measure $t(u,v)*p(u,v)$, but $t(u,v)*p(u,v)$ is sampled at various points in the (u,v) plane. Let $s(u,v) = \sum W_k \delta(u-u_k)\delta(v-v_k)$ represent the sampling where W_k is a weighting factor for the kth point. The summation is over some finite set of points $[u_k,v_k]$ where measurements were made. The corresponding transform $S(x,y)$ is the dirty beam, and $\Big(T(x,y)P(x,y)\Big)*S(x,y)$ is the dirty map.

Next a set of point sources are found which when convolved with the dirty beam gives back the dirty map. Let $D(x,y) = \sum A_j \delta(x-x_j)\delta(y-y_j)$ be a set of point sources which satisfies the equation

$$D(x,y)*S(x,y) = \Big(T(x,y)P(x,y)\Big)*S(x,y)$$

One can then infer that the corresponding Fourier transforms are also equal.

$$d(u,v)s(u,v) = \Big(t(u,v)*p(u,v)\Big)s(u,v)$$

Thus a set of point sources has been found whose complex visibility at the sampled points is the same as that measured by the interferometer. It is also possible to make some statement about how well $d(u,v)$ and $t(u,v)*p(u,v)$ must

agree in regions between the sampled points. $t(u,v)*p(u,v)$ must be a relatively smooth function since a convolution operation produced it. Assume $s(u,v)$ satisfies the sampling theorem, i.e. $t(u,v)*p(u,v)$ has been measured at points sufficiently close that interpolation can determine its value continuously. If $d(u,v)$ can be guaranteed to be as smooth as $t(u,v)*p(u,v)$, then $d(u,v)$ and $t(u,v)*p(u,v)$ must agree continuously (not just at the sampled points) over the sampled region in the (u,v) plane. Naturally $d(u,v)$ can be made as smooth as $t(u,v)*p(u,v)$ by limiting the area over which point sources are allowed to a region comparable to $P(x,y)$, i.e. no point sources in $D(x,y)$ are allowed outside the primary beam.

Because $D(x,y)$ is a set of point sources, its fringe amplitude will be appreciable well beyond the maximum limits in the (u,v) plane where observations were made. By convention one usually sets the visibility to zero in this outer region. In other words the final map should not contain spatial structures which would have been smeared out by the limited resolution available. Let $b(u,v)$ be some function (usually a Gaussian) which is about unity inside and zero outside the region of the (u,v) plane which was actually sampled. Multiply $d(u,v)$ by $b(u,v)$, or equivalently $D(x,y)$ is convolved with $B(x,y)$, the clean

beam, to form $D(x,y)*B(x,y)$ the clean map.

To summarize, the interferometer measures the Fourier transform of $T(x,y)P(x,y)$ over some limited region in the (u,v) plane. The reduction program produces a clean map $M(x,y)$ equal to $D(x,y)*B(x,y)$. In that part of the (u,v) plane where measurements were made, $m(u,v)$ is consistent with the data. $m(u,v)$ approaches zero in areas far from the origin where no measurements were made. The value of the visibility near the origin is generated by the clean program and will probably differ considerably from $t(u,v)*p(u,v)$. The remaining discussion will consider combining single dish observations and interferometer data to produce one map. The purpose of performing single dish observations is to fill the gap near the origin in the (u,v) plane where interferometer data is missing.

Let $F(x,y)$ be the power pattern of the antenna used for single dish observations and $T_a(x,y)$ be a quantity proportional to the antenna temperature when the antenna is pointed at position (x,y).

$$T_a(x,y) = T(x,y)*F(x,y)$$

$T_a(x,y)$ is usually known at some grid of points; however, for simplicity assume it is known continuously. The

corresponding operation in (u,v) space is $t(u,v)f(u,v)$. The objective is to determine $t(u,v)*p(u,v)$ near the origin; therefore, we may perform a convolution $\Big(t(u,v)f(u,v)\Big)*p(u,v)$ whose corresponding operation is $T_a(x,y)P(x,y)$. If the single dish beam width is considerably less than the interferometer primary beam, then $f(u,v)$ will be a very broad smooth function as compared to $p(u,v)$. In such a case

$$\Big(t(u,v)f(u,v)\Big)*p(u,v) \simeq f(u,v)\Big(t(u,v)*p(u,v)\Big)$$

Suppose the interferometer data is not available within some distance u_{min} of the origin in the (u,v) plane. From the above equation, it is seen $f(u,v)$ must be close to unity out to u_{min} and $T_a(x,y)$ must be known out to where $P(x,y)$ is small in order for $t(u,v)*p(u,v)$ to be determined near the origin. Assume that such conditions are satisfied.

Let $g(u,v)$ be a function that is unity if $u^2 + v^2$ is less than u_{min} but zero otherwise. Modify the clean map by forming $m(u,v)[1 - g(u,v)]$ or equivalently calculating

$$M'(x,y) = M(x,y) - M(x,y)*G(x,y)$$

Take the single dish observations and calculate

$$T'(x,y) = [T_a(x,y)P(x,y)]*G(x,y).$$

Then M'(x,y) and T'(x,y) can be added directly to form a map whose visibility is the same as t(u,v)*p(u,v) from the zero spacing out to the maximum limit where interferometer measurements were made.

REFERENCES

Allen, C. W. 1973, Astrophysical Quantities, London, Athlone Press

Bieging, J. H. 1973, California Institute of Technology, Ph. D. dissertation

Blaauw, A. 1964, Ann. Rev. Astr. and Ap., 2, 213

Bok, B. J. 1956, Astr. J., 61, 309

Bok, B. J., Cardwell, C. S., Cromwell, R. H. 1970, Symposium on Dark Nebulae, Globules, and Protostars, Tuscon: Univ. Arizona Press

Bok, B. J., Lawrence, R. S., Menon, T. K. 1955, P.A.S.P., 67, 108

Bok, B. J., Reilly, E. 1947, Ap. J., 185, 857

Crutcher, R. M. 1973, Ap. J., 185, 857

Cudaback, D. D., Heiles, C. 1969, Ap. J. (Letters), 155, L21

Davies, R. D. 1956, M.N.R.A.S., 116, 443

Davies, R. D. 1958, Rev. Mod. Phys., 30, 931

Dieter, N. H. 1973, Ap. J., 183, 449

Garzoli, S. L., Varsavsky, C. M. 1966, Ap. J., 145, 79

Garzoli, S. L., Varsavsky, C. M. 1970, Ap. J., 160, 83

Greisen, E. W. 1973, California Institute of Technology, Ph. D. dissertation

Habing, H. J. 1968, B.A.N., 19, 421

Heiles, C. 1967, Ap. J., 148, 299

Heiles, C. 1968, Ap. J., 151, 919

Heiles, C. 1969, Ap. J., 156, 493

Heiles, C. 1971, Ann. Rev. Astr. and Ap., 9, 293

Heiles, C. 1973, Ap. J., 183, 441

Herbig, G. H. 1960, Ap. J. Supp., 4, 337

Herbig, G. H. 1962, Adv. Astr. and Ap., 1, 47

Hollenbach, D. J., Werner, M. W., Salpeter, E. E. 1971, Ap. J., 163, 165

Jenkins, E. B., Savage, B. D. 1974, Ap. J., 187, 243

Kerr, F. J., Garzoli, S. 1968, Ap. J., 152, 51

Knapp, G. R. 1974, Astr. J., 79, 527

Larson, R. B. 1973, Ann. Rev. Astr. and Ap., 11, 219

Lilley, A. E. 1955, Ap. J., 121, 559

Loren, R. B., Vanden Bout, P. A., Davis, J. H. 1973, Ap. J. (Letters), 185, L67

Lynds, B. T. 1962, Ap. J. Supp., 7, 1

Lynds, B. T. 1965, Ap. J. Supp., 12, 163

Lynds, B. T. 1968, In Nebulae and Interstellar Matter, ed. B. M. Middlehurst, L. H. Aller, Chicago: Univ. of Chicago Press

Mc Gee, R. X., Murray, J. D., Milton, J. A. 1963, Aust. J. Phys., 16, 136

Palmer, P., Zuckerman, B., Buhl, D., Snyder, L. E. 1969, Ap. J. (Letters), 156, L147

Penzias, A. A., Solomon, P. M., Jefferts, K. B., Wilson, R. W. 1972, Ap. J. (Letters), 174, L43

Quiroge, R. J., Varsavsky, C. M. 1970, Ap. J., 160, 83

Racine, R. 1968, Astr. J., 73, 233

Raimond, E. 1966, B.A.N., 18, 191

Rogstad, D. H., Shostak, G. S. 1971, Astr. and Ap., 13, 99

Sancisi, R. 1971, Astr. and Ap., 12, 323

Sancisi, R., Wesselius, P. R. 1970, Astr. and Ap., 7, 341

Solomon, P. M., Werner, M. W. 1971, Ap. J., 165, 41

Sturch, C. 1969, Astr. J., 74, 82

van den Berg, S. 1966, Astr. J., 71, 991

Zuckerman, B., Palmer, P., Snyder, L. E., Buhl, D. 1969, Ap. J. (Letters), 157, L167